Revealing the earliest events of auxin perception

Sigurd Ramans Harborough

Submitted in accordance with the requirements for the degree of
Doctor of Philosophy

The University of Leeds
Faculty of Biological Sciences
Centre for Plant Sciences

September, 2016

The candidate confirms that the work submitted is his own and that appropriate credit has been given where reference has been made to the work of others.

Acknowledgements

Firstly, I would like to thank my supervisory team of Stefan, Richard and Iain for their support and guidance during my PhD. I would also like to especially thank Arnout and Gary for teaching me how to use NMR. I would also like to thank the research groups of the Kepinski and Napier labs for all their support during my PhD. I would like to thank my sponsors of BBSRC and Syngenta and especially John and Nathan for training me to use the computational modelling software Maestro. I would also like to thank Gatsby plant sciences for all their support during my PhD. I would also like to make a special thank you to my teachers and all my family and friends for their help and support.

Abstract

Auxin signalling involves the ubiquitin-mediated degradation of Aux/IAA transcriptional repressor proteins. This is dependent on the interaction between a TIR1/AFB auxin co-receptor protein, an auxin molecule, and the Aux/IAA protein. Here we characterise the structure of an Aux/IAA protein AXR3 domains I and II, focussing in particular on the conformations adopted within the region of the Aux/IAA protein known as the degron before and during its interaction with the auxin molecule and TIR1. We use of a range of biophysical techniques including Nuclear Magnetic Resonance (NMR) Spectroscopy, Isothermal Titration Calorimetry (ITC) and Surface Plasmon Resonance (SPR). Our work provides the first evidence that a large component of an Aux/IAA's structure is intrinsically disordered with tendencies to form secondary structure around the degron. We show that *cis* and *trans* isomer states of Pro 87 within the degron core are approximately equal in abundance and that binding to TIR1 is stronger for the *cis* state, but nevertheless apparent for both conformations highlighting the possibility of a distinct encounter complex that precedes the fully-docked complex revealed by previous crystallographic analysis. Residues flanking the degron core are shown to be important for the interaction with TIR1 and we show that by mutation of these peripheral sequences it is possible to both decrease and increase the kinetics of complex formation. We also report on apparent low affinity auxin binding to the Aux/IAA degron in the *trans* conformation. We discuss the possible regulatory significance of apparent conformation shifts within the degron core that may act as a molecular switch to control the Aux/IAA's intrinsic disorder and how this disorder may relate to its hypothesised function as a co-receptor for auxin.

Table of Contents

List of Tables

List of Figures

List of abbreviations

AFBs: (AUXIN SIGNALLING F-BOX) Members of a small family of auxin receptors.

AREs: (Auxin response elements) Conserved regions of DNA commonly associated with the promoters of auxin regulated genes.

ARFs: (Auxin response factors) Transcription factors which bind to AREs.

ARF^{A}: Activating ARFs

ARF^{R}: Repressor ARFs

Auxinole: [α-(2,4-dimethylphenylethyl-2-oxo)-IAA] An anti-auxin.

Aux/IAAs: (Auxin/INDOLE ACETIC ACID) Repressor proteins of auxin-regulated genes.

AXR3/IAA17: A member of the Aux/IAA family of repressor proteins of auxin regulated genes.

BH-IAA: (*tert*-butoxycarbonyl-minohexyl-IAA) An anti-auxin.

CNB: 4-chloro-3-nitrobenzoic acid

COI1: (CORONATINE INSENSITIVE 1) An F-box protein of jasmonate signalling.

DD: Dimerisation domain.

DI: Domain I of an Aux/IAA protein. Contains the motif required for co-repressor recruitment.

DII: Domain II of an Aux/IAA protein. The location of the degron which forms the critical interface with TIR1

DIII: Domain III of an Aux/IAA protein, mediates dimerisation between other Aux/IAA proteins and ARF transcription factors

DIV: Domain IV of an Aux/IAA protein, mediates dimerisation between other Aux/IAA proteins and ARF transcription factors

EAR: Ethylene response factor-associated amphilic repression motif.

ER7: (Everted repeat 7) A nucleotide sequence which contains two AuxREs.

HDAC: Histone deacetylase complexes

IAA: (Indole-3-acetic acid) An endogenous auxin, which is biologically active.

IBA: (Indole-3-butyric acid) An endogenous auxin, considered to be a storage form of auxin which is not biologically active.

IDP: intrinsically disordered protein.

IDR: intrinsically disordered region.

IPTG: Isopropyl 1-thio-β-D-galactopyranoside

$IP_{6:}$ inositol hexakisphosphate

ITC: Isothermal titration calorimetry.

JA-Ile: [(*3R,7S*)-jasmonoyl-L-isoleucine] A bioactive molecule of jasmonate signalling.

JAZ: (JASMONATE ZIM DOMAIN) transcriptional repressor proteins of jasmonate signalling.

MR: The non-conserved middle region of an ARF

NAA: (1-naphthaleneacetic acid) A synthetic auxin.

NMR: Nuclear magnetic resonance spectroscopy

NMSA (I-naphthylsulphide acetic acid) An anti-auxin.

NMSP: [*α*-(I-napthylmethylsulphide) propionic acid] An anti-auxin.

PAA: (phenylacetic acid) An endogenous auxin, which is biologically active.

PCIB: (*p*-chlorophenoxy-*iso*-butyric acid) An anti-auxin.

Picloram: (4-amino-3,5,6-trichloropicolinic acid) A synthetic auxin.

SCF: SCF-type E3 ubiquitin ligase complex.

SPR: Surface plasmon resonance

TCEP: Tris(2-carboxyethyl)phosphine hydrochloride solution.

TIR1: (TRANSPORT INHIBITOR RESPONSE 1) An F-box protein and a member of a small family of six auxin receptors.

TPD: TPL domain.

TPL: (TOPLESS) Co-repressor protein.

U2AF: (U2 auxiliary factors) Essential splicing factors in humans.

2,4-D: (2,4-dichlorophenoxyacetic acid) A synthetic auxin.

4-Cl-IAA: (4-chloroindole-3-acetic acid) An endogenous auxin, which is biologically active.

Chapter 1

General introduction

Auxin perception within the plant cell nucleus

The plant hormone auxin is essential for plant growth and development. From the earliest events of embryogenesis through to flowering auxin is involved in almost every aspect of development (Jenik and Barton, 2005; Vanneste and Friml, 2009). For example, the formation of lateral organs in both the root and shoot of higher plants depends on the formation of local auxin maxima (Sassi and Vernoux, 2013). The exquisite spatio-temporal control of auxin distribution and response is most clearly demonstrated with the precise arrangement of leaves and flower petals in the form of a spiral phyllotaxis observed in Arabidopsis and many other species (Sassi and Vernoux, 2013).

The most well-studied endogenous auxin is indole-3-acetic acid (IAA). In *Arabidopsis thaliana* there are three other chemically distinct auxins: 4-chloroindole-3-acetic acid (4-Cl-IAA) and phenylacetic acid (PAA), and indole-3-butyric acid (IBA) (Figure 1.1). As well as these endogenous auxins, synthetic auxins have been developed since the 1940s as herbicides where their stability within a cell disrupts normal plant development (Grossmann, 2010). Among the earliest of these compounds are: 2,4-dichlorophenoxy acetic acid (2,4-D), and 1-naphthalene acetic acid (1-NAA). A selection of these synthetic auxins is presented (Figure 1.1).

The endogenous IAA can be actively transported to specific locations within the plant to mediate developmental responses, a feature unique amongst the plant hormones (Leyser, 2006). This is achieved by a series of influx and efflux carrier proteins which can distribute asymmetrically around the cell to establish a flux of auxin within the tissue of the plant. This enables the

hormone to be distributed throughout the plant, in addition to its long distance transport down the plant phloem (Friml, 2003; Leyser, 2005).

The transport and biosynthesis of auxin provides a mechanism to control auxin gradients and establish tissue patterning (Teale *et al.,* 2006). This is most clearly observed during root tissue specification, but there is uncertainty on whether auxin functions as a typical morphogen throughout the rest of the plant (Bhalerao and Bennett, 2003). It is likely that this simple signal is fine-tuned by variation of the components involved in its perception, allowing for a wide range of developmental responses.

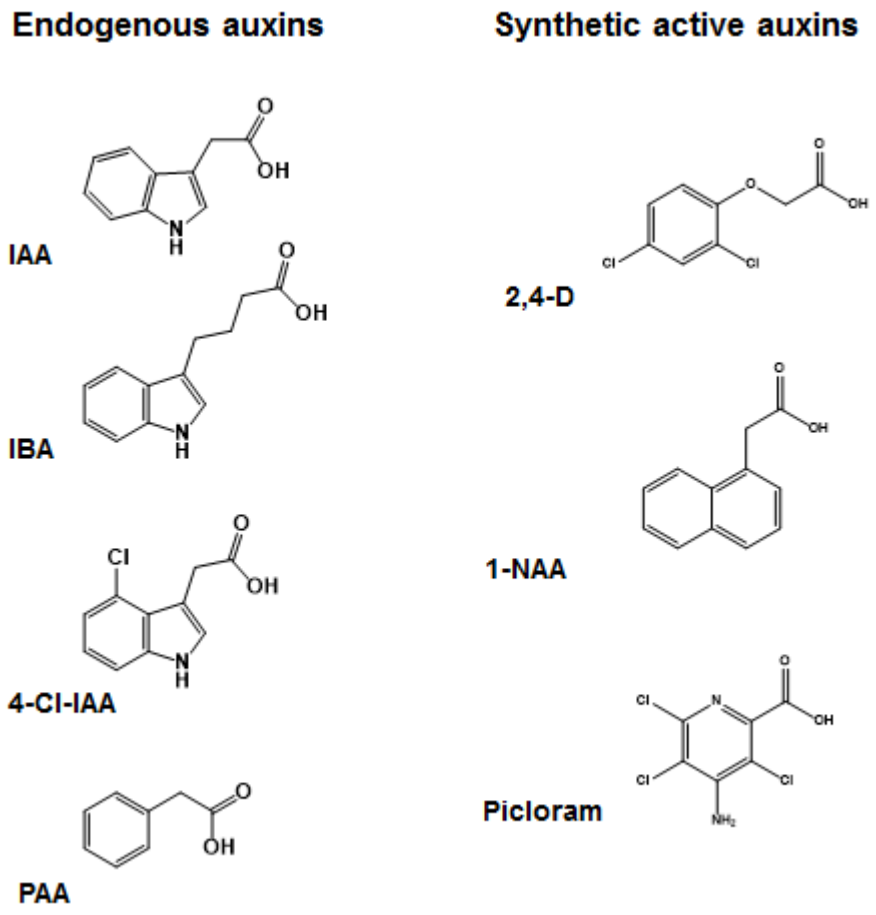

Figure 1.1 Chemical structures of endogenous and synthetic auxins.
Endogenous auxins: (IAA) indole-3-acetic acid, (IBA) indole-3-butyric acid, (4-Cl-IAA) 4-chloroindole-3-acetic acid, (PAA) phenylacetic acid. Selection of synthetic auxins: (2,4-D) 2,4-dichlorophenoxyacetic acid, (1-NAA) 1-naphthaleneacetic acid, (picloram) 4-amino-3,5,6-trichloropicolinic acid.

Here auxin signal transduction in the nucleus is reviewed, focusing particularly on the structural biology of the components within this mechanism. We will also consider similarities in the perception between auxin and the plant hormone jasmonate. This review will outline the future perspectives of this signal transduction, highlighting our limited understanding of the molecular detail in the earliest events of auxin perception.

1.1 Schematic overview of auxin signal transduction in the plant cell nucleus

Our understanding of auxin perception in the plant cell nucleus has developed from the simple models of activators and repressors controlling gene expression, to the targeted proteasome-mediated degradation of the Auxin/INDOLE ACETIC ACID (Aux/IAA) transcriptional repressor proteins (Theologis, 1986; Walker and Estelle, 1998; Mockaitis and Estelle, 2008; Hayashi, 2012).

A recent review has studied the role of instability elements termed degrons involved in the ubiquitin-mediated degradation of a wide range of protein families (Guharoy *et al*., 2016). The report suggests protein degradation is mediated by a tripartite system of instability elements. The primary degron is the region of the protein which defines it as a substrate for ubiquitin-mediated degradation. In close proximity to this primary degron there is typically a secondary instability element, which is less well defined as it can be represented by at least one lysine residue and is the site for ubiquitin modification (Guharoy *et al*., 2016). This may not be the case for Aux/IAA proteins as a report has shown that substituting all lysine residues with arginine did not stop the rapid degradation of the protein IAA1 (Gilkerson *et al*., 2015). The third part of the degradation model is a long disordered segment usually within ten residues of the primary degron (Guharoy *et al*., 2016). How this tripartite degron system relates to the ubiquitin-mediated degradation of Aux/IAA proteins is uncertain and is a key question considered in our research.

Presented here is the current model for auxin signal transduction within the plant cell nucleus (Figure 1.2). This model describes the molecular interactions at low and high auxin levels to regulate gene expression, a process tightly linked to the stability of the Aux/IAA protein.

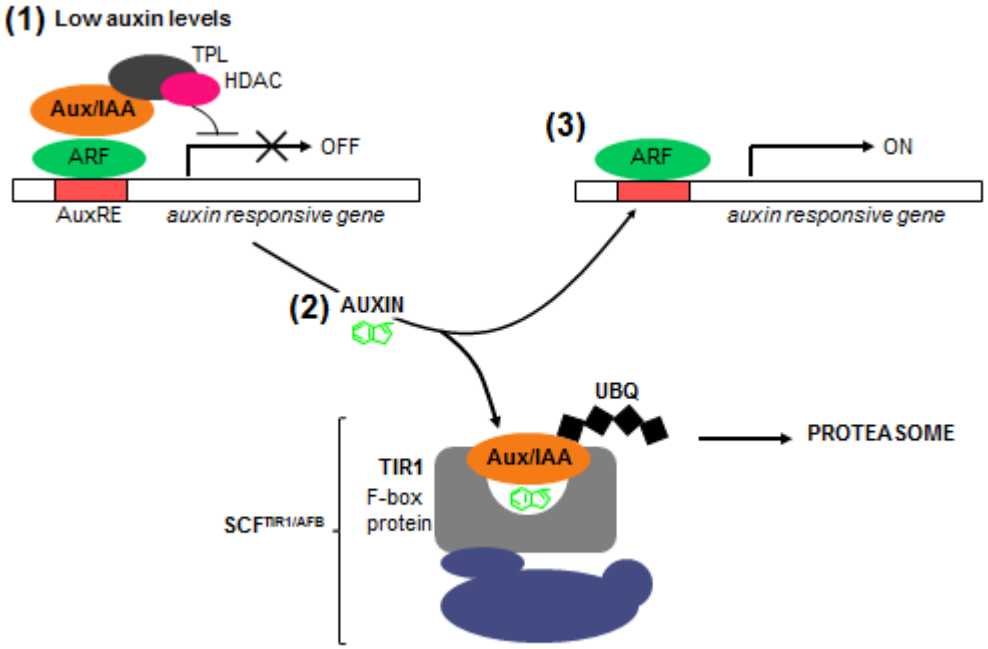

Figure 1.2 Schematic diagram of auxin signal transduction in the nucleus of a plant cell. (1) The first step shown in the diagram is transcriptional repression, which occurs at low auxin levels. Promoters of auxin-regulated genes typically contain a sequence region known as an auxin response element (AuxRE) which acts as a recognition site for the binding of auxin response factors (ARFs). These transcriptions factors form a heterodimer with the functional domains DIII and DIV of the transcriptional repressor protein Aux/IAA. The Aux/IAA recruits the co-repressor TOPLESS (TPL), which in turn may recruit histone deacetylase complexes (HDAC) to repress gene transcription. (2) An increase in auxin levels promotes the formation of the auxin receptor complex. This is composed of an SCF E3 ubiquitin ligase complex ($SCF^{TIR1/AFB}$), where the F-box protein TRANSPORT INHIBITOR RESPONSE1 (TIR1) acts as the substrate receptor. Auxin binds to TIR1 and enhances the affinity of the receptor for the binding of the Aux/IAA protein. Consequently the Aux/IAA protein gains a polyubiquitin chain which targets the protein for degradation in the 26S proteasome. (3) The degradation of the Aux/IAA protein results in the de-repression of the auxin-regulated genes.

1.1.1 Transcriptional repression at low auxin levels

Transcriptional repression of auxin-regulated genes is mediated by two inter-linked mechanisms of transcription factors and repressor proteins. The transcription factors, termed auxin response factors (ARFs) are able to modulate expression of auxin-regulated genes through chromatin remodeling. This involves interactions between members of the ARF protein family of which there are 23 in *A. thaliana* and can be broadly defined into transcriptional activators and repressors (reviewed by Guilfoyle and Hagen, 2007; Chandler, 2016).

The activator ARFs (ARF5-8, and 19) share the characteristic amino acid enrichment of glutamine, serine, and leucine in the non-conserved middle region (MR) of their structures, located between a DNA binding domain and a C-terminal region of functional domains III and DIV. The rest of the ARF protein family is composed of transcriptional repressors with their MR domain enriched in the amino acids serine, proline, leucine, and glycine (reviewed by Guilfoyle and Hagen, 2007; Chandler, 2016).

The repressor ARFs (ARF^R) may heterodimerise with activating ARFs (ARF^A), but also with other ARF^R proteins through a dimerisation domain (DD) located within the DNA binding region of the protein, or through the C-terminal DIII and DIV (Ulmasov et al., 1999; Korasick *et al*., 2014; Chandler, 2016). The interaction with an ARF^R is expected to mediate transcriptional repression by the recruitment of the co-repressor TOPLESS (TPL). This protein is then considered to recruit histone deacetylase complexes (HDAC) resulting in DNA condensation (Chandler, 2016).

These transcription factors are recruited to promoters of auxin-regulated genes, by recognizing a short nucleotide sequence motif of TGTCTC. Mutation of any one of these nucleotides prevents auxin-mediated regulation of gene expression; consequently the sequence motif defines an auxin response element (AuxRE) (Ulmasov *et al*., 1995; Ulmasov *et al*., 1997).

The interaction between an ARF and AuxRE has been observed in a recent crystallography study of the ARF1 DNA binding domain (Figure 1.3) (Boer *et al*., 2014; reviewed by Parcy *et al*., 2016). The crystal structure shows the

protein bound to DNA as a dimer. In this case the partner monomer interacts with an inverted repeat of the TGTCTC sequence, consistent with earlier investigations (Ulmasov *et al*., 1997). Spacing between these AuxREs has the potential to introduce specificity for the recruitment of particular ARF dimers to the promoter of an auxin-regulated gene with protein ARF1 showing sensitivity to spacing while protein ARF5 was able to bind sites at very different spacing (Boer *at al*., 2014).

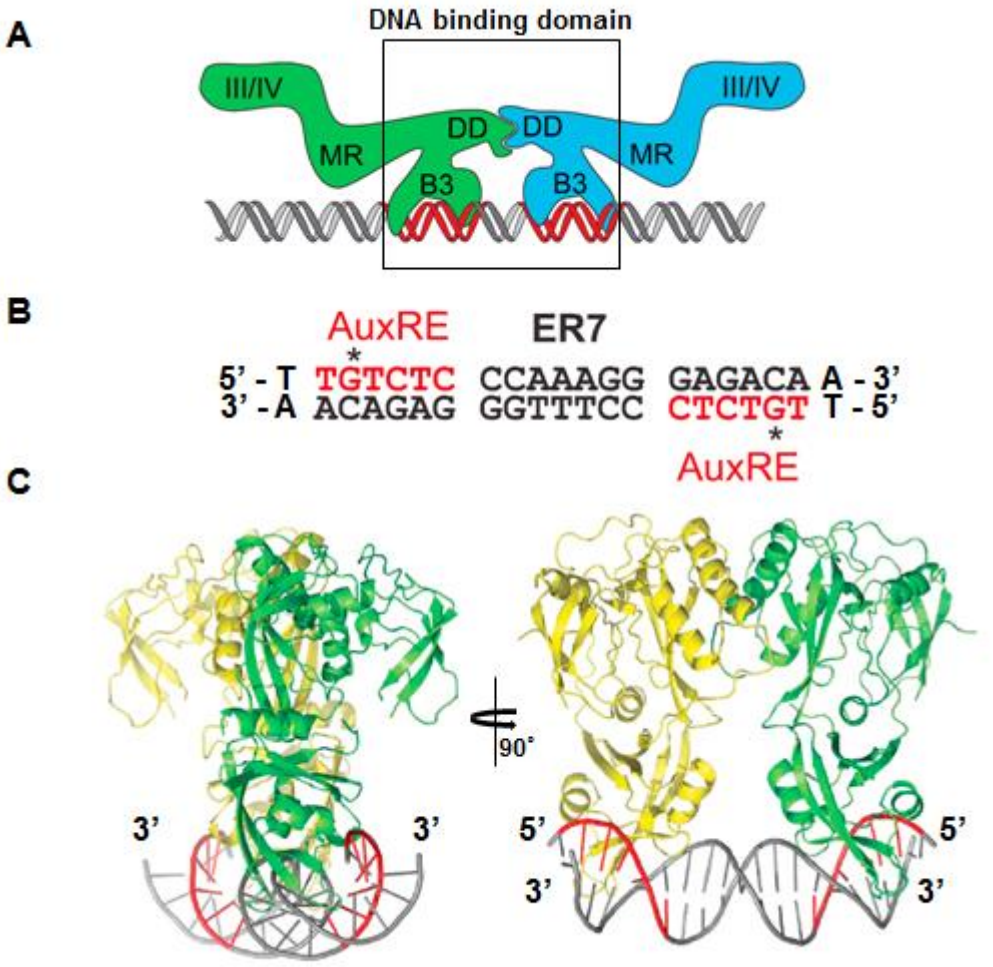

Figure 1.3 Crystal structure of the DNA binding domain dimer of ARF1, figure adapted from Boer *et al*., 2014. (A) Schematic diagram of an ARF dimer, with each monomer shown in a different colour. A box highlights the DNA binding domain which is composed of three regions: a B3 domain, flanked by two regions which from a dimerisation domain (DD). The B3 domains are shown bound to AUXREs coloured red. (B) Nucleotide sequence of everted repeat 7 (ER7) with the AUXREs highlighted. (C) Crystal structure of a DNA binding domain dimer of ARF1. The monomers are coloured green and yellow to separate the structures.

The ARF C-terminal domains III and IV are also the location for the binding of Aux/IAA transcriptional repressor proteins, which mediate transcriptional repression at low auxin levels and are the proteins via which auxin can affect the transcription of ARF-bound genes. At low auxin levels the Aux/IAA protein typically interacts with the ARF^{A} transcription factors, with lower affinity for ARF^{R} proteins (Guilfoyle and Hagen, 2007; Vernoux *et al*., 2011). The ARFs and Aux/IAA proteins form heterodimers through structurally homologous regions referred to as domains DIII and DIV in both proteins, a process which is independent of the ARF DNA binding domain. After dimerizing with an ARF the Aux/IAA protein is positioned above its target gene and mediates transcriptional repression by the recruitment of the co-repressor TPL which is then expected to recruit HDAC, resulting in the DNA condensation (Figure 1.2 [1]) (Mockaitis and Estelle, 2008; Hayashi, 2012).

A recent review has suggested a further development to this model of auxin signal transduction (Wang and Estelle, 2014). The review highlights the possibility of the Aux/IAA proteins and ARFs forming long polymer chains. These occur where opposite-charged surfaces across DIII and DIV form electrostatic interactions allowing higher-order structures to be established (Han *et al*., 2014; Dinesh *et al*., 2015). It is suggested that such chains may enhance the recruitment of TPL and HDAC for efficient transcriptional repression (Wang and Estelle, 2014).

1.1.2 The auxin receptor complex

An increase in auxin levels results in the ubiquitin mediated degradation of the Aux/IAA protein and consequently the de-repression of the auxin-regulated gene (Figure 1.2 [2 to 3]) (reviewed by Mockaitis and Estelle, 2008; Hayashi, 2012). The targeted degradation of Aux/IAA proteins involves an SCF E3 ubiquitin ligase complex, where auxin enhances the binding of the Aux/IAA protein to the complex by forming an interaction with the F-box receptor protein TRANSPORT INHIBITOR RESPONSE1 (TIR1) (Kepinski and Leyser, 2005; Dharmasiri *et al*., 2005). TIR1 is part of a small family of six auxin receptors, with the other members termed AUXIN

SIGNALLING F-BOX proteins (AFBs) (Dharmasiri *et al*., 2005 a; Parry and Estelle, 2006).

Crystallographic analysis has revealed the structure of TIR1 in complex with the auxin molecule IAA, and a 13 amino acid peptide of the Aux/IAA protein AXR2 (Figure 1.4) (Tan *et al*., 2007). The peptide represents the conserved amino acids of functional domain II, an instability element within the protein which is termed the degron (Abel *et al*., 1994; Ramos *et al*., 2001; Kepinski and Leyser, 2005; Dharmasiri *et al*., 2005).

The crystal structure of TIR1 shows a fold in the receptor surface formed from a leucine-rich repeat loop (loop-2), which creates a ridged hydrophobic pocket (Figure 1.4A). The IAA molecule is observed tethered to the base on this binding pocket via its carboxyl tail, which forms a salt bridge and two hydrogen bonds with the TIR1 residues Arg 403 and Ser 438 (Figure 1.4B). The interaction between IAA and TIR1 is further stabilized by two phenylalanine residues (Phe 83 and Phe 380), which are positioned in close proximity to the IAA indole ring structure (Tan *et al*., 2007).

The bound IAA molecule is believed to extend the hydrophobic surface, functioning as molecular glue by enhancing the affinity of the receptor for Aux/IAA binding (Tan et al., 2007). This is consistent with previous observations of auxin promoting the binding of Aux/IAA degron peptides to TIR1 (Kepinski and Leyser, 2005; Dharmasiri *et al*., 2005).

The crystal structure shows that the degron peptide partly inserts into the upper region of the auxin binding pocket (Figure 1.4C and D) (Tan *et al*., 2007). This inserted region consists of the highly conserved residues Trp 86, Pro 87, and Pro 88. It is likely that this crystal structure represents the final stages of binding of the complex, when the interaction is most secure. How the auxin receptor complex forms remains a central question to auxin biology. Currently literature has not reported on how auxin may bind to the TIR1/AFB receptors in absence of the Aux/IAA co-receptors. Furthermore, our understanding of the protein structure surrounding the degron is limited as the N-terminal half of an Aux/IAA protein has currently not been characterised.

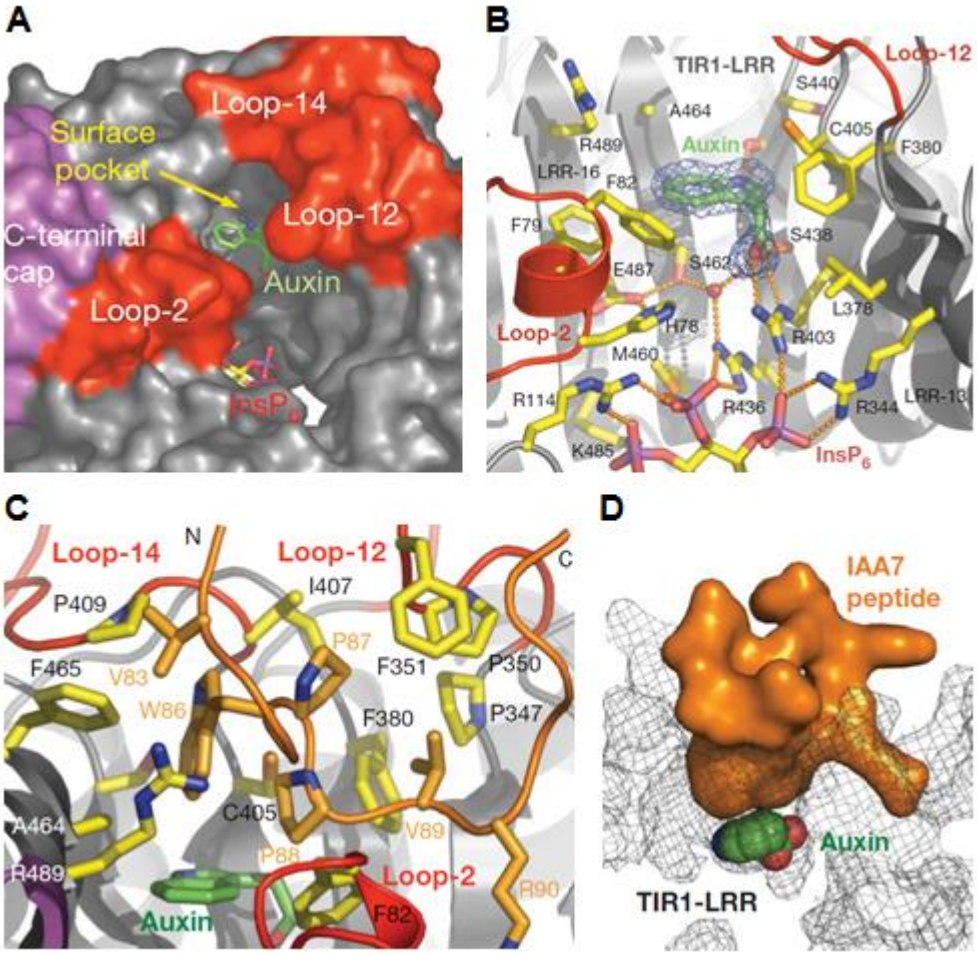

Figure 1.4 Crystal structure of the auxin receptor complex, figure adapted from Tan *et al*., 2007. (A) The molecular surface of the TIR1 receptor. Regions of the TIR1 surface are highlighted red to indicate the loop forming leucine-rich repeats considered important for ligand binding. Auxin (shown in green) is observed at the base of surface pocket. This is adjacent to a larger cavity, where inositol hexakisphosphate (IP_6) is observed through gaps in the pocket floor. (B) The molecular interaction between IAA and the TIR1 binding pocket are presented as dashed-lines. The pocket floor is defined by the polar residues Arg 403 and Ser 438 and forms the main contact via a salt bridge and two hydrogen bonds with the carboxyl chain of IAA. (C) The AXR2 / IAA7 peptide is shown bound to the auxin pocket. The degron core residues of Trp 86, Pro 87, and Pro 88 are shown in bold within the pocket. (D) Molecular surface of the degron peptide and auxin are displayed, with TIR1 surface displayed as a mesh.

1.2 Anti-auxins

In addition to the endogenous and synthetic auxins, there is a possibility of a group of molecules which function as anti-auxins within plants. Early studies indicated a group of potential anti-auxins which antagonised IAA induced growth stimulation of excised pea-root sections (Audus and Das, 1955). Within this study three molecules were observed to inhibit growth at 10^{-4} and 10^{-5} ppm: *α*-(I-napthylmethylsulphide) propionic acid (NMSP), I-naphthylsulphide acetic acid (NMSA), 4-chloro-3-nitrobenzoic acid (CNB). A fourth molecule *p*-chlorophenoxy-*iso*-butyric acid (PCIB) was shown to be a far more potent antagonist of IAA growth stimulation compared to NMSP, NMSA, and CNB (Audus and Das, 1955).

Interestingly, without IAA treatment PCIB is a very effective growth promoter at concentrations below 10^{-6} molar (Burström, 1950). A more recent study has revealed PCIB treatment reduces Aux/IAA gene transcripts in the plant cell and suggested a possible influence on the gene expression feedback loops (Oono *et al*., 2003).

Building on these early studies a recent report has shown by in-silico docking a possible molecular mechanism of anti-auxins (Hayashi *et al*., 2012). The anti-auxin *tert*-butoxycarbonyl-minohexyl-IAA (BH-IAA) can be docked into the auxin binding pocket of TIR1 (Figure 1.5A and B). The long alkyl side group of BH-IAA fills the upper region of the pocket and prevents binding of the Aux/IAA degron core. Consequently without the stabilising effect of the Aux/IAA degron to the complex, BH-IAA has a low affinity interaction with TIR1 as observed in pull-down assays and reduces its antagonistic potency within plants (Hayashi *et al*., 2008; Hayashi *et al*., 2012).

Subsequently a new anti-auxin has been developed, α-[2,4-dimethylphenylethyl-2-oxo]-IAA, termed auxinole (Figure 1.5C) (Hayashi *et al*., 2012). This compound has increased potency as an antagonist compared to BH-IAA, due to an increased affinity to TIR1. This is likely to be due to an electrostatic interaction between the phenyl ring of auxinole and the TIR1 residue Phe 82 in the upper-regions of the auxin binding pocket as shown by in-silico docking (Figure 1.5D). Consequently auxinole prevents

Pro 88 of the Aux/IAA degron from binding (Hayashi *et al*., 2012). This is likely to lead to increased stability of Aux/IAA proteins in the plant cell as suggested from previous studies (Oono *et al*., 2003). The low potency of BH-IAA highlights the stabilising role of the Aux/IAA degron in the auxin receptor complex.

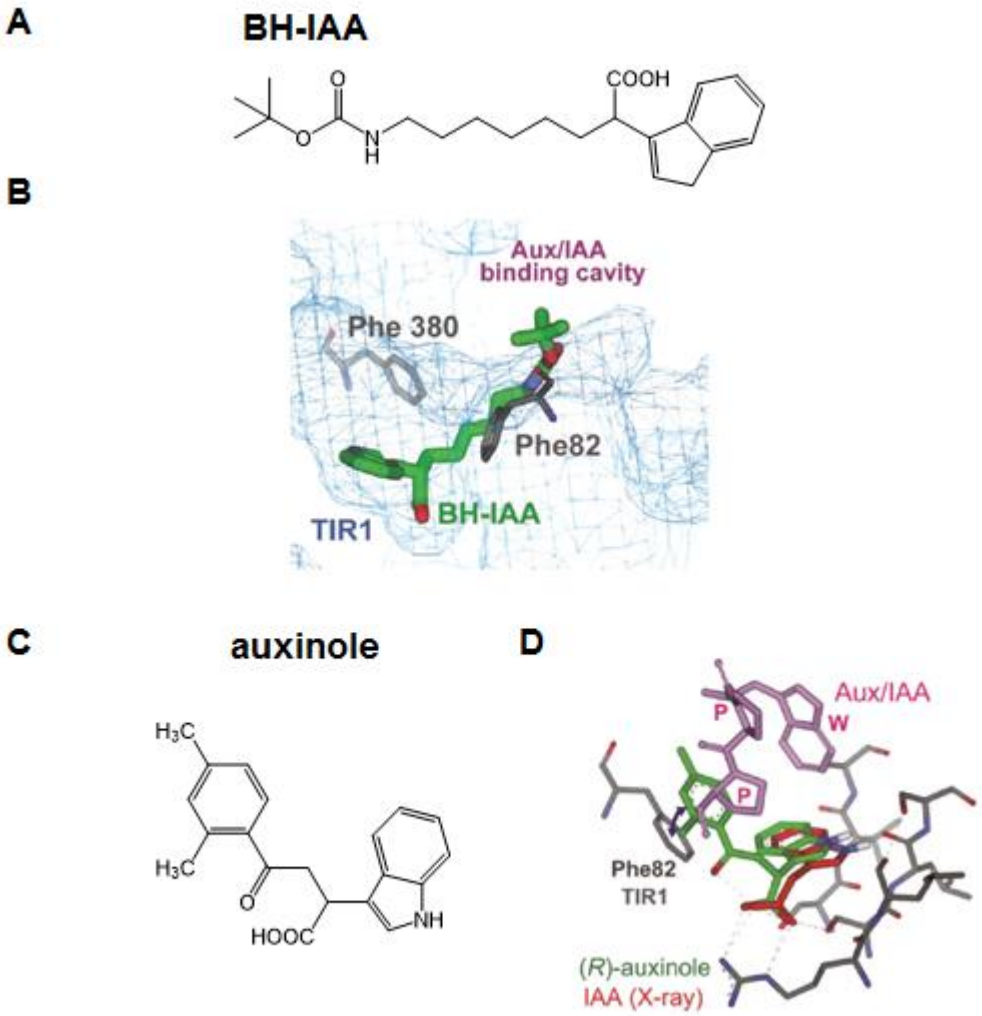

Figure 1.5 Anti-auxins BH-IAA and auxinole prevent Aux/IAA binding to TIR1, figure adapted from Hayashi *et al.,* 2012. (A) Chemical structure of the IAA antagonist *tert*-butoxycarbonyla-minohexyl-IAA (BH-IAA). (B) Below is shown the in-silico docking of BH-IAA into the auxin binding pocket of TIR1. (C) Chemical structure of α-[2,4-dimethylphenylethyl-2-oxo]-IAA, termed auxinole. (D) Molecular docking of auxinole into TIR1 auxin binding pocket shows a π-π stacking between Phe 82 (TIR1) with the phenyl ring of auxinole, preventing Pro 88 of the Aux/IAA degron from binding to the pocket.

1.3 A comparison between auxin and jasmonate perception

We have seen how Aux/IAA proteins are targeted for degradation by the formation of the auxin receptor complex. Remarkably a similar mechanism is observed for the perception of the plant hormone jasmonate. Before jasmonate can bind to its SCF complex it must first be conjugated with the amino acid isoleucine to form a bioactive molecule (*3R,7S*)-jasmonoyl-L-isoleucine (JA-Ile) (Fonseca *et al*., 2009). The equivalent process for IAA results in its inactivation as an auxin.

In jasmonate perception the active JA-IIe binds to its F-box protein CORONATINE INSENSITIVE 1 (COI1), which acts as the substrate receptor of the SCF^{COI1} E3 ubiquitin ligase complex. This complex targets for degradation the jasmonate signalling equivalent of the Aux/IAA proteins, the JASMONATE ZIM DOMAIN (JAZ) transcriptional repressors (Thines *et al*., 2007). The jasmonate receptor complex, containing the JAZ1 degron peptide has been observed in a crystallography study (Sheard *et al*., 2010).

The F-box proteins COI1 and TIR1 share a similar overall-structure, except for the distinct hormone binding pockets, where the COI1 pocket is polar and in TIR1 the auxin pocket is hydrophobic (Sheard *et al*., 2010; Tan *et al*., 2007). Another striking feature between these signalling systems is the divergent structure of the degron peptides (Figure 1.6A and B). The crystal structure of JAZ1 degron peptide shows a C-terminal helix and is in contrast to the unstructured AXR2 degron peptide within the auxin receptor complex.

The formation of a C-terminal helix in JAZ1 may relate to the stability of the immediate interface with the bound JA-Ile. Unlike the auxin receptor complex where the degron inserts into the upper half of the auxin binding pocket, the JA-IIe occupies its entire pocket in COI1 (Figure 1.7). The main contact between the N-terminal half of JAZ1 peptide and COI1 is a single leucine (Leu 201) which binds to a small pocket above the JA-IIe cavity (Figure 1.7A and B) (Sheard *et al*., 2010). To ensure a secure complex, the JAZ C-terminal degron forms a helix which fills an adjacent cavity and blocks the JA-Ile from dissociating (Figure 1.7C). There is also a second cavity adjacent to the auxin binding pocket and currently there is limited structural data for the C-terminal half of the degron (Figure 1.4A).

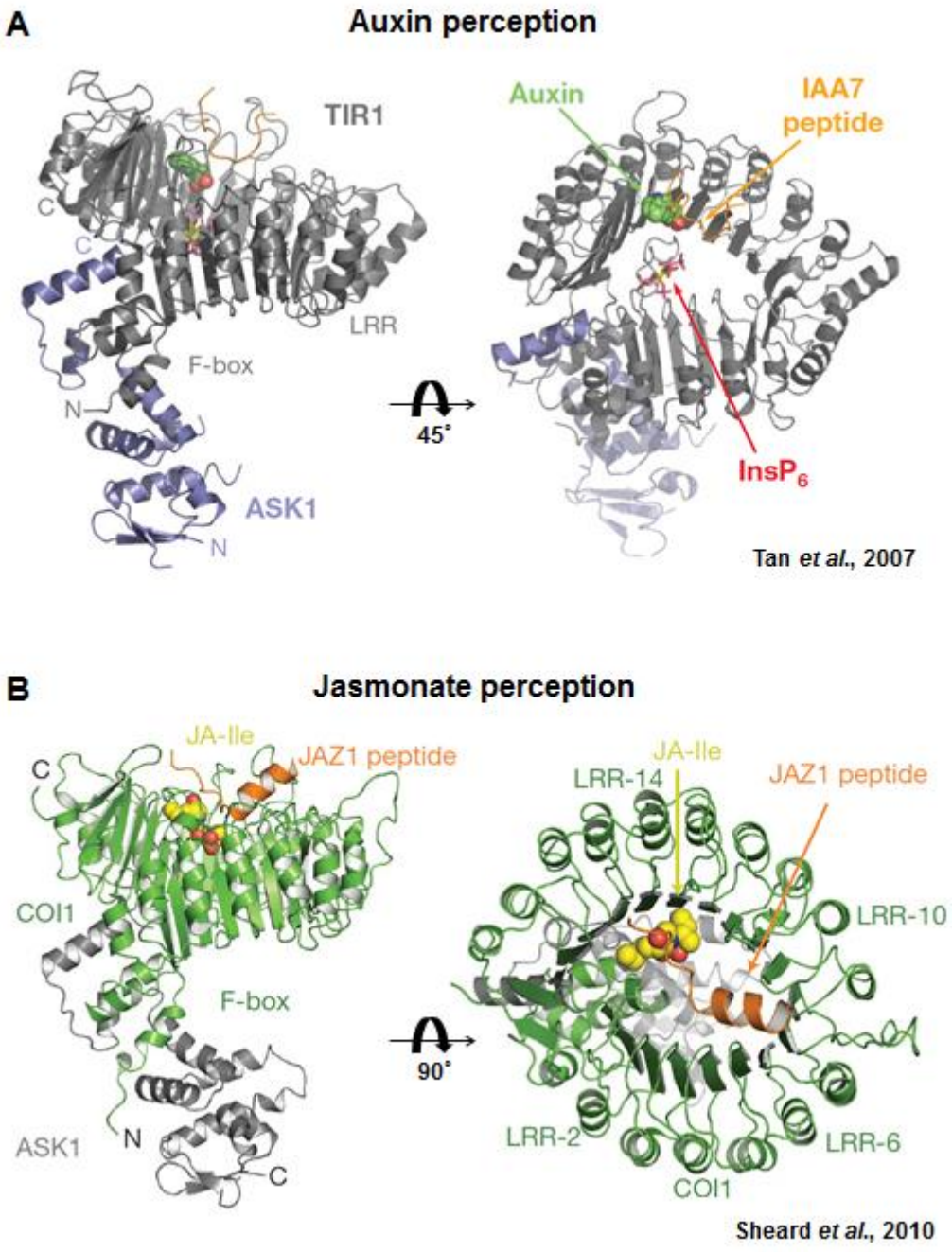

Figure 1.6 Crystal structures of the auxin and jasmonate receptor complexes, adapted from Tan *et al*., 2007 and Sheard *et al*., 2010. (A) The auxin receptor complex, consisting of the receptor TIR1 (grey), the auxin molecule IAA (green), the degron peptide of the AXR2 transcriptional repressor (orange), and the co-factor IP_6 (red). The adapter molecule ASK1 of the $SCF^{TIR1/AFB}$ complex is also displayed (light-purple). (B) The crystal structure of the jasmonate receptor complex. This includes the bioactive JA-Ile (yellow) and the JAZ1 degron peptide (orange) bound to the receptor COI1 (green) attached to the adapter molecule ASK1 (grey) of the SCF^{COI1} complex.

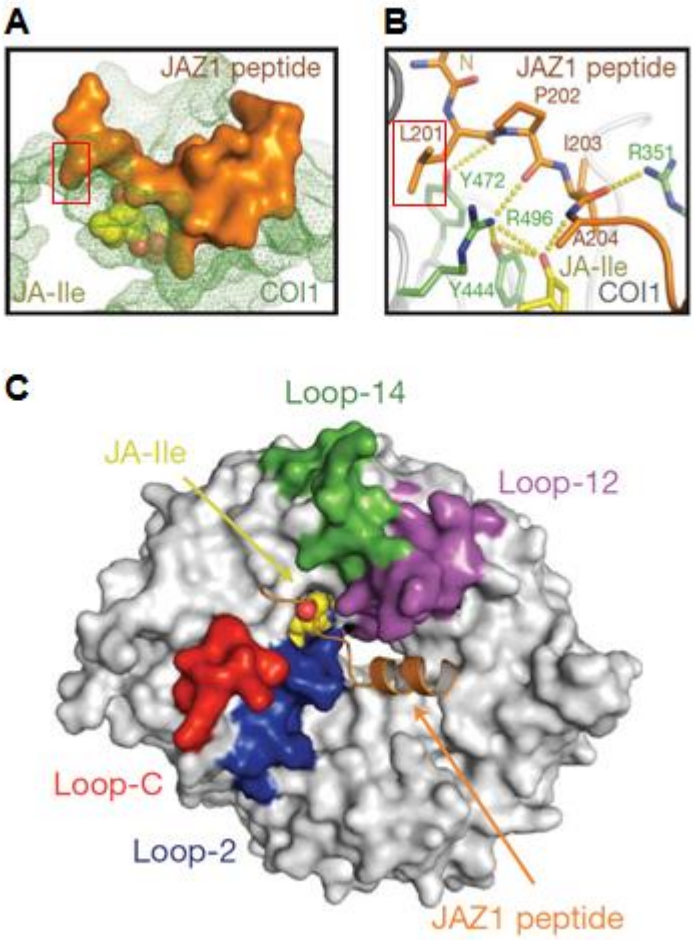

Figure 1.7 Crystal structure of the jasmonate receptor complex focusing on the JAZ1 peptide, figure adapted from Sheard *et al*., 2010. (A) The molecular surface of the degron peptide JAZ1 (orange) is shown bound to COI1 (green), where it covers the bound JA-Ile molecule (yellow). The N-terminal half of the JAZ1 peptide has a limited binding interface with the receptor and is highlighted by a red box. (B) This highlighted region corresponds to the JAZ1 residue Leu 201. (C) Molecular surface of the jasmonate receptor complex, including colour coding of the surface loops formed by leucine-rich repeats. The position of the helix formed by the C-terminal half of the degron is shown, securing the JA-Ile to COI1.

1.4 Outlook: the potential for a fuzzy auxin receptor complex

Crystallography of the auxin receptor complex has provided an insight into the degron as a binding interface, but questions still remain on how this important region relates the rest of the Aux/IAA protein structure. It is not

known if the surrounding region displays secondary structure, and this may have major implications for how the auxin receptor complex forms.

Here we will consider the possibility of the degron being located within an unstructured region of the Aux/IAA protein, the N-terminal half of which has not been characterised. This idea of an important binding interface being within an unstructured region is based on a growing trend within the literature. At the centre of cellular signalling events there are often proteins which exhibit extreme conformational flexibility, fluctuating between states, where structural organization can be triggered by interactions with other molecules (Wright and Dyson, 1999; Kiefhaber *et al*., 2012). Such intrinsic disorder can be localized to specific regions within a protein or dominate the entire structure (Uversky *et al*., 2005).

When these intrinsically-disordered proteins participate in molecular interaction they can be either static or highly dynamic, and are described as forming fuzzy complexes (Tompa and Fuxreiter, 2008). Usually in these interactions the disordered regions remain unstructured (Hazy and Tompa, 2009; Gruet *et al*., 2016). This has the advantage of targeting an interaction to a specific location within the protein which contributes the majority of the binding free energy (Wright and Dyson, 2015).

Such interaction hot spots are often characterised with highly-conserved sequence motifs which provide molecular identification for specific interactions (Tompa *et al*., 2015). These primary interface sites are typically associated with pre-defined structural elements or regions where folding is induced upon binding (Fuxreiter *et al*., 2004; Mészáros *et al*., 2007).

There is a spectrum of potential binding mechanisms of fuzzy complexes which can be split into four general categories: polymorphic, clamp, flanking, and random (Sharma *et al*., 2015). These mechanisms will be summarised in turn. Polymorphic binding includes static interactions where a specific conformation is induced with a binding partner. A clamp mechanism describes disordered regions functioning as flexible linkers to highly structured protein regions which act as the main binding interfaces. A flanking mechanism describes disordered regions and adjacent secondary structure both contributing to a binding event. The last mechanism is a

random binding model which involves multiple binding motifs in the protein interconnected by disordered regions (figure 1.8) (Sharma *et al*., 2015).

These four categories can be further refined into conformational selection, entropy modulation, competitive binding, and tethering where multiple binding motifs enhance the affinity of an interaction (figure 1.8) (Dogan *et al*., 2014; Sharma *et al*., 2015). The most interesting of these categories is conformational selection where currently the only example is found within a flanking binding model (Sharma *et al*., 2015). An example of this binding model is observed in the dimerisation of splicing factors, which enable an interaction with RNA. This mechanism was shown by the U2 auxiliary factors involving a reciprocal interaction of Trp residues, establishing conformational selection during heterodimerisation (Figure 1.9) (Kielkopf *et al*., 2001). In this binding event both disordered and structured regions function together as a binding interface.

These presented categories form a matrix of possible binding mechanisms for disordered proteins, but this should not be seen as absolute as there is potential for many different combinations to form. This matrix is particularly intriguing when considering the formation of the auxin receptor complex. It is a possibility that Aux/IAA proteins form fuzzy complexes and that the earliest events of auxin perception follow one of the outlined mechanisms.

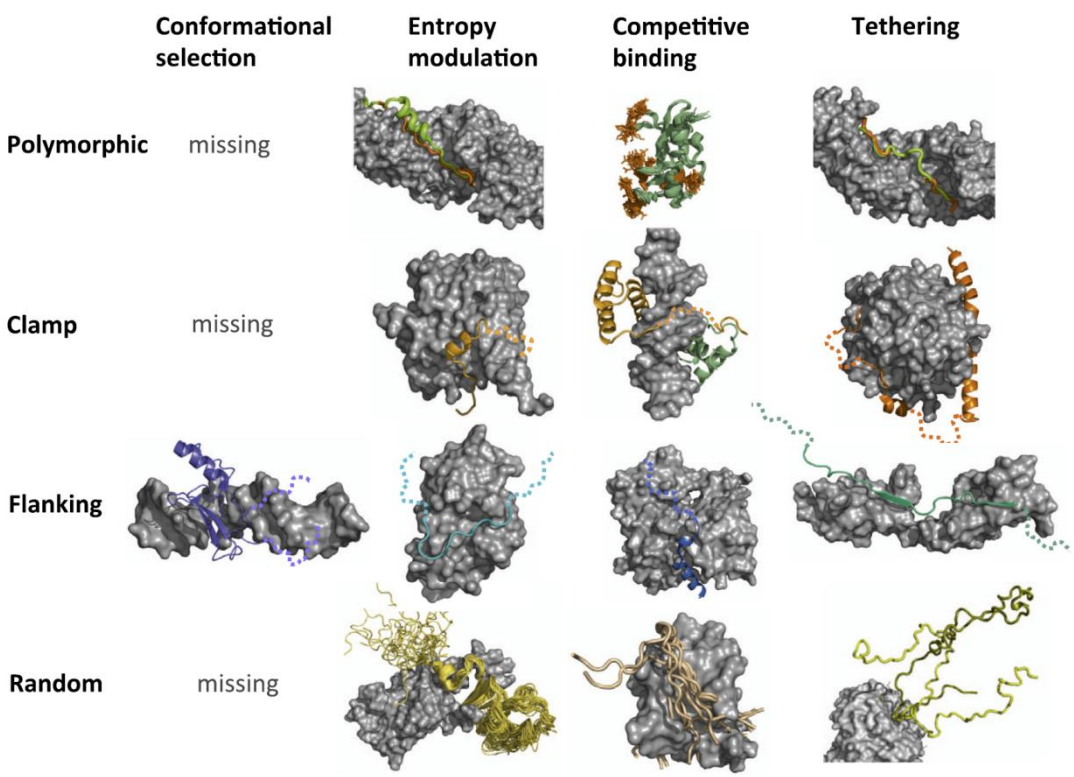

Figure 1.8 Matrix of potential binding mechanisms for the formation of fuzzy complexes, figure from Sharma *et al*., 2015. The binding mechanisms presented can be split into four general models, reflecting the function of the intrinsic disorder within the binding event: polymorphic, clamp, flanking, and random. These models can be further divided into the following: conformational selection, entropy modulation, competitive binding, and tethering. These categories form a matrix of possible binding mechanisms of disordered proteins when forming fuzzy complexes. These complexes are based on published structures within the literature and are reviewed by Sharma *et al*., 2015.

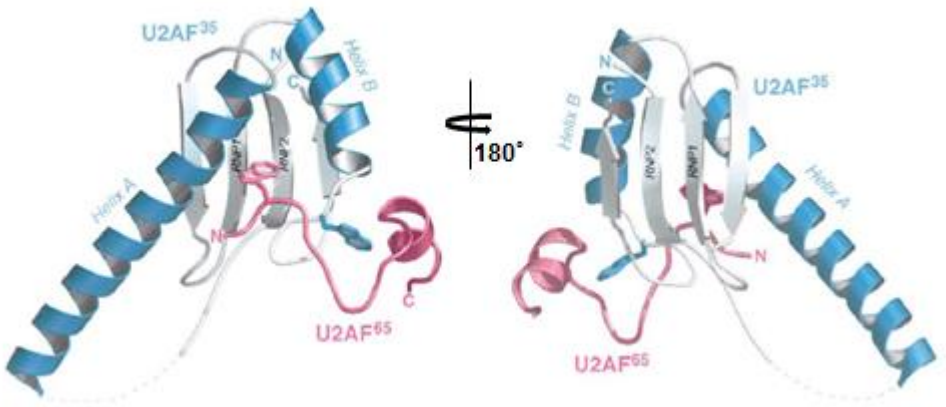

Figure 1.9 Example of a flanking mechanism in a fuzzy complex, figure adapted from Kielkopf *et al*., 2001. Presented is the crystal structure of the U2 auxiliary factors (U2AF) forming a heterodimer required for RNA binding. These are essential splicing factors in humans. The RNA recognition motif $U2AF^{35}$ (blue) forms a hydrophobic pocket between two helixes. A peptide of the linker region $U2AF^{65}$ (pink) contains a short helical region in the C-terminal half, in contrast the N-terminal half is disordered and rich in prolines. A Trp residue within this disordered region of $U2AF^{65}$ is observed inserted into the hydrophobic pocket of $U2AF^{35}$. This is reciprocated by the $U2AF^{35}$ with its own Trp residue interacting with the disordered loop of $U2AF^{65}$. The reciprocal Trp interaction is considered essential for U2AF dimerisation.

1.5 Project aims

The potential for intrinsic disorder in auxin signalling, and the observation of a large cavity adjacent to the auxin binding pocket raises important questions on how the Aux/IAA protein interacts with the receptor complex beyond the degron core. These questions must be addressed in order to develop our understanding on how the auxin receptor complex forms in the earliest events of auxin perception.

Here our research uses biophysical and structural biology to study the auxin receptor complex. Nuclear magnetic resonance (NMR) spectroscopy has been used to characterise the structure of the N-terminal half of the Aux/IAA protein AXR3 (DI and DII) and observe the interactions this protein forms with auxin receptor TIR1. We will consider the possible co-receptor functions of an Aux/IAA protein and study the potential for *cis* and *trans* isomer states

within the degron core and what effect this may have on auxin receptor complex formation. Together this research examines potential interactions not captured by the previous crystallography study of the auxin receptor complex (Tan *et al.,* 2007) and develops and enhances our understanding of the earliest events of auxin perception within the plant cell nucleus. The specific objectives of the project are as follows:

1. Characterise the structure of the N-terminal half of the Aux/IAA protein AXR3 (DI and DII).

2. The study of interactions formed by the AXR3 (DI and DII) protein upon receptor and auxin binding.

3. Explore determinants of specificity for Aux/IAA degron binding to the auxin receptor TIR1.

Chapter 2

General Methods

2.1 Acknowledgments

All DNA constructs used in this project were made and transformed into competent cells by Dr Martin Kieffer and Dr Lynne Armitage, and are part of the Kepinski research group plasmid and glycerol stock libraries**.**

2.2 DNA constructs and transformation of *Escherichia coli*

The vector pET28a (Novagen; product code: 69864-3) with the appropriate DNA insert was transformed into *Escherichia coli* strain Rosetta^{TM} DE3 competent cells (Novagen; product code: 70954). The transformation was by heat-shock as in the manufacturer's protocol (Page 7, User Protocol TB009 Rev. F 0104, Novagen). SOC medium at room temperature was added to the transformed competent cells and grown for 30 minutes (37˚C / 200 rpm) as recommended by the manufacturer.

2.3 Glycerol stocks of transformed competent cells

After the competent cells were transformed with the particular DNA construct the cells were plated on Luria-Bertani (LB) agar plates (LB media: peptone (10 g/L), yeast extract (5 g/L), NaCl (5 g/L) was adjusted to pH 7.0 with NaOH solutions and agar added to 15 g/L for solid media). All plates contained kanamycin selection (0.1 mg /mL).

A single colony was used to inoculate a new plate from which a single colony was used to inoculate 5 mL of liquid LB media with kanamycin selection. The cell culture was grown for approximately 16 hours (37 ˚C / 200 rpm) and then aliquoted. To each aliquot sterilized glycerol was added to form 25 % (w/v) of the final sample followed by snap freezing in liquid nitrogen and stored at -80 ˚C.

2.4 Growing cell cultures in enriched media and inducing protein expression

A starter culture of 5 mL LB medium with kanamycin (0.1 mg /mL) was inoculated with the required transformed cells from a glycerol stock. The inoculated starter culture was grown for approximately 16 hours (37 ˚C / 200 rpm) and then used to inoculate 500 mL of 2YT media (peptone (16 g/L), yeast extract (10 g/L), NaCl (5 g/L) was adjusted to pH 7.0 with NaOH solutions with kanamycin (0.1 mg /mL) in a 2 L conical flask. The cell culture was grown (37 ˚C / 200 rpm) to obtain an optical density of 0.5 to 0.8 measured with a spectrophotometer at wavelength 600 nm.

At this cell density range protein expression was induced with 0.5 mM isopropyl 1-thio-β-D-galactopyranoside (IPTG) and the cell culture grown for 16 hours (18 ˚C / 200 rpm). At the end of this incubation period a sample of the cell culture was collected to be run on an SDS-PAGE gel beside a sample of the un-induced culture, to confirm protein expression.

The remainder of the cell culture was then centrifuged (4000 x g / 30 minutes / 4 °C) to pellet the cells, with each pellet formed from 250 mL of cell culture. The supernatant was carefully decanted without re-suspending the pellet. The cell pellet was then stored at -80 °C to minimise any potential degradation of the expressed protein.

2.5 Protocol for SDS-PAGE gels

Protein samples were analysed on pre-cast SDS-PAGE gels (Invitrogen; NuPAGE 4-12 % Bis-Tris gel). The protocol was as recommended by the manufacturer. The samples were treated with DTT (100 mM) and heated (70 ˚C / 10 minutes) followed by electrophoresis (30 minutes / 200 V). The gel was then stained with SimplyBlue^{TM} safe stain (Invitrogen; product code: LC6060) following the manufacturer’s instructions.

2.6 Protein purification

2.6.1 Preparing stock solution of protease inhibitor

The following protease inhibitor cocktail tablets were used: cOmplete, Mini, EDTA-free protease inhibitor cocktail (Roche product code: 04693 15900); and cOmplete, mini protease inhibitor cocktail (Roche product code: 11836153001).

A stock solution was prepared by dissolving one tablet in 1 mL of filter sterilised (filter unit pore size: 0.2 µm) distilled H_2O, vortexed thoroughly. The stock solution was used as 2 % (v/v) of any sample buffer.

The EDTA-free protease inhibitor cocktail was used in the cell lysate before affinity protein purification on a HiTrap TALON crude 1 mL column (Product code: 29-0485-65) as recommended by the manufacturer GE Healthcare Life Sciences.

2.6.2 Cell lysis and protein extraction

To each cell pellet (pelleted from 250 mL cell culture) His-A buffer (sodium phosphate 20 mM pH 8.0, NaCl 500 mM, imidazole 10 mM) was added (30 mL), including EDTA-free cOmplete mini protease inhibitor cocktail (2 % v/v; Roche Molecular Biochemicals).This was then mixed thoroughly (vortex) until no clumps of cells could be observed. At this stage the re-suspended cells were kept on ice. Lysozyme and triton X-100 were added to final concentrations of 0.5 mg/ml and 0.2 % (v/v) for cell lysis. The mixture was incubated at room temperature (5 minutes), swirling gently. This was followed by the addition of $MgCl_2$ and DNAsel to 3 mM and 3.3 µg/ mL respectively. DNAsel stock solution was prepared in Tris.HCl 10 mM pH 7.9, NaCl 150 mM. The reaction was incubated at room temperature (5 minutes), swirling gently until the suspension became free-flowing again.

The cell lysate was sonicated (wavelength 10 microns / 9 mm probe / 3 x 10 seconds) to further ensure cell lysis. After each round of sonication the sample was mixed by being poured into another container and transferred back into a beaker for further sonication. During the sonication process the

sample was kept on wet-ice. A sample was collected at this stage for SDS-PAGE analysis, representing both soluble and insoluble proteins from the lysed cells.

The sonicated sample was centrifuged (7500 x g / 30 minutes / 4 °C) to pellet the cell debris and insoluble protein. The supernatant was carefully decanted into a clean container, without disturbing the pellet and stored on ice. To minimise degradation of the expressed protein EDTA-free cOmplete mini protease inhibitor (2 % v/v; Roche Molecular Biochemicals) was added to the sample. The pellet was also kept and re-suspended in approximately 30 mL of His-A buffer for further analysis on a SDS-PAGE gel.

2.6.3 Ni-NTA affinity chromatography for protein purification

The soluble extract was purified on a His-Trap 1 mL TALON Crude column (GE Healthcare Life Sciences) and the protein eluted on a gradient of increasing imidazole concentration. Chromatography buffers contained sodium phosphate 20 mM pH 8.0, NaCl 500 mM and either 10 mM or 500 mM imidazole for wash and elution buffers respectively, using ÄKTA Explorer (GE Healthcare Life Sciences). The elution was collected into 5 mL fractions. Fractions which corresponded to an increase in absorbance (mAU) at wavelength 280 nm were placed on ice and cOmplete mini protease inhibitor cocktail (2 % v/v; Roche Molecular Biochemicals) was added to the selected elution fractions. Samples of these fractions were analysed by SDS-PAGE to confirm the presence of protein and to observe the purity and integrity of the protein.

2.7 Protein expression and purification of the TIR1 receptor

2.7.1 Acknowledgments

TIR1 protein was expressed using a baculovirus vector system in insect cells (Invitrogen; *Trichoplusia ni* High-Five™ BTI-TN-5B1-4). All insect cell pellets used in this research were produced by Professor Richard Napier's laboratory at the University of Warwick.

2.7.2 TIR1 protein purification protocol

Two cell pellets (each from 100 mL of cell culture) were re-suspended in 2.25 mL of cytobuster protein extraction reagent (Novagen; product number: 71009) with one-tablet of EDTA-free cOmplete mini protease inhibitor cocktail (Roche Molecular Biochemicals). The cell suspension was incubated for 30 mins at 4 ˚C on a rotating mixer. The re-suspended cells were then diluted with His-A buffer (final volume 30 mL).The standard protocol was then followed for protein extraction as previously described (section 2.7.2) with the addition of $MgCl_2$ (to 3 mM) and DNAse1 (to 3.3 µg/ mL).

After centrifugation (7500 x g / 30 minutes / 4 ˚C) a blunt needle attached to a syringe was used to collect the soluble protein from the supernatant below a layer of lipids. This soluble fraction was filtered (filter unit: 0.2 µm; GE Healthcare Life Sciences Whatman; product code: 6896-2502) and passed through a HiTrap 1 mL TALON Crude column (GE Healthcare Life Sciences). At this stage the same protocol was followed as outlined in the histidine affinity chromatography for protein purification section (2.6.3).

The elution from histidine affinity chromatography was passed through a column of ANTI-FLAG® M2 affinity gel (Sigma-Aldrich, product code: A2220) (1 mL bed volume; gravity flow). This second affinity column was washed with a HEPES buffer (HEPES buffer pH 7.4 (10 mM); NaCl (150 mM); DTT (1 mM); IP_6 (1 mM)) for three column volumes.

The TIR1 protein was then eluted by competitive binding with FLAG® peptide (Sigma-Aldrich; product code: F4799-4MG) at 174.7 µM (0.5 mg / mL) dissolved in HEPES buffer. For this elution stage, the tap of the gravity controlled column was closed for 15 minutes with the elution buffer in the gel matrix. After this time period elution fractions were collected and cOmplete mini protease inhibitor cocktail (2 % v/v; Roche Molecular Biochemicals) was added to the purified TIR1 before storage at 4 ˚C.

2.8 Sample concentration and buffer exchange

All purified protein samples were concentrated by ultrafiltration using a Vivaspin2 ultrafiltration device with a hydrosart membrane, 2000 molecular weight cut off (Generon; product number: VS02H91). The manufacturer's protocol was followed to prepare the ultrafiltration device for the protein sample. This included an initial wash of the device with filter sterilised (filter unit pore size: 0.2 µm) distilled H_2O. The protein sample was loaded to the recommended maximum volume (2 mL for product number: VS02H91) and centrifuged (4000 x g / 30 minutes / 4 ˚C). The filtrate was removed and more of the protein sample loaded into the device and centrifuged again. This process was repeated until the entire protein sample was concentrated (< 0.5 mL).

The concentrated protein sample was then diluted to 2 mL in the desired buffer solution and the volume reduced again by ultrafiltration. This process was repeated three times for buffer exchange. This process resulted in a concentrated sample of the purified protein in the desired buffer for experimental analysis. The final concentration was measured using a Nanodrop spectrophotometer at wavelength 280 nm.

2.9 Surface plasmon resonance

2.9.1 Bio-sensor chip and Biacore 3000

Sensor chip SA (GE Healthcare Life Sciences; product code: BR100032). The surface of the chip consisted of carboxymethylated dextran covalently attached to a gold surface. The matrix is pre-immobilised with streptavidin. This enabled the immobilisation of biotinylated ligands to the SA chip surface. This sensor chip is compatible with the Biacore 3000 Processing unit (manufacture: GE Healthcare Life Sciences; product code: BR110045), which was used in all SPR experiments.

2.9.2 SPR running buffer

The buffer used in all SPR experiments within this research was HBS-EP Buffer (GE Healthcare Life Sciences; product code: BR100188). The buffer is obtained from the manufacturer degassed and ready to use. The buffer is composed of the following: 10 mM HEPES pH 7.4, 150 mM NaCl, 3 mM EDTA, 0.005 % (v/v) surfactant P20.

2.9.3 Peptide synthesis and immobilising biotinylated peptides to an SA sensor chip

All peptides used in this research were synthesised by Thermo Scientific to a high level of purity (> 80 %). For consistency all peptides studied were 17 amino acids in length with an N-terminal biotin-tag. The amino acid sequences of the peptides studied are shown in Table 2.1. Stock solutions of the peptides were prepared by dissolving the lyophilised powder in filter sterilised (filter unit pore size: 0.2 µm) distilled H_2O (1 mg / mL).

Table 2.1 Biotinylated degron peptides analysed by SPR. All peptides were synthesised by Thermo Scientific to a high level of purity (> 80 %). For consistency all peptides were designed to be 17 amino acids in length with an N-terminal biotin-tag and a C-terminal carboxyl group.

Peptide identification	N-terminal biotin-tag peptides
AXR3	**AKAQVVGWPPVRSYRKN**
AXR3-1	**AKAQVVGWPLVRSYRKN**
AXR3-3	**AKAQVVGWPPGRSYRKN**
IAA28	**EVAPVVGWPPVRSSRRN**
Transition-P	**AKAPVVGWPPVRSYRKN**
Transition-SS	**AKAPVVGWPPVRSSRKN**
Transition -RR	**AKAPVVGWPPVRSYRRN**
Transition-EVAP	**EVAPVVGWPPVRSYRKN**
Transition-SSRR	**AKAQVVGWPPVRSSRRN**

An SA sensor chip (GE Healthcare Life Sciences) was conditioned by injecting over a conditioning solution (NaOH 50 mM, NaCl 1.0 M) for one minute (flow-rate 40 µL / minute). Peptides were immobilised onto the SA chip by injecting a diluted sample of a peptide in HBS-EP buffer (10 µg / mL) onto a specific flow cell of the SA chip (flow rate: 5 µL / minute). Flow cell one was left blank and provided a control for non-specific binding and refractive index mismatches. Flow cells two, three, and four were immobilised separately with specific peptides. Each injection of the peptide was stopped after the addition of approximately 800 RUs (response difference) onto the sensor chip surface.

2.9.4 IAA stock solution for surface plasmon resonance

A 10 mM stock solution of indole-3-acetic acid (IAA) sodium salt (Sigma-Aldrich; product number: I5148-2G) was dissolved in 10 mL of the HBS-EP buffer and vortexed thoroughly. This was followed by sonication (60 seconds) and then filtered (0.2 µm pore size). The prepared stock solution was then stored at 4 ˚C.

2.9.5 Protocol for SPR assay

Each SPR experiment consisted of a 600 second period of only HBS-EP (GE Healthcare Life Sciences) running buffer (flow-rate: 25 µL / minute) passing over the SA chip surface to establish a base-line. This was followed by a 96 second injection of a sample of TIR1 protein (diluted 50 %) in HBS-EP buffer with 50 µM IAA. At the end of the injection a period of at least 600 seconds was allowed to observe the dissociation phase of the auxin receptor complex.

2.9.6 SPR assay, chemical compound screen for binding to the degron

The SPR assay was performed with the N-terminal biotin tagged peptides AXR3, AXR3-1 and AXR3-3 immobilised on to an SA sensor chip to a density of around 1000 RU. The peptide sequences are shown in Table 2.1.

All the chemical compounds tested were dissolved in the HBS-EP buffer (composition described in 2.9.2), to a final concentration of 500 µM. The chemical compounds were injected over the sensor chip for a minimum of 90 seconds. This was followed by a minimum dissociation phase of approximately 150 seconds.

2.9.7 Processing the SPR data

All SPR data was processed using BIAevaluation software 3.2 RC1 (GE Healthcare Life Sciences; product code: 29017513). The manufacturer's protocol (Pages 47 to 49; Evaluation of results; Biacore 3000 GxP Getting

Started Edition AB; GE Healthcare Life Sciences) was followed to operate the BIAevaluation software. The software enabled the averaging of the response difference before the injection to establish a base-line. This was important as the starting response values recorded vary between the flow cells of the sensor chip. This difference in starting values was corrected by selecting the data 60 seconds before the injection and averaging the selection (software option selected: “zero at average of selection”). In addition, the start of each injection period for the four flow cells can be selected in the software to align the curves for the different flow cells. The final stage in the processing of the data was to subtract the RU of the reference cell as a control for non-specific binding from the data of the remaining flow cells. The analysed data displays changes in RU over time.

2.9.8 Non-linear fitting of SPR data for the chimeric peptides

Non-linear fitting of the SPR response curves was performed using BIAevaluation software 3.2 RC1 (GE Healthcare Life Sciences; product code: 29017513). The binding model selected was 1:1 Langmuir binding. TIR1 was classified as the analyte, at approximately 4 µM. The TIR1 concentration used to estimate the rate constants for this assay was based on TIR1 concentration measurements using a Nanodrop spectrophotometer at wavelength 280 nm.

2.10 Nuclear magnetic resonance (NMR) spectroscopy

2.10.1 Isotope labelled AXR3 N-terminal (DI and DII) protein

2.10.1.1 Isotope labels

3 g / L of ^{13}C D-Glucose ($13C^{6}$, 99 %; Cambridge isotope laboratories; product code: LM-1396-5)

1 g / L of ^{15}N ammonium chloride (15N, 99 % Cambridge isotope laboratories; product code: NLM-467-10)

2.10.1.2 Preparing minimal media

The maximisation of isotope labelling of the expressed protein required the restriction of other sources of nitrogen and carbon sources within the growth media. This was achieved by preparing minimal media. M9 (-) salts (10 X) stock solution was first prepared (Na_2HPO_4 (35.9 mg / mL), KH_2PO_4 (30 mg / mL), NaCl (8.3 mg / mL). The M9 (-) salts stock solution was autoclaved before use. The M9 (-) salts (10 X) stock solution was diluted (to 1 X) in the minimal growth media (M9 (-) salts (10 X, 100 mL / L), ^{13}C D-Glucose (3 g / L), ^{15}N NH_4Cl (1 g /L), $MgSO_4$ (1 M, 2 mL / L), $CaCl_2$ (1 M, 100 µL), $FeCl_3$ (5 %, 800 µL / L), Minimal essential medium (MEM) vitamins Biochrom product number: K0373 (100 X, 10 mL / L).

The isotope labels of ^{15}N and ^{13}C were dissolved first in 5 mL of filter sterilised (filter unit pore size: 0.2 µm) distilled H_2O before addition to the media. The antibiotic kanamycin (0.1 mg / mL) was added as the selection reagent for the cells transformed with the plasmid for N-terminal AXR3 protein (DI and DII).

2.10.1.3 Expression of isotope labelled protein and purification

For the expression of isotopically labelled protein 5 mL LB medium with kanamycin (0.1 mg / mL) was inoculated with a glycerol cell stock. The inoculated media was grown for 8 hours (37 ˚C / 200 rpm) in a 50 mL tube. After the growth period a 100 µL sample of the initial cell culture was used to inoculate 12.5 mL of minimal media in a 100 mL conical flask and grown (37 ˚C / 200 rpm) for 16 hours.

The entire 12.5 mL of minimal media starter culture was used to inoculate 500 mL of minimal media in a 2 L conical flask and grown (37 ˚C / 200 rpm) until an optical density of 0.5 to 0.8 was obtained, as previously described. Expression was induced with the addition of 0.5 mM IPTG and the cell culture grown (18 ˚C / 200 rpm) for a further 12 hours. The cells were pelleted and stored as previously described (section 2.5).

Resuspension of the cell pellets and extraction of the isotope labelled N-terminal AXR3 (DI and DII) protein followed the protocol previously described (section 2.7.2). This isotope-labelled protein was purified by histidine affinity chromatography (as in section 2.7.3). A selection of elution fractions were concentrated by ultrafiltration, followed by buffer exchange (section 2.9).

2.10.2 NMR sample buffer

NMR sample buffer contained: sodium phosphate pH 6.0 (20 mM), NaCl (150 mM), EDTA (3 mM), DTT (10 mM), cOmplete mini protease inhibitor cocktail (2 % v/v; Roche Molecular Biochemicals). Before NMR analysis a final component of $^{2}H_2O$ (5 % to 10 % v/v depending on frequency of spectrometer) was added to the sample.

2.10.3 HSQC experiment

The parameters for the ^{1}H-^{15}N Heteronuclear single-quantum correlation (HSQC) experiment are described in Table 2.2.This experiment was used to analyse ^{15}N labelled N-terminal AXR3 protein (DI and DII).

Table 2.2. Parameters for heteronuclear single-quantum correlation (HSQC) experiment. HSQC experiments were performed at 17 ˚C, frequency of 600 MHz.

Experiment	Recycling delays (S)	Scans	Nuclei		Spectral width (Hz)		Number of complex data points	
			t1	t2	t1	t2	t1	t2
HSQC	1	4	^{15}N	^{1}H	1600.0	8620.7	1024	256

2.10.4 NMR backbone assignment of the AXR3 (DI and DII) carbon backbone

The ^{13}C, ^{15}N isotopically labelled AXR3 (DI and DII) protein was concentrated by ultrafiltration, followed by ultrafiltration in NMR buffer as previously stated in sections 2.9 and 2.10.2. A final concentration of 290 µM was used in the assignment experiments.

The following NMR experiments were used in the assignment of the backbone of AXR3 (DI and DII): HNCA, HNcoCA, HNcaCB, CBcacoNH, HNcaCO, HNCO. The parameters for the assignment experiments are described in Table 2.3. All the assignment experiments were performed at a frequency of 600 MHz at 17˚C using an Agilent DDX3 NMR spectrometer with a RT HCN triple resonance probe. The assignment data was analysed with minimal automation in the software CcpNmr Analysis.

Table 2.3 Parameters for assignment experiments in the analysis of ^{13}C and ^{15}N isotopically labelled AXR3 (DI and DII) protein. All experiments were performed with the following parameters: 17˚C, frequency of 600 MHz, recycling delays of 1 second, 4 scans.

Experiment	Nuclei			Spectral width (Hz)			Number of complex data points		
	t1	t2	t3	t1	t2	t3	t1	t2	t3
HNCA	^{15}N	^{13}C	^{1}H	4525.3	1600.0	6613.8	1024	2048	64
HNcoCA	^{15}N	^{13}C	^{1}H	6613.8	4525.3	1600.0	1024	32	64
HNCACB	^{15}N	^{13}C	^{1}H	10558.9	1600.0	6613.8	1024	2048	64
CBCAcoNH	^{15}N	^{13}C	^{1}H	12067.3	1600.0	6613.8	1024	2048	64
HNcaCO	^{15}N	^{13}C	^{1}H	1600.0	1600.0	6613.8	1024	2048	64
HNCO	^{15}N	^{13}C	^{1}H	1600.0	2500.0	9615.4	1024	2048	64

2.10.5 Sequential NMR backbone assignment through the prolines in the AXR3 (DI and DII)

A set of 2D ^{13}CO detected NMR experiments CON, hCAnCO, and hCACO were used in the assignment of prolines in the carbon backbone of AXR3 (DI and DII). The parameters for the NMR experiments are described in Table 2.4. The experiments were performed at a frequency of 950 MHz at 17˚C using a TCI cryoprobe with a cooled amplifier on carbon.

Table 2.4 Parameters for proline assignment experiments in the analysis of ^{13}C, ^{15}N isotopically labelled AXR3 (DI and DII) protein. All experiments were performed with the following parameters: 17˚C, frequency of 950 MHz, recycling delays of 1.5 seconds and acquisition time of 71.3 ms.

Experiment	Scans	Nuclei		Spectral width (Hz)		Number of complex data points	
		t1	t2	t1	t2	t1	t2
CON	8	^{13}C	^{15}N	7183.9	3851.5	512	160
hCACO	8	^{13}C	^{13}C	7183.9	7168.5	512	64
hCAnCO	16	^{13}C	^{13}C	7183.9	7168.5	512	180

2.10.6 ^{15}N R_2 relaxation of AXR3 (DI and DII)

A ^{15}N R_2 relaxation experiment was performed at 17˚C at a frequency of 950 MHz following the parameters in Table 2.5. 10 values of the R2 relaxation delay (S) were used, including two repeat values and recorded in a random order of 0.06, 0.39, 0.84, 0.26, 0.64, 0.13, 0.52, 0.26, 1.03, 0.64. The ^{15}N R_2 relaxation parameter used in this study are shown in Table 2.5. The protein sample was prepared as described in section sections 2.9 and 2.10.2.

Table 2.5 ^{15}N R_2 relaxation experiment of AXR3 (DI and DII) protein. All experiments were performed with the following parameters: 17˚C, frequency of 950 MHz.

Experiment	Recycling delay (S)	R_2 Recycling delay (S)	Scans	Nuclei		Spectral width (Hz)		Number of complex data points	
				t1	t2	t1	t2	t1	t2
R_2 relaxation	2.8	0.01612 x L*	4	^{15}N	^{1}H	15243.9	2599.7	200	1024

* where L value was changed after each run in the following sequence:4, 24, 52, 16, 40, 8, 32,16, 64, 40. Giving relaxation delay values of 0.06, 0.39, 0.84, 0.26, 0.64, 0.13, 0.52, 0.26, 1.03, 0.64.

2.10.7 Estimating the occupancy of the *cis* and *trans* isomer population with the NMR data

The height and volume of NMR signals assigned to Trp 86 were determined from the assignment peak list for the ^{1}H-^{15}N HSQC spectrum within the software CcpNmr Analysis. The values were automatically calculated within the software when the peak picking option was activated. The height of the NMR signals was measured by a parabolic method and the NMR peak volumes measured by a box-method.

2.10.8 NMR analysis of the auxin receptor complex

^{15}N isotopically-labelled AXR3 (DI and DII) protein was expressed and purified following the protocol in section 2.10.1.3. TIR1 protein was purified as described in section 2.7. All protein samples were concentrated by ultrafiltration, followed by buffer exchange as in section 2.8. The same NMR sample buffer was consistently used in the NMR experiments as described in section 2.10.2.

A sample of AXR3 (DI and DII) protein and TIR1 protein was prepared in a 1:1 ratio (7 µM) with 10 % D_2O and measured using a ^{1}H-^{15}N HSQC experiment following the parameters described in Table 2.2. The temperature was set to 4˚C to maintain the stability of the TIR1 protein. The full auxin receptor complex was studied by the titration of 50 µM IAA into the sample.

2.10.9 NMR analysis of the IAA binding to AXR3 (DI and DII)

A sample of ^{15}N isotopically labelled AXR3 (DI and DII) protein was prepared as described in sections 2.8 and 2.10.2 to a final concentration of 50 µM. This sample was used as a reference and HSQC spectra were measured using the parameters outlined in Table 2.2. This was followed by the addition of IAA (2000 µM; in NMR buffer, composition given in section 2.11.2) to give a ratio 1:40 (AXR3:IAA) and repeating the experiemnt.

2.10.10 NMR analysis by WaterLOGSY (Water-Ligand Observed via Gradient Spectroscop Y)

Un-labelled AXR3 (DI to DIV) protein was expressed and purified as described in sections 2.4 to 2.8. The protein sample was prepared for NMR analysis by buffer exchange into the NMR sample buffer (2.8 and 2.10.2). A series of AXR3 (DI toDIV) : IAA ratios were prepared, from 1:40, to the highest ratio of 1:200; each sample contained 10 % D_2O and 15 µM AXR3 DI to DIV). Reference samples in the absence of AXR3 (DI to DIV) were prepared for each IAA concentration tested. These samples were measured by the NMR method WaterLOGSY using the parameter described in Table 2.6.

Four of the proton peaks associated with the aromatic rings found in IAA were selected within the WaterLOGSY spectrum and the integrals calculated for each selected peak. This was repeated for all the samples to calculate the difference in signal intensities for each ratio of protein to ligand.

Table 2.6 Parameters for the NMR experiment WaterLOGSY used in the study of IAA binding with AXR3 (DI to DIV). WaterLOGSY experiments were performed at 17˚C, at a frequency of 500 MHz. The experiments were performed using a 15 ms Gaussian inversion pulse for water inversion, a 1 s mixing time, excitation sculpting for readout and water suppression and a 2.5 second relaxation delay

Experiment	Recycling delays (S)	Scans	Nuclei	Spectral width (Hz)	Number of complex data points
			t1	t1	t1
WaterLOGSY	2.5	1024	^{1}H	8000	13108

2.11 Isothermal titration calorimetry (ITC)

The expression and purification of AXR3 (DI and DII) was as described in the general methods chapter 2 (sections 2.5 to 2.7). The protein sample was concentrated by ultrafiltration (section 2.9) followed by buffer exchange into the following buffer: 20 mM sodium phosphate pH 6.0, 150 mM NaCl, 3 mM EDTA, 1 mM Tris(2-carboxyethyl)phosphine hydrochloride solution (TCEP).

The isothermal titration calorimetry (ITC) was performed using a MicroCal iTC200 system. AXR3 (DI and DII) was vacuum treated (2 minutes) and transferred using a syringe into the MicroCal sample cell. Any air bubbles were removed from the sample cell by slowly moving the plunger of the syringe up and down. In each case IAA was dissolved in the ITC buffer to a final concentration of 4 mM and was loaded into the automated pipette using the software supplied.

The following parameters were selected for the ITC experiment: total number of injections 20, cell temperature 25 ˚C, reference power 5 (µCal / second), initial delay 60 seconds, feedback mode high, filter period 2 seconds. IAA was injected into the sample cell with an initial 0.5 µL injection

of the length 1 second, followed by a 4 second long 2 µL injection repeated 19 times; the injections were each separated by a delay of 120 seconds.

2.12 Computational modelling

2.12.1 Analysing the crystal structure 2P1Q of the auxin receptor complex

The crystal structure 2P1Q by Tan *et al*., 2007 was imported from the Protein Data Bank (RCSB PDB) into the modelling software Maestro, version 9.0, Schrodinger suite and analysed following the manufacturer's protocol (Pages 35 to 42; Maestro 9.0 User Manual).

The imported molecular structure was optimised for residue orientation by selecting the option, refine-protein-ligand-complex within the tasks menu-bar of the wizard-based interface. In this section, the IAA molecule was selected as the ligand and the refinement radius specified from this molecule. Only residues within the refinement radius were optimised by the software. The structure was refined three times with an increasing radius from the IAA molecule of 10 Å, 12 Å, and 14 Å respectively. The energy minimised structure was further analysed by changing the display of the structure to show the molecular surface of the TIR1 molecule, not including the IAA and IP_6 molecules (Pages 93 to 116; Maestro 9.0 User Manual).

2.12.2 Modelling chimeric peptides by modifying the AXR2 crystal structure from 2P1Q

Residues within the AXR2 peptide were replaced by selecting the mutate residue option within Maestro Schrodinger suite (Pages 81 to 83, Maestro 9.0 User Manual). The residues replaced in the AXR2 structure are shown in Table 2.7. The minimise option within the Task menu-bar was performed for each of the replaced residues and then for the remainder of the peptide. This was followed by energy minimisation of the peptide and auxin binding pocket by selection of the option refine-protein-ligand-complex as previously described (2.12.1).

Table 2.7 Peptides analysed using Maestro Schrodinger suite. All peptides modelled were based on the AXR2 peptide from the structure 2P1Q (Tan *et al*., 2007). Residue changes from the AXR2 peptide are shown in red.

Peptide identification	Modelled peptides
AXR2	**QVVGWPPVRNYRK**
AXR2-1	**QVVGWSPVRNYRK**
SHY2-2	**QIVGWSPVRSYRK**
AXR3	**QVVGWPPVRSYRK**
AXR3-1	**QVVGWPLVRSYRK**
AXR3-3	**QVVGWPPGRSYRK**
IAA28	**PVVGWPPVRSSRR**
Transition-P	**PVVGWPPVRSYRK**
Transition-SS	**PVVGWPPVRSSRK**
Transition -RR	**PVVGWPPVRSYRR**
Transition-SSRR	**QVVGWPPVRSSRR**

Chapter 3

Structural characterisation of the N-terminal half of AXR3 protein domains I and II by NMR spectroscopy

3.1 Introduction

3.1.1 Current structural elements of Aux/IAA proteins

To date there has been no structural information of a full-length Aux/IAA protein. Although the C-terminal half of an Aux/IAA is well characterised more limited structural information is known for the N-terminal half of an Aux/IAA protein, where the only data is from crystallography of peptides. Structural characterization of this N-terminal region is important for developing our understanding of how the auxin receptor complex forms.

Here, a selection of the key structural data showing elements of Aux/IAA proteins is reviewed. These transcriptional repressors of auxin regulated genes typically contain four conserved sequence motifs, which are referred to in the literature as functional domains I to IV (Abel *et al*., 1994; Abel *et al*., 1995; Reed, 2001).

3.1.1.1 NMR structure of C-terminal AXR3 DIII and DIV

The most complete structures of Aux/IAA proteins are of the C-terminal half and include DIII and DIV (Han *et al*., 2014; Dinesh *et al*., 2015). Secondary structure analysis of a range of DIII and DIV Aux/IAA and ARF sequences suggested similar structural homology of a β-clasp fold (Guilfoyle and Hagen, 2012). This was confirmed by recent NMR analysis of the C-terminal half of the Aux/IAA protein AXR3 and the transcription factor ARF5 (Han *et al*., 2014). Analysis shows positive and negative charges on opposite sides of the DIII and DIV structures which allows for electrostatic interaction and dimerisation between Aux/IAAs and ARFs (Han *et al*., 2014) (Figure 3.1).

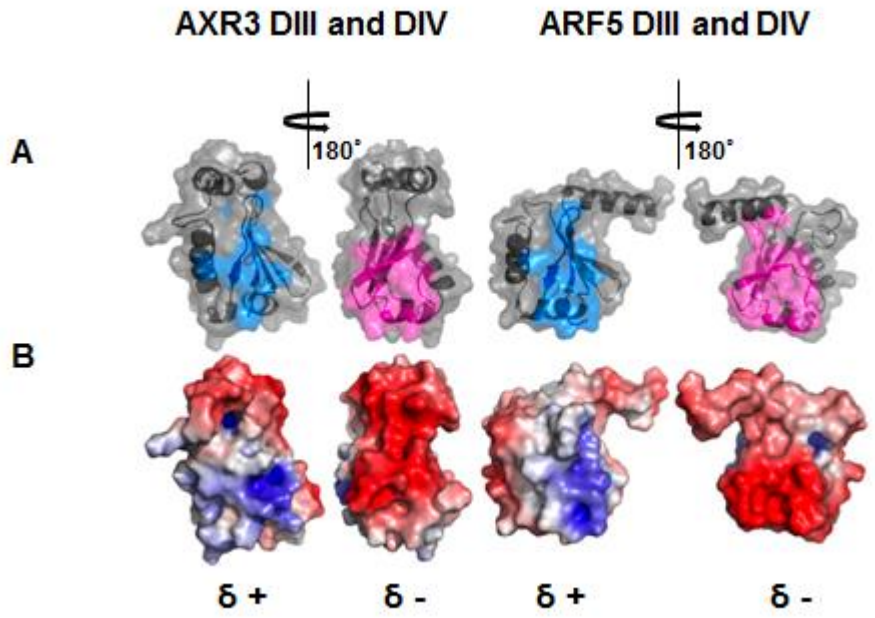

Figure 3.1 NMR structures of domains III and IV for AXR3 and ARF5 adapted from Han *et al*., 2014. The molecular structures are presented in two views which are rotated 180˚. (A) DIII and DIV for AXR3 and ARF5 are presented with secondary structure showing through the molecular surface. Blue indicates positively charged surfaces and Red negatively charged regions. (B) Electrostatic potentials mapped onto the molecular surfaces of the DIII and DIV structures.

3.1.1.2 The limited structural data of the N-terminal half of an Aux/IAA

More limited structural information is known for the N-terminal half of an Aux/IAA protein, where the only structural data is of peptides representing the conserved residues of DI, and DII. DI mediates transcriptional repression by forming a binding site for the co-repressor TPL. The primary interface for this interaction is a conserved sequence motif of three leucine residues of LXLXL within domain I, at residue positions 14 to 18 in AXR3 (Abel *et al*., 1994). A weak redundancy for this interaction is provided by a second LXLXL motif located between DI and DII at residue positions 40 to 44 in AXR3 (Lee *et al*., 2016). These leucine sites represent a sub-class of repressor elements common to many transcriptional repressor systems in plants, known as the ethylene response factor-associated amphilic

repression (EAR) motifs (Tiwari *et al*., 2004; Szemenyei *et al*., 2008; Causier *et al*., 2012; Wang and Estelle, 2014).

A recent crystallography study has captured the interaction between a TPL domain (TPD) and peptides of the EAR motif from the Aux/IAA proteins IAA1 and IAA10 (Ke *et al*., 2015) (Figure 3.2). The formation of this complex is assumed to recruit histone deacetylases, resulting in the condensation of chromatin and transcriptional repression of auxin regulated genes (Kagale and Rozwadowski, 2011; Strader and Zhao, 2016).

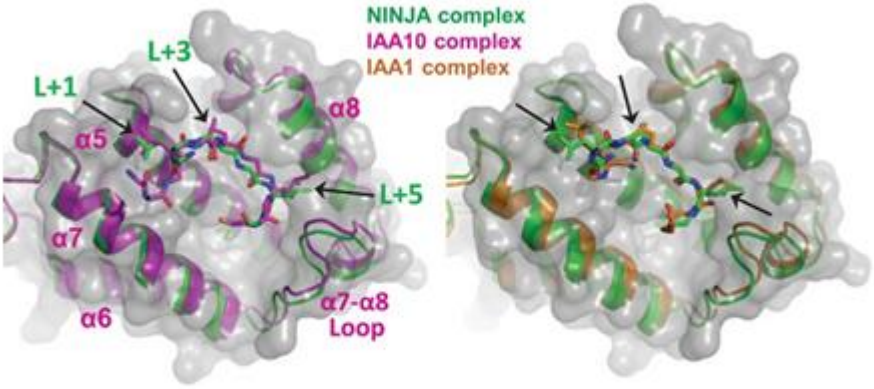

Figure 3.2 Crystal structures of the TOPLESS domain protein (OsTPR2) with three different EAR motif peptides adapted from Ke *et al*., 2015. The secondary structure of the TOPLESS domain protein (TDP) is shown through the molecular surface (grey). The secondary structure is colour coded according to the bound EAR motif peptide. Three EAR peptides are presented and include the sequence motifs from the Aux/IAA's IAA1 (orange), IAA10 (Purple), compared to the protein NINJA (green) which is a transcriptional repressor in jasmonate signalling. The crystal structure showed TDP is composed of nine α-helices with connecting loops and forms a physiological relevant tetramer. The helices within this oligomer form crevices which provide a positively charged and hydrophobic interface for EAR peptide binding, with each monomer of the TDP complex associated with one EAR peptide.

Early analysis of the Aux/IAA protein sequences showed that the N-terminal half of the protein contained two conserved regions, the first forming DI and the second DII represented by a consensus sequence of 13 amino acids. This second region consisted of a highly conserved core motif of VGWPP,

flanked by less well conserved regions rich in lysine and arginine residues and was termed DII (Abel *et al*., 1994; Ramos *et al*., 2001).

The motif GWPPV of DII has a critical role in the ubiquitin-mediated degradation of the Aux/IAA protein and is consequently termed the degron (Kepinski and Leyser, 2005; Dharmasiri *et al*., 2005). This region forms the main interface with the substrate receptor of the SCF-type E3 ubiquitin ligase complex as reveled by crystallography (Tan *et al*., 2007) (Figure 3.3).

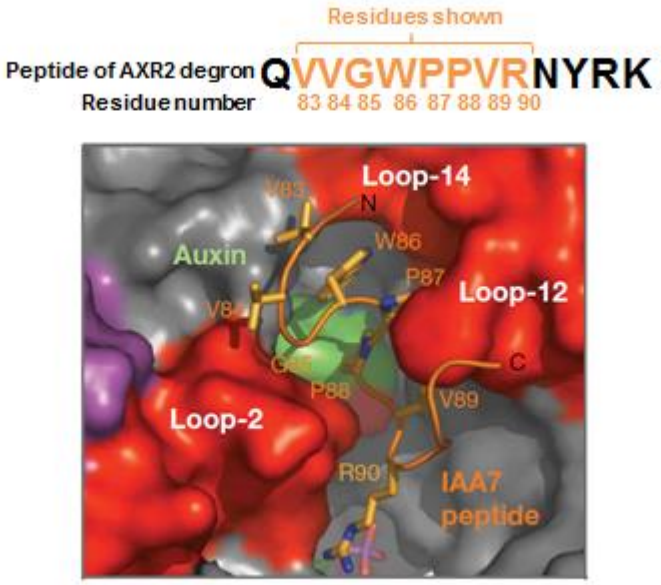

Figure 3.3 Crystal structure of a peptide of the AXR2 degron forming the auxin receptor complex, adapted from Tan *et al*., 2007. The full peptide sequence from the published crystal structure is shown at the top of the figure. Only a section of the degron is displayed in the molecular model and these residues are highlighted orange in the peptide sequence. The AXR2 degron peptide is observed above the auxin molecule IAA in a binding pocket of the receptor TIR1. Regions of the TIR1 surface are highlighted red to indicate the loop forming leucine reach repeats considered important for ligand binding.

Despite the importance of the degron, the structure of the surrounding region has not been reported. This limited structural knowledge has been commented on in a recent review (Weijers and Wagner, 2016). Characterizing the structure of the N-terminal half of an Aux/IAA protein will develop our knowledge on how this protein interacts with its binding partners to form the auxin receptor complex.

3.1.2 The potential for intrinsic disorder in the N-terminal half of an Aux/IAA protein

Currently auxin signalling has not been associated with intrinsic disorder, but it forms a central question when considering the structure of the N-terminal half of an Aux/IAA protein. A typical indicator of an intrinsically disordered region (IDR) is the enrichment of prolines, which contribute rigidity to the backbone of an intrinsically disordered protein (IDP) and disfavor the formation of secondary structure, due to lack of an NH group for hydrogen bonding (Theillet *et al*., 2013). Early analysis of the Aux/IAA amino acid sequences highlighted an enriched region of prolines separating the conserved functional domains I and II (Abel *et al*., 1994). This amino acid composition is a indicator of a possible disordered loop dominating the center of the N-terminal Aux/IAA protein.

This potential for intrinsic disorder in an Aux/IAA has previously been discussed to act as filler-loops between the domains, allowing conformational freedom for each of the four domains to adopt their required structure (Reed, 2001). This hypothesis is consistent with the idea that IDRs disfavor protein-protein interactions, with many IDPs remaining disordered upon binding (Hazy and Tompa, 2009; Gruet *et al*., 2016).

It is in these regions of conformational flexibility that recognition elements often form the primary interface with a binding partner, typically associated with pre-defined structural elements or regions primed to fold when in contact with a binding partner (Fuxreiter *et al*., 2004; Mészáros *et al*., 2007).

Here we have used nuclear magnetic resonance spectroscopy (NMR) to characterize the structure of the N-terminal half of the Aux/IAA protein AXR3 (DI and DII). This structural analysis evaluates the possibility of intrinsic disorder and the recognition sites within the protein, with particular interest in the region surrounding degron.

3.2 Results

3.2.1 Expression and purification of AXR3 protein

The AXR3 protein has been studied in this thesis as a full-length protein with all four functional domains and as a truncated protein. This truncated version consisted of only the N-terminal half with the functional domains I and II. The amino acid sequences of the AXR3 proteins studied are shown (Figure 3.4).These proteins were expressed using a Novagen pet28a vector in *Escherichia coli* strain Rosetta™ DE3 competent cells with kanamycin as the selection reagent. The pet28a vector encodes an N-terminal six histidine-tag for affinity chromatography of the expressed protein.

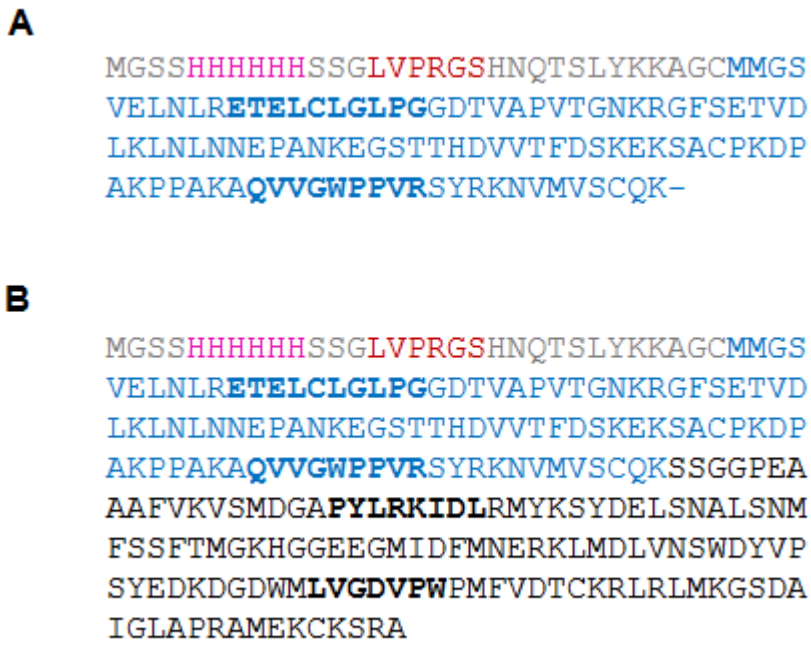

Figure 3.4 Amino acid sequences of the proteins expressed: AXR3 N-terminal half (domains I and II) and full-length protein (domains I to IV). (A) Amino acid sequence for the C-terminal truncated protein. The sequence highlighted in blue represents the sequence of AXR3 N-terminus (domains I and II). The consensus sequences for the domains are shown in bold (domain I: ETELCLGLPG; domain II: GWPPVRSY). Pink represents the six histidine tag; dark red represents a thrombin cleavage site; grey indicates the rest of the N-terminal sequence which surrounds the histidine tag and thrombin cleavage site and is not encoded in the AXR3 gene.

(B) Amino acid sequence for AXR3 full-length protein showing the histidine-tag thrombin and cleavage site. The N-terminal half remains highlighted in blue with the sequence of the C-terminal half shown in black including domains III and IV. The consensus sequences are shown in bold (domain III: PYLRKIDL; domain IV: LVGDVPW).

3.2.1.1 Secondary structure prediction for AXR3 (DI and DII)

My research focused on the N-terminal half of the AXR3 protein (DI and II) for structural characterisation by NMR spectroscopy. The amino acid sequence for AXR3 (DI and DII) was analysed using the secondary structure prediction server JPred4 (Drozdetskiy *et al*., 2015). This analysis predicted secondary structure in the regions of the functional domains I and II, where the separate predictions for helical and β-secondary structure overlapped (Figure 3.5). The JPred4 analysis also indicated a large region relative to the rest of the protein of intrinsic disorder. This disorder was predicted between DI and II, interspersed with small areas of predicted β-secondary structure. These smaller regions of predicted secondary structure are in close proximity to the KR motif, which is predicted to form a bi-partite nuclear localisation signal.

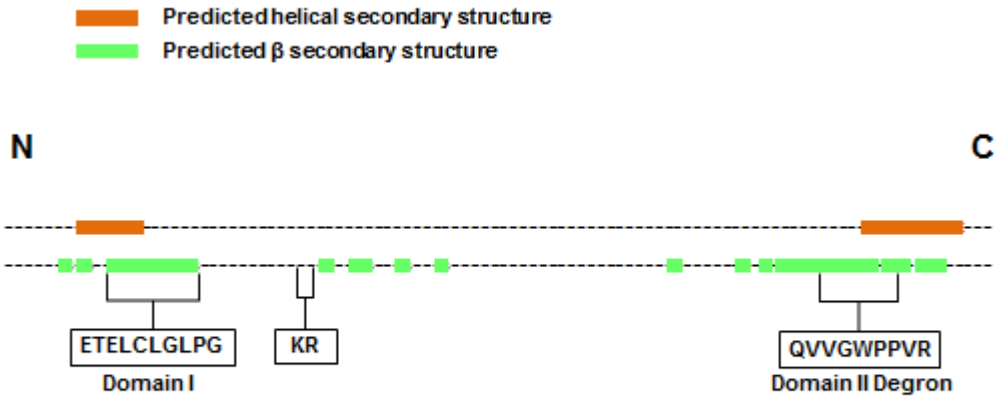

Figure 3.5 Secondary structure prediction of AXR3 (DI and DII). The amino acid sequence for AXR3 (DI and DII) was analysed by the secondary structure prediction server JPred4 (Drozdetskiy *et al*., 2015). The amino acid sequence for AXR3 (DI and DII) is represented by the dashed line with N- and C-terminals indicated. Regions of helical structure and β-secondary structure were predicted and are indicated by the coloured segments, orange and green respectively on two separate diagrams of the AXR3 (DI and DII) sequence. Regions of the N- and C-terminus are predicted to form helical and β-secondary structure, with predictions overlapping in these regions. These more extensive regions of predicted secondary structure co-inside with the functional domains I and II and are annotated with the consensus sequences shown. Smaller regions of β-secondary structure are also predicted within an intrinsically disordered region between DI and DII. The KR motif which is known to influence auxin receptor complex formation is located in close proximity to a predicted region of β-secondary structure.

3.2.1.2 Purification of ^{13}C and ^{15}N isotopically labelled AXR3 (DI and DII) protein for NMR spectroscopy

The isotopically labelled AXR3 (DI and DII) protein was purified by histidine affinity chromatography for NMR spectroscopy (Figure 3.6A). SDS-PAGE analysis shows the progression through the purification process of the AXR3 (DI and DII) protein, resulting in the observation of a single protein band (Figure 3.6B). The position of AXR3 (DI and DII) protein on the SDS-PAGE gel was above the predicted molecular weight of 14.4 KDa. This slower migration of the protein is consistent with the predicted intrinsic disorder for AXR3 (DI and DII). The higher net-charge and low hydrophobicity compared to a more ordered protein makes the AXR3 (DI and DII) structure resistant to the heat treatment used in SDS-PAGE analysis (Hazy and Tompa, 2009).

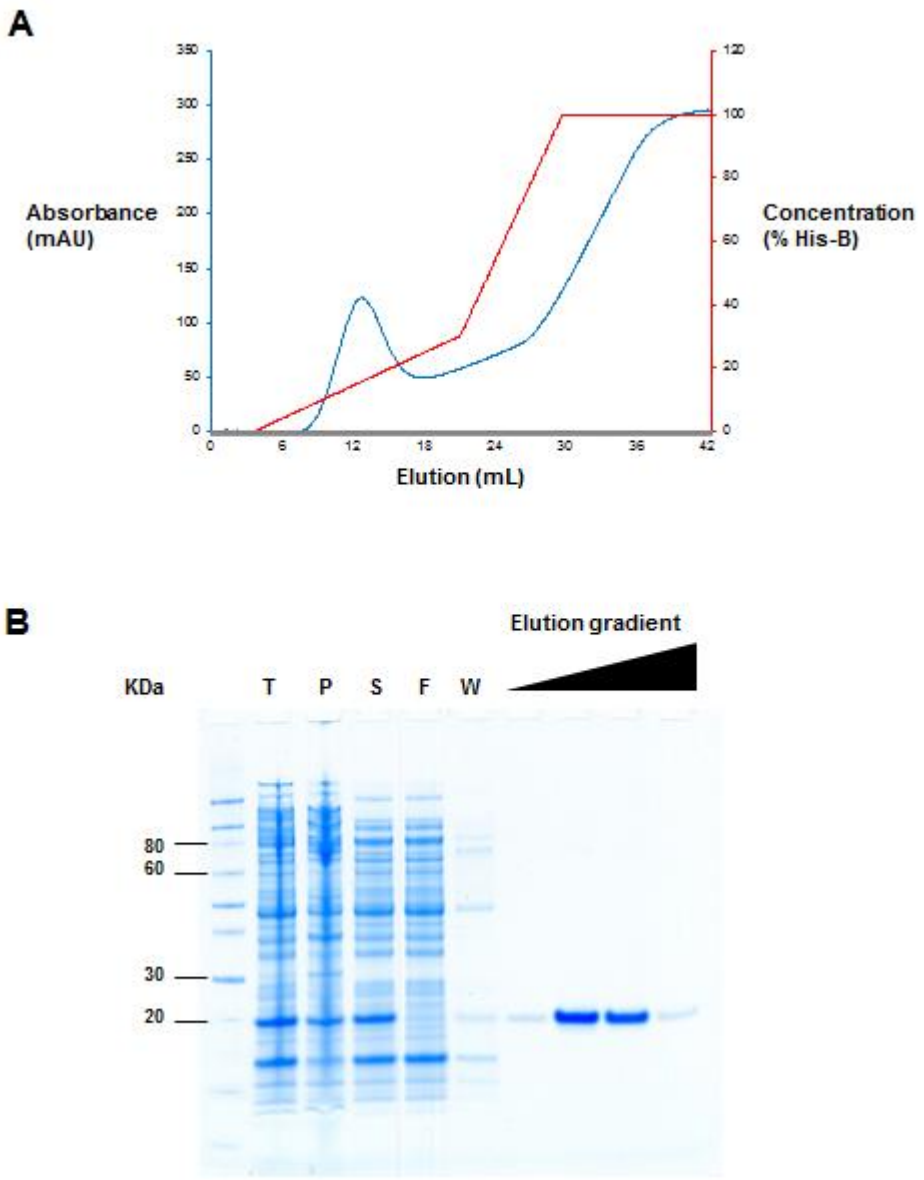

Figure 3.6 Purification of AXR3 N-terminal (DI and DII) protein double labelled (^{15}N, ^{13}C) for NMR analysis. (A) Chromatogram showing the Histidine affinity purification. The blue line represents the absorbance at wave-length 280 (mAU). The red line shows the concentration of the elution buffer (His-B). (B) SDS-PAGE gel of samples collected during the purification of the double labelled IAA17 C-terminal truncated protein. The letter T represents the total protein sample of the re-suspended and lysed cell pellet before purification. P represents the pelleted material after cell lysis. S represents the soluble protein fraction. F represents the Flow-through from the HiTrap crude TALON column. W represents the wash fraction from the column. This followed by the samples collected during the elution of protein from the column by an increasing concentration of imidazole.

3.2.2 NMR backbone resonance assignment of AXR3 (DI and DII)

The assignment of AXR3 (DI and DII) required data from a combination of experiments where magnetisation is transferred through the protein backbone to detect correlated ^{1}H, ^{15}N, $^{13}C_{\alpha,}$ $^{13}C_{\beta}$, and $^{13}C'$ signals. These are associated with two different residue positions, the C_i and C_{i-1} which represents the current and previous residue along the protein backbone respectively relative to the ^{1}H-^{15}N amide signals being detected (Figure 3.7).

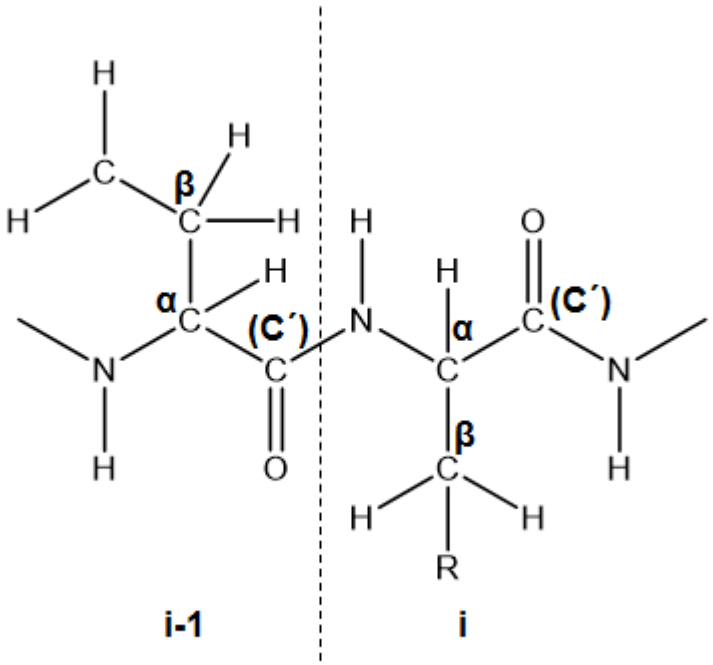

Figure 3.7 C_i and C_{i-1} showing the C_{α}, C_{β}, and C' positions. Representation of the carbon backbone of a protein, where i-1 is the previous residue along the chain. The C_{α} refers to the carbon atom within the same or previous residue as the NH group; the next carbon along the side chain is the C_{β}; and the C' indicates the carbon in the carboxyl group.

The assignment experiments included the following: HNCA, HNcoCA, HNcaCB, CBCAcoNH, HNcaCO, and HNCO. Together these experiments allowed the assignment of the majority of residues in the carbon backbone for the protein AXR3 (DI and DII). Here the assignment process is demonstrated with the degron residues Val 84 to Trp 86.

The first combination of assignment data presented are from the spectra of HNCA and HNcoCA (Figure 3.8). The HNCA experiment detects nuclei from the $^{13}C_{\alpha\, i}$ and $^{13}C_{\alpha\, i-1}$ positions along the carbon backbone. This was achieved due to the simultaneous evolution of the chemical shifts for both positions.

The $^{13}C_{\alpha\, i}$ and $^{13}C_{\alpha\, i-1}$ signals from HNCA are distinguished by comparison with the HNcoCA spectrum which shows only the $^{13}C_{\alpha\, i-1}$ signal. This enables a connection to be established between adjacent residues through equal ^{13}C chemical shift values of the $^{13}C_{\alpha\, i}$ and $^{13}C_{\alpha\, i-1}$ signals, a process repeated for each residue along the carbon backbone.

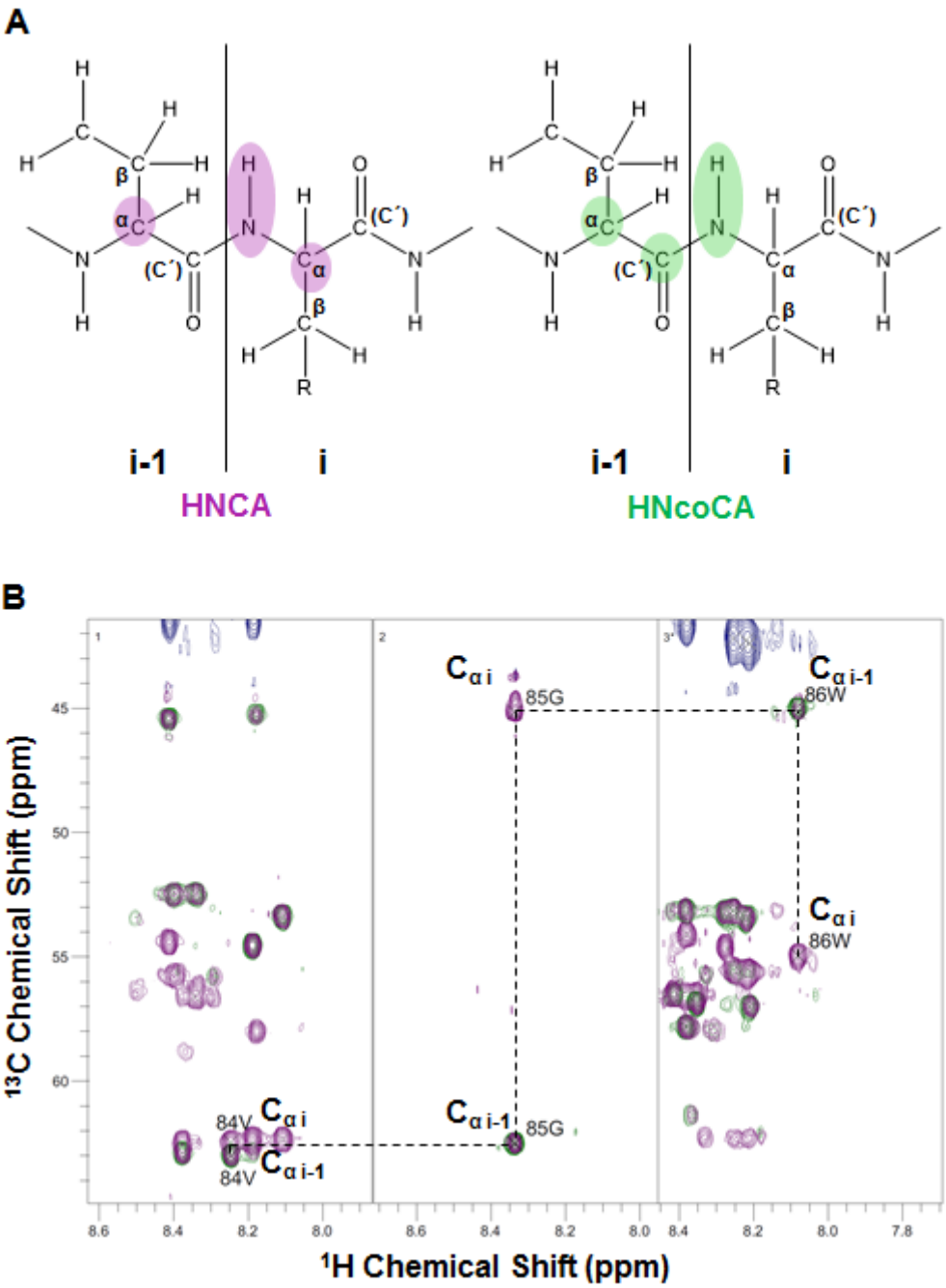

Figure 3.8 Assignment of the carbon backbone of AXR3 (DI and DII) using HNCA and HNcoCA spectra. (A) Representation of the carbon backbone of a protein is shown at the top of the figure. The magnetisation transfer in the HNCA and HNcoCA are shown with the nuclei involved highlighted-purple and green respectively. (B) Assignment of the degron residues Val 84 to Trp 86 are shown using the overlaid spectra of HNCA (purple) and HNcoCA (green). The spectra are split into three sections to observe each of these residues. HNCA shows the $^{13}C_{\alpha\, i}$ and $^{13}C_{\alpha\, i-1}$ signals. This is compared with the HNcoCA spectrum which shows only the $^{13}C_{\alpha\, i-1}$ signal. Connections between the $^{13}C_{\alpha\, i-1}$ and $^{13}C_{\alpha\, i}$ signals are indicated by the dashed line.

The connections established between the $^{13}C_{\alpha\, i}$ and $^{13}C_{\alpha\, i-1}$ signals from the HNCA and HNcoCA spectra were confirmed by the analysis of the $^{13}C_{\beta}$ signals. The HNCACB detects the $C_{\alpha\, i}$ and $C_{\beta\, i}$ nuclei of an amino acid and the $^{13}C_{\alpha\, i-1}$ and $^{13}C_{\beta\, i-1}$ of the previous residue along the carbon backbone (Figure 3.9A). The two sets of signals associated with the HNCACB spectrum can be distinguished by overlaying the CBCAcoNH, which only detects the $^{13}C_{\alpha\, i-1}$ and $^{13}C_{\beta\, i-1}$ signals of the previous residue along the carbon backbone.

The data presented here shows the connection between the $^{13}C_{\beta\, i}$ and $^{13}C_{\beta\, i-1}$ of Val 84 and Gly 85 (Figure 3.9B). Further along the carbon backbone no connection is detected between Gly 85 and Trp 86, as glycine does not contain a C_{β} atom and consequently no $^{13}C_{\beta\, i}$ signal. Instead, the connection between Gly 85 and Trp 86 is confirmed through the C' signals, detected through the HNcaCO and HNCO experiments (Figure 3.10).

HNcaCO detects the $^{13}C'_{i}$ and $^{13}C'_{i-1}$ signals (Figure 3.10A). These are distinguished by the HNCO experiment which detects only the $^{13}C'_{i-1}$ signals. Overlaying the spectra from these two experiments enabled connections to be made between C'_{i} and C'_{i-1} positions. This is demonstrated with the degron residues Val 84 to Trp 86 and confirms the connections observed in the previous spectra (Figure 3.10B). It was by this process that the majority of the carbon backbone of AXR3 (DI and DII) was assigned.

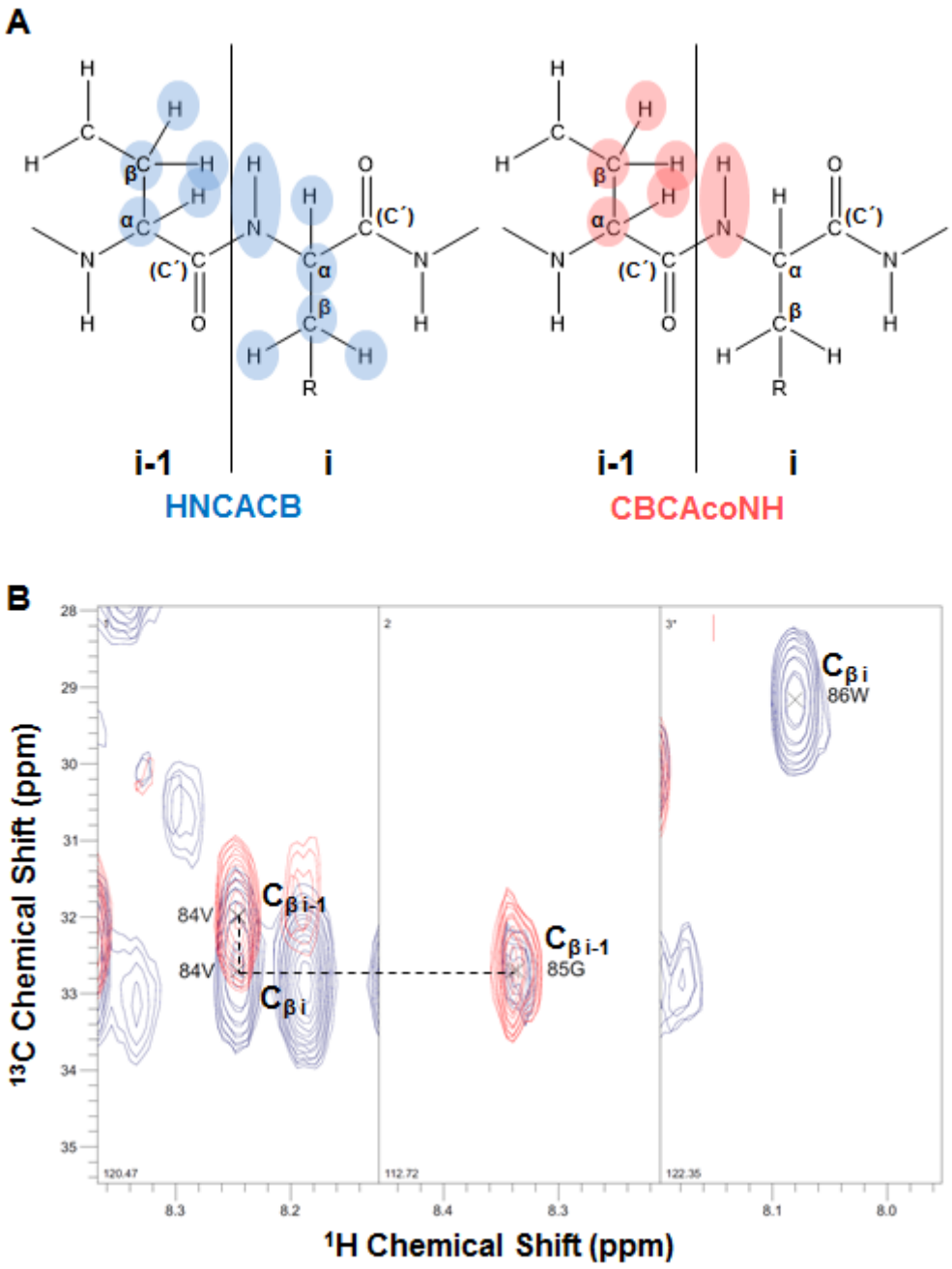

Figure 3.9 Assignment of the carbon backbone of AXR3 (DI and DII) using HNCACB and CBCAcoNH spectra. (A) Representation of the carbon backbone of a protein is shown at the top of the figure. The magnetisation transfer in the HNCACB and CBCAcoNH are shown with the nuclei involved highlighted blue and red respectively. (B) The overlaid spectra from HNCACB (blue) and CBCAcoNH (red) are presented for the degron residues Val 84 to Trp 86. The HNCACB spectrum shows the $^{13}C_{\beta\ i}$ and $^{13}C_{\beta\ i-1}$ signals for each residue. The HNCACB spectrum is shown overlaid by the CBCAcoNH spectrum showing only the $^{13}C_{\beta\ i-1}$ of the previous residue along the carbon backbone. The connections between the residues are indicated by the dashed line. The connection stops between the Gly

85 and Trp 86 in HNCACB and CBCAcoNH spectra, as glycine does not have a C_β carbon atom.

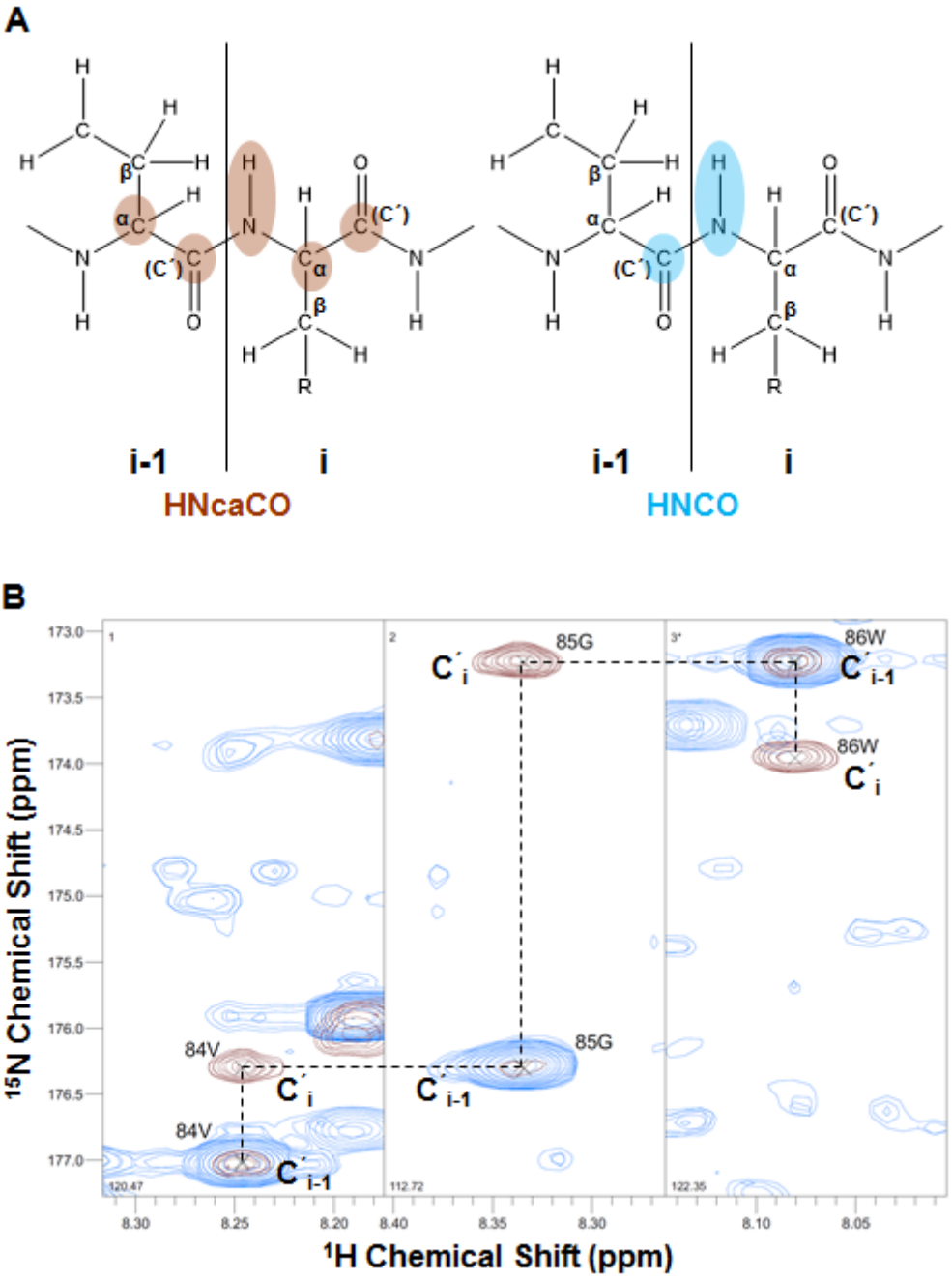

Figure 3.10 Assignment of the carbon backbone of AXR3 (DI and DII) using HNcaCO and HNCO spectra. (A) Representation of the carbon backbone of a protein is shown at the top of the figure. The magnetisation transfer in the HNcaCO and HNCO are shown with the nuclei involved highlighted brown and light-blue respectively. (B) The spectra of HNcaCO (brown) and HNCO (blue) are overlaid to show the $^{13}C'_i$ and $^{13}C'_{i-1}$ signals. The spectra are divided into three for each of the

presented residues of Val 84, Gly 86, and Trp 86. The connections between the residues Val 84 to Trp 86 are indicated by the dashed line.

3.2.2.1 Assignment of resonances from proline residues in AXR3 (DI and DII) and the identification of *cis-trans* isomer states within the degron

The AXR3 (DI and DII) protein contains 10 prolines, including one (-15P) in the thrombin cleavage site. Eight of these residues were assigned by establishing connections with the carbon backbone through the $^{13}C_{\alpha\, i}$ and $^{13}C_{\alpha\, i+1}$ signals from the hCAnCO and hCACO spectra. Continuous assignment through the prolines is then feasible in combination with the amide detected backbone assignment experiment from the proline surrounding residues. Connections were supported by similar chemical shifts between the hCACO spectrum for position i and CON spectrum for position i + 1. The nuclei involved in the magnetisation transfer are demonstrated in the chemical structures for the degron residues Trp 86 and Pro 87 (Figure 3.11). The CON spectrum with the assigned prolines is presented (Figure 3.12).

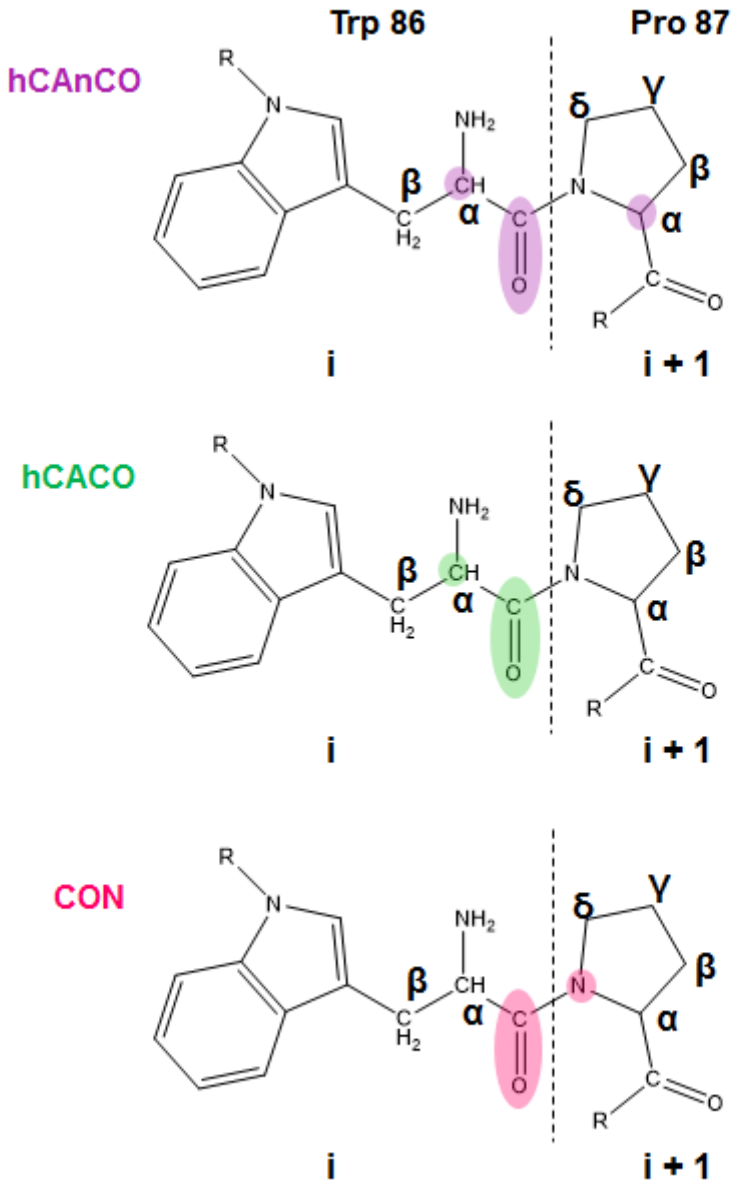

Figure 3.11 Nuclei involved in the assignment experiments hCAnCO, hCACO, and CON. The chemical structures of Trp 86 and Pro 87 are shown, where Trp 86 is in position i and Pro 87 in position i + 1. The nuclei involved in magnetisation transfer for the NMR experiments hCAnCO, hCACO, and CON are colour coded purple, green, and pink respectively.

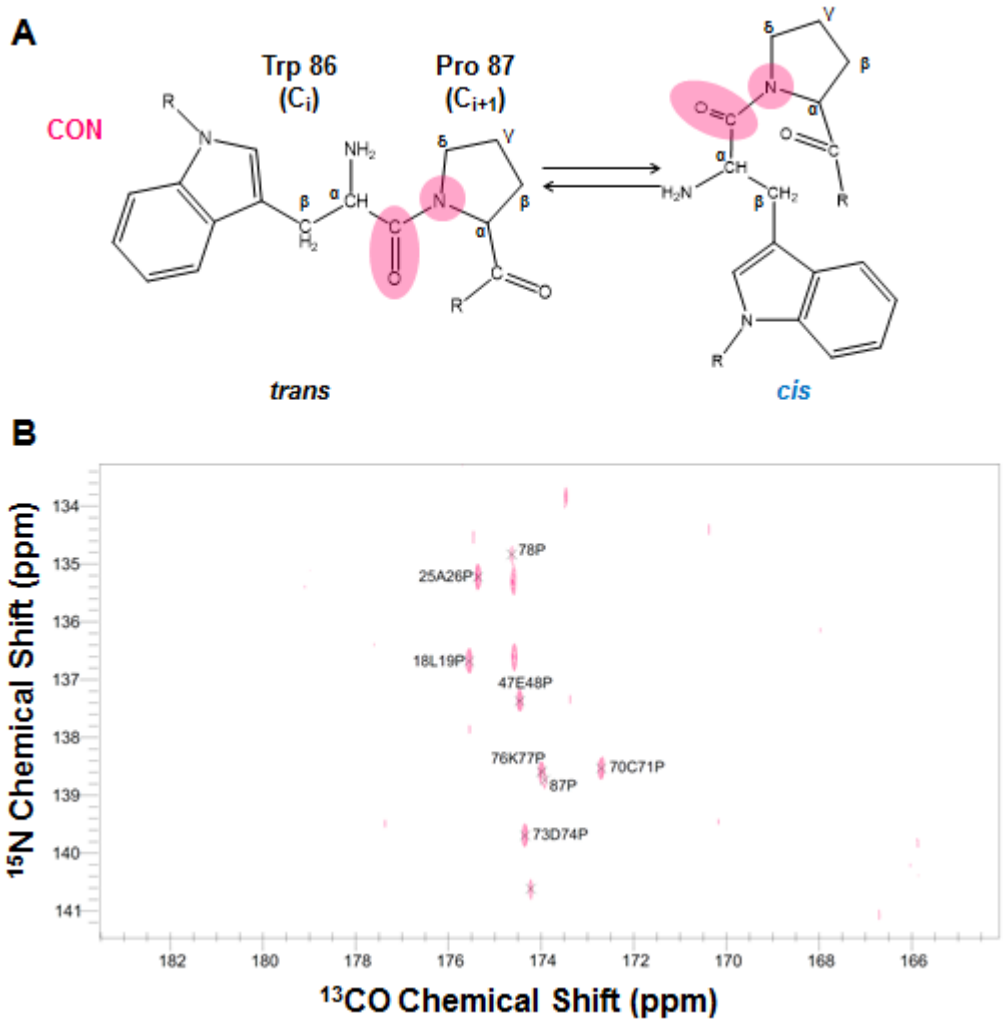

Figure 3.12 Assignment of prolines using the NMR experiment CON. (A) The chemical structure of Trp 86 and Pro 87 representing positions i and i +1along the carbon backbone. The nuclei involved in the magnetisation transfer in the CON experiment are highlighted pink. (B) Spectrum of CON of proline residues.

Although there are ten proline residues in AXR3 (DI and DII) an eleventh signal similar in intensity to other proline signals was observed in the $^{13}C_{\alpha}$ and $^{13}C_{\delta}$ signals associated with Pro 87. Such duplicate peaks indicate *cis-trans* isomerisation of the prolyl bond.

The peptide conformers with *cis* and the *trans* populations at Pro 87 (described as '*cis'* and '*trans'* for the rest of this chapter) were distinguished by observing the $^{13}C_{\alpha}$ chemical shift difference between the isomer signals. The $^{13}C_{\alpha}$ *cis* population was predicted to have an up-field chemical shift of around 0.5 ppm as described by Richarz and Wüthrich, 1978; and Shen and

Bax, 2010. The hCAnCO and hCACO spectra for AXR3 (DI and DII) show an up-field $^{13}C_{\alpha}$ chemical shift difference of around 0.3 ppm for the *cis* isomer population of Pro 87 compared to the *trans* isomer position (Figure 3.13).

The *cis-trans* isomerisation of the prolyl amide bond between Pro 87 and Trp 86 appeared to effect the chemical environment of residues further along the carbon backbone in both the N-terminal and C-terminal directions. As a result duplicate peaks were observed for residues within a specific region of the degron from Val 84 to Arg 90.

A connection was established between the C_{i+1} signal of the *cis* Pro 87 with the corresponding C_i signal of the Trp 86 (figure 3.14). The results show a $^{13}C_{\alpha}$ chemical shift difference of around 0.3 ppm with the cis conformation of Tpr 86 now down-field to the *trans* signal (Figure 3.14). This chemical shift change was used to identify the isomer populations of the other degron residues from Val 84 to Arg 90.

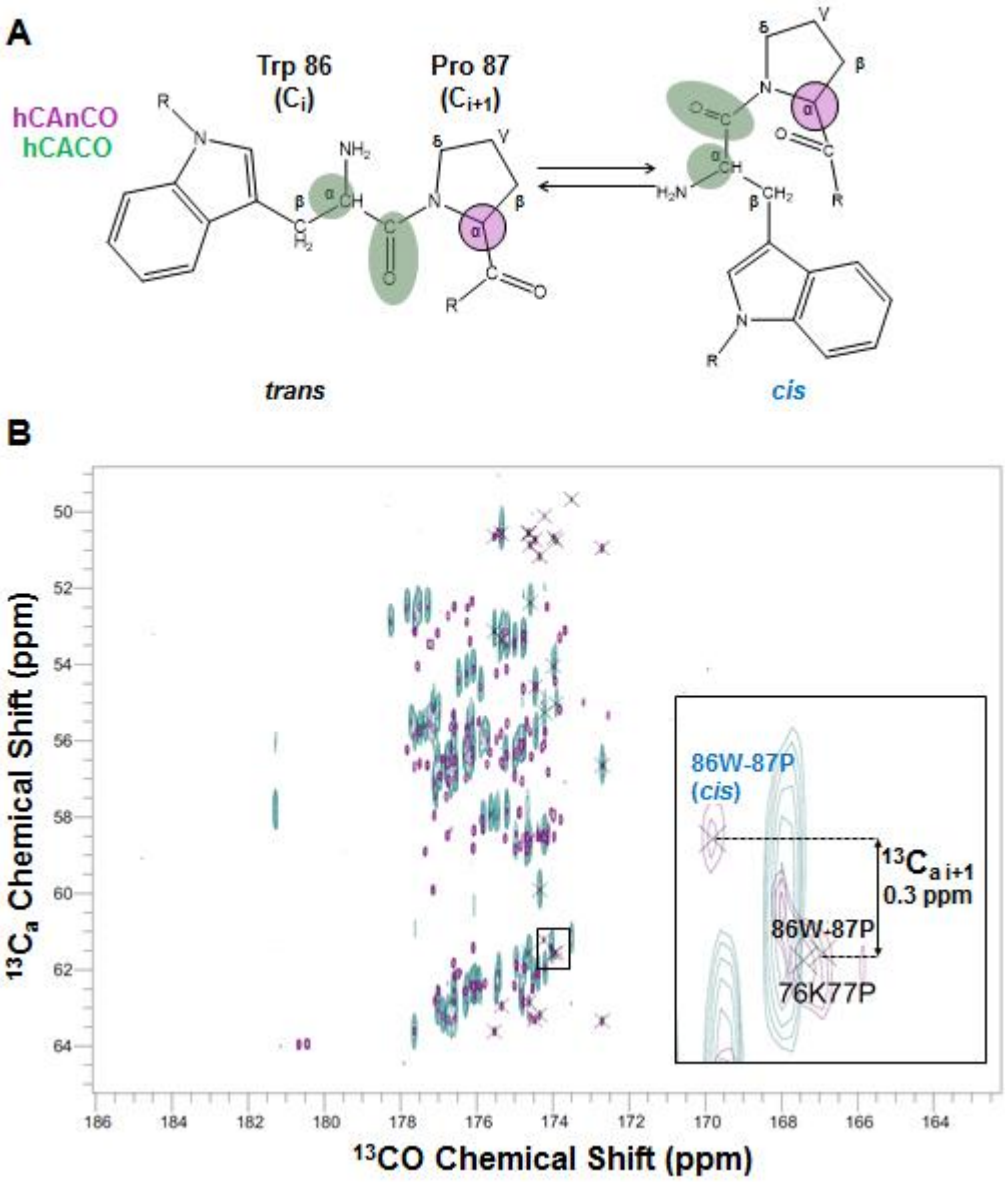

Figure 3.13 Assignment of *cis* and *trans* isomer states for Pro 87 $^{13}C_{\alpha}$ in AXR3 (DI and DII) using hCAnCO and hCACO spectra. (A) Trp 86 (C_i) and Pro 87 (C_{i+1}) in the *trans* and *cis* conformations. The nuclei of these structures involved in magnetisation transfer are highlighted purple and green for the hCAnCO and hCACO respectively. Nuclei involved in both experiments are highlighted in dark green. The $C_{\alpha\, i+1}$ position is outlined in black. (B) hCAnCO (purple) spectrum is overlapped with the hCACO (green) spectrum. In the $^{13}C_{\alpha}$ signal of Pro 87 the *cis* conformation is observed up-field to the *trans* conformation with a chemical shift difference of approximately 0.3 ppm.

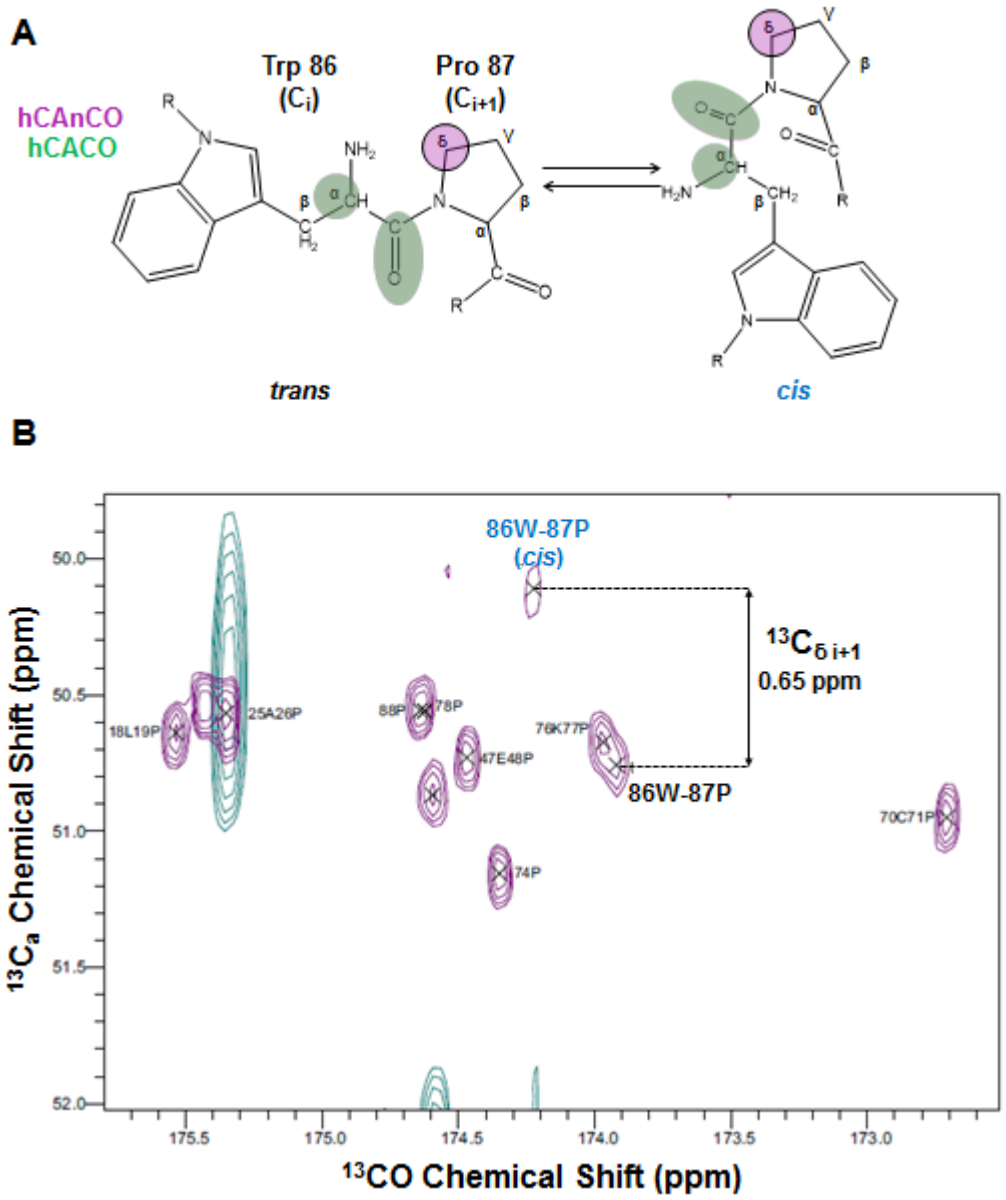

Figure 3.14 The hCAnCO and hCACO assignment of Trp 86 in the *cis* state.
(A) The chemical structures of Trp 86 (C_i) and Pro 87 (C_{i+1}) are shown. The nuclei of these structures involved in magnetisation transfer are highlighted purple and green for the hCAnCO and hCACO respectively, overlapped nuclei are shown in dark green. (B) The spectra of hCAnCO (purple) and hCACO (green). The $^{13}C_\alpha$ chemical shift difference of around 0.3 ppm is shown between the *cis* and *trans* signals of Trp 86.

The ^{13}C chemical shift difference between the *cis* and *trans* conformations of Pro 87 are observed to be greater for the C_δ nuclei of the proline relative to the C_α. This chemical shift difference approximately doubles from a difference of around 0.3 ppm for $^{13}C_\alpha$ to 0.65 ppm for the $^{13}C_\delta$ (Figure 3.15).

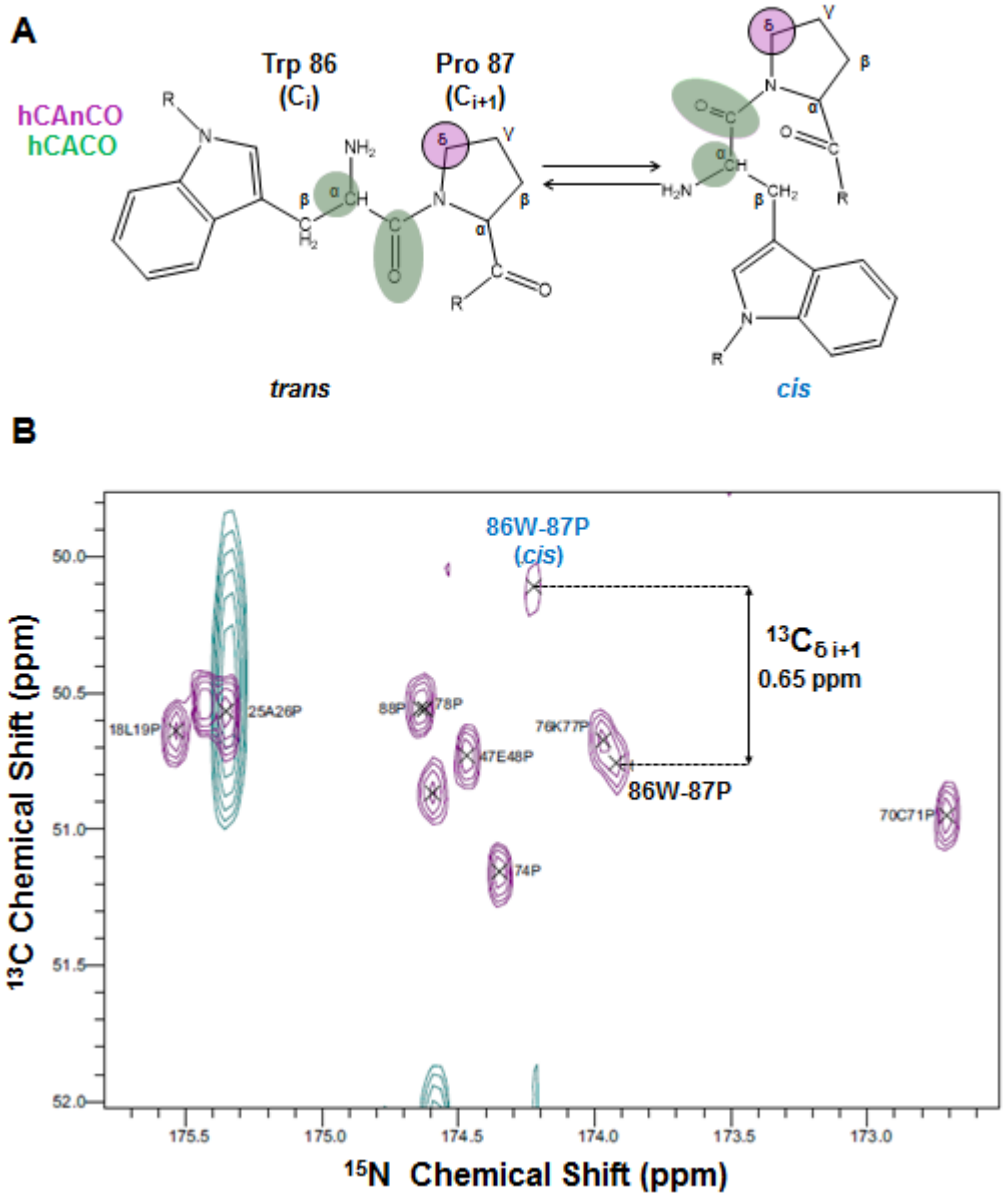

Figure 3.15 Assignment of *cis* and *trans* isomer states for Pro 87 $^{13}C_\delta$ in AXR3 (DI and DII) using hCAnCO and hCACO spectra. A) The nuclei of Trp 86 (C_i) and Pro 87 (C_{i+1}) involved in magnetisation transfer are highlighted purple and green for the hCAnCO and hCACO respectively. Nuclei involved in both experiments are highlighted in dark green. The $C_{\delta\,i}$ position is outlined in black. (B) hCAnCO (purple) spectrum is overlapped with the hCACO (green) spectrum. A $^{13}C_\delta$ chemical shift

difference of around 0.65 ppm is recorded between the cis and trans isomers for the $^{13}C_{\delta}$ signals of Pro 87. The $^{13}C_{\delta}$ signal for the *cis* conformation is observed up-field to the *trans* conformation.

3.2.2.2 HSQC of the assigned protein AXR3 (DI and DII)

The assigned residues of AXR3 (DI and II) are shown in a ^{1}H-^{15}N HSQC spectrum (Figure 3.16). The clustering of signals in a narrow ^{1}H chemical shift region of 7.9 to 8.6 ppm is consistent with the predicted intrinsic disorder of the protein. The degron residues Val 84 to Arg 90 were each observed to have two resonances within the ^{1}H-^{15}N HSQC spectrum and can be linked to the *cis* and *trans* isomers of Pro 87 (Figure 3.17).

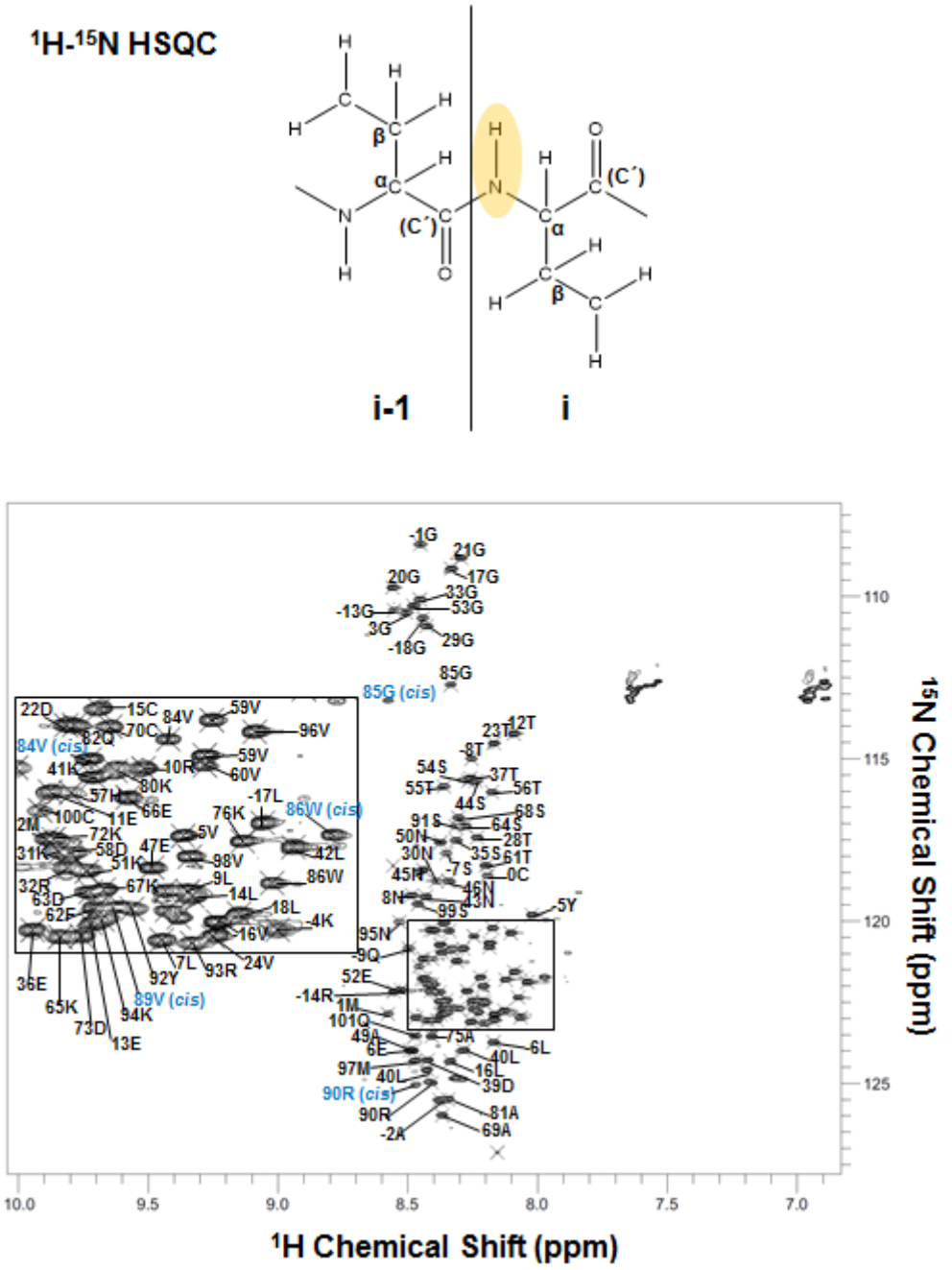

Figure 3.16 HSQC of the assigned protein AXR3 (DI and DII). At the top of the figure is a diagram of the magnetisation transfer in a HSQC experiment, where only the amide bond is detected. Shown below is the ^{1}H-^{15}N HSQC spectrum of the protein AXR3 (DI and DII). The peaks associated with Pro 87 in the *cis* isomer conformation the annotated light-blue.

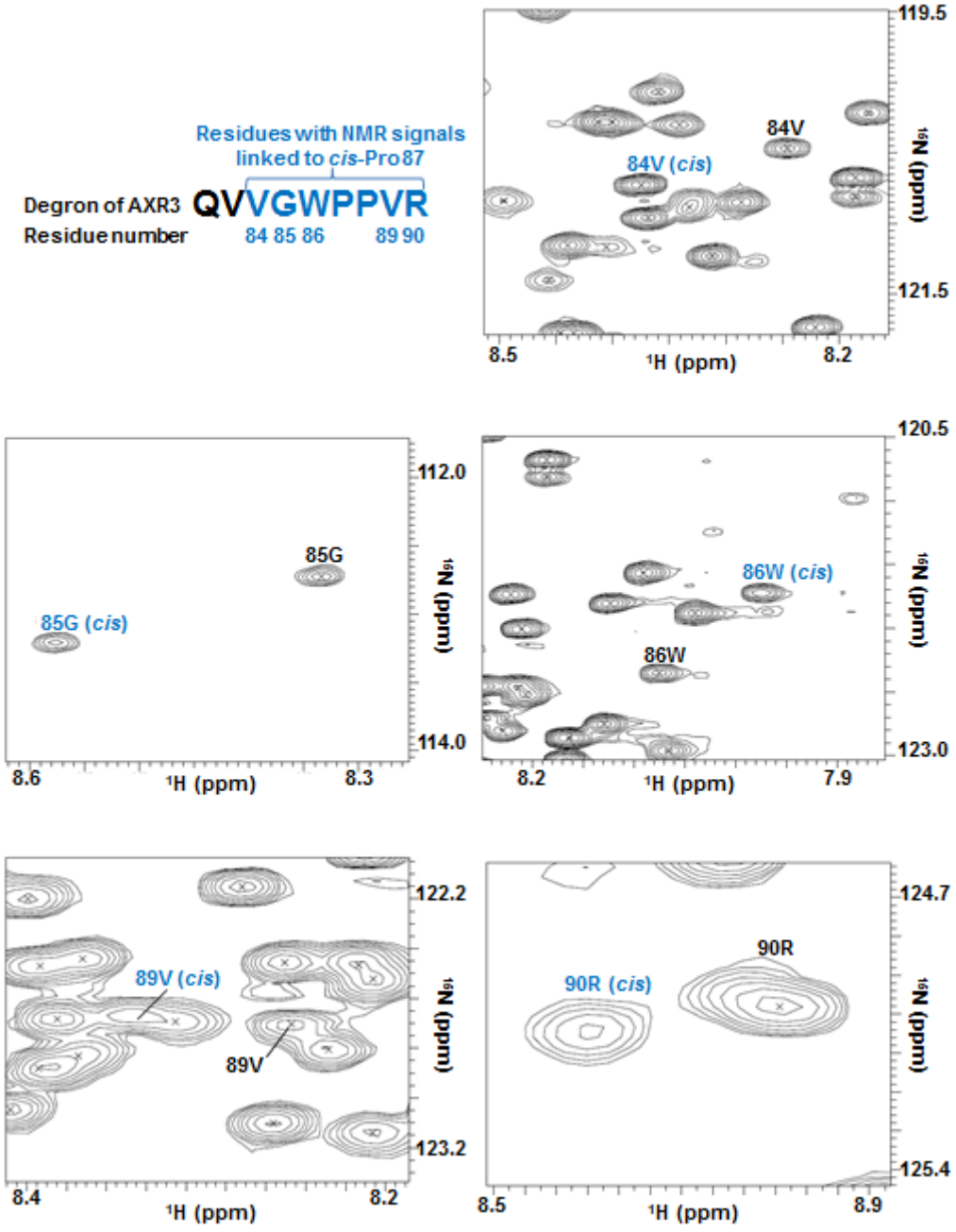

Figure 3.17 HSQC spectra of AXR3 (DI and DII) showing the paired signals of degron residues, linked to the cis and trans isomer states of Pro 87. Enlarged images from the HSQC spectrum showing the *cis* and *trans* isomers of the degron residues Val 84 to Arg 90, not including the residues Pro 87 and Pro 88. The peaks associated with Pro 87 in the *cis* isomer conformation the annotated light-blue.

3.2.3 Evidence for secondary structure in AXR3 (DI and DII)

The chemical shift values for $^{13}C_{\alpha,}$ $^{13}C_{\beta}$, and $^{13}C'$ signals recorded in the assignment of AXR3 (DI and DII) were used to identify secondary structure within the protein. Standard chemical shift values recorded at pH 5.0 in a random coil as reported by Wishart *et al*., 1994, were subtracted from the values for each residue recorded in the assignment experiments for AXR3 (DI and DII), to give the secondary chemical shift.

Positive chemical shift differences ($\Delta\delta$) for the $^{13}C_{\alpha}$ and $^{13}C'$ signals indicate tendencies for the formation of helical secondary structure, while a negative $\Delta\delta$ indicates a tendency for β-secondary structure. The opposite scenario applies to the $^{13}C_{\beta}$ chemical shift differences (Wishart *et al*., 1994; Shen and Bax, 2010).

Comparison between the $^{13}C_{\alpha,}$ $^{13}C'$, and $^{13}C_{\beta}$ chemical shift indices are shown (Figure 3.18). The results indicate a tendency for helical formation from Leu 7 to Leu 16 of AXR3 (DI and DII). This nascent helical region corresponds to functional domain I, where the consensus sequence extends from Glu 11 to Gly 20.

Further along the carbon backbone towards functional domain II, the chemical shift indices indicate a region of intrinsic disorder (Figure 3.18). This disordered region contains a small region with a tendency to form β-secondary structure, most likely a β-strand or region of extended structure between residues Val 59 and Asp 63. Further tendencies for the formation of a possible β-strand are observed in the regions flanking the degron core and include Ala 79 to Gln 82 and Val 89 to Arg 93. The region N-terminal to the degron (Ala 79 to Gln 82) shows a weaker trend for a tendency to form β-secondary structure compared to the other identified regions. There is no indication that these regions associate to form any higher order structure.

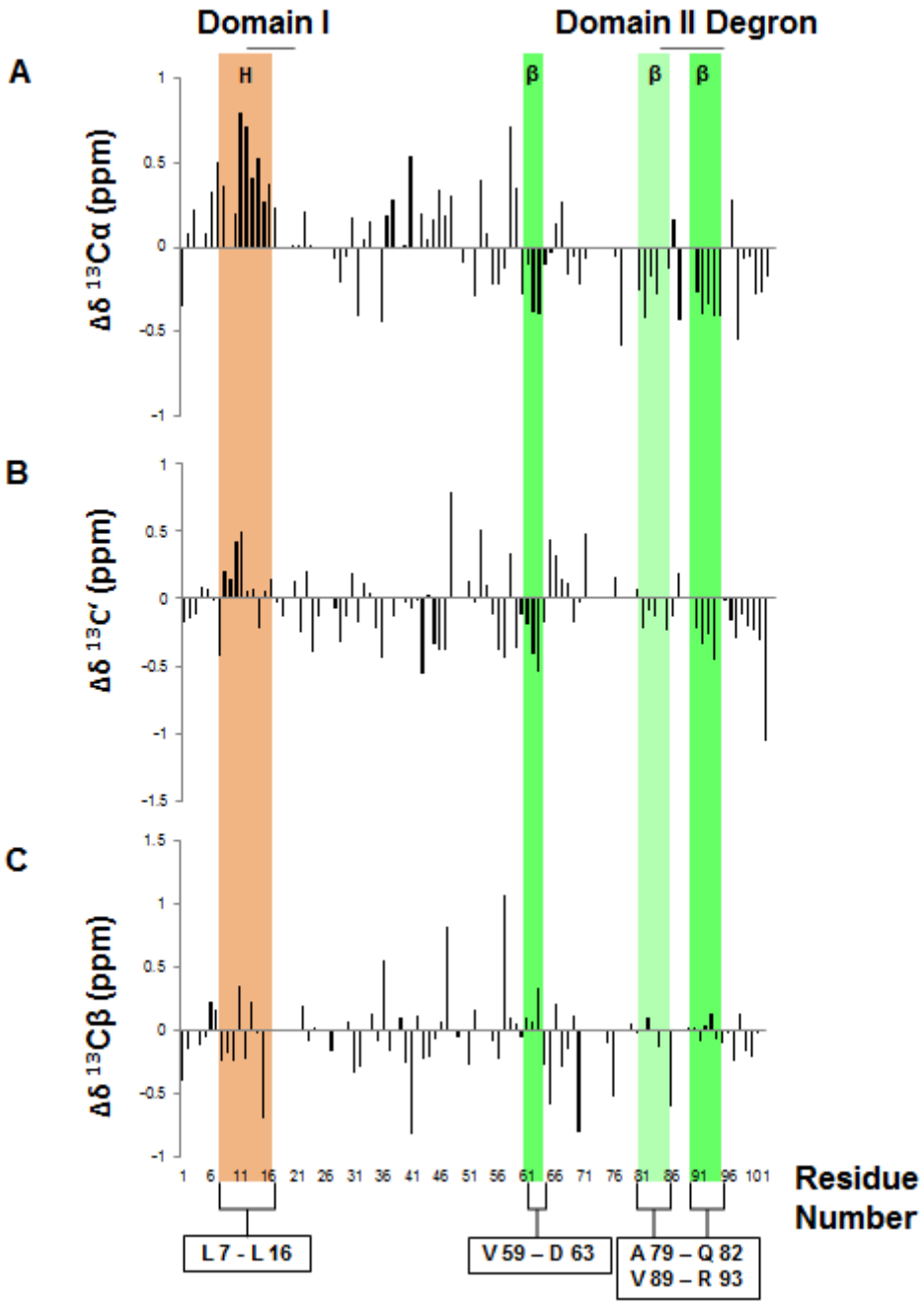

Figure 3.18 Chemical shift indices for $^{13}C_{\alpha}$, $^{13}C'$, and $^{13}C_{\beta}$. Positive chemical shift differences ($\Delta\delta$) for the $^{13}C_{\alpha}$, $^{13}C'$ indices indicate a tendency for helical secondary structure. Negative $\Delta\delta$ for the $^{13}C_{\alpha}$, $^{13}C'$ indices indicate a tendency for β-secondary structure. The opposite scenario applies to the $\Delta\delta$ $^{13}C_{\beta}$ index. Consensus regions for secondary structure tendencies between the $\Delta\delta$ $^{13}C_{\alpha}$, and $^{13}C'$ indexes are highlighted orange and green, for the helical and β-secondary structure respectively. The region from A 79 to Q 82 is highlighted lighter to indicate a weaker trend for a tendency to form β-secondary structure. Residues forming the termini of the consensus regions are annotated.

Residues within secondary structure or involved in hydrophobic clusters or other tertiary interactions are associated with higher transverse relaxation rate (R_2) values relative to residues in more flexible regions of a protein. The change in R_2 values for residues across the carbon backbone of AXR3 (DI and DII) are shown and compared with consensus regions for the tendency to form secondary structure, as indicated by the $\Delta\delta$ indices (Figure 3.19).

A higher relative R_2 value coincided with the region Leu 7 to Leu 16, which show tendencies to form helical secondary structure from the $\Delta\sigma$ indices. These observations support the secondary structure prediction for helices within functional domain I (Figure 3.19A to B). This region was immediately followed by a decrease in the R_2 rate corresponding to the end of the consensus sequence for DI and the location of the primary EAR motif.

The R_2 rate was observed to decrease within the intrinsically disordered region indicated by the $\Delta\delta$ indices. A number of small rises are seen in the R_2 rate, the most prominent of which is in the NLS region at the C-terminus (Val 89 to Arg93). Together these data sets indicate evidence for small elements with nascent structural tendencies within the intrinsic disorder of AXR3 (DI and DII) and they indicate a protein with a considerable higher level of complexity than a random coil.

The R_2 rate was compared between *cis* and *trans* isomer states for the degron residues Val 85 to Arg 90 and was found to have no significant changes in R_2 values (Figure 3.19C). Interestingly, a small general trend was observed for a decrease in R_2 values for degron residues closest to the central degron core (WPP), suggesting the centre of the degron remains similarly disordered.

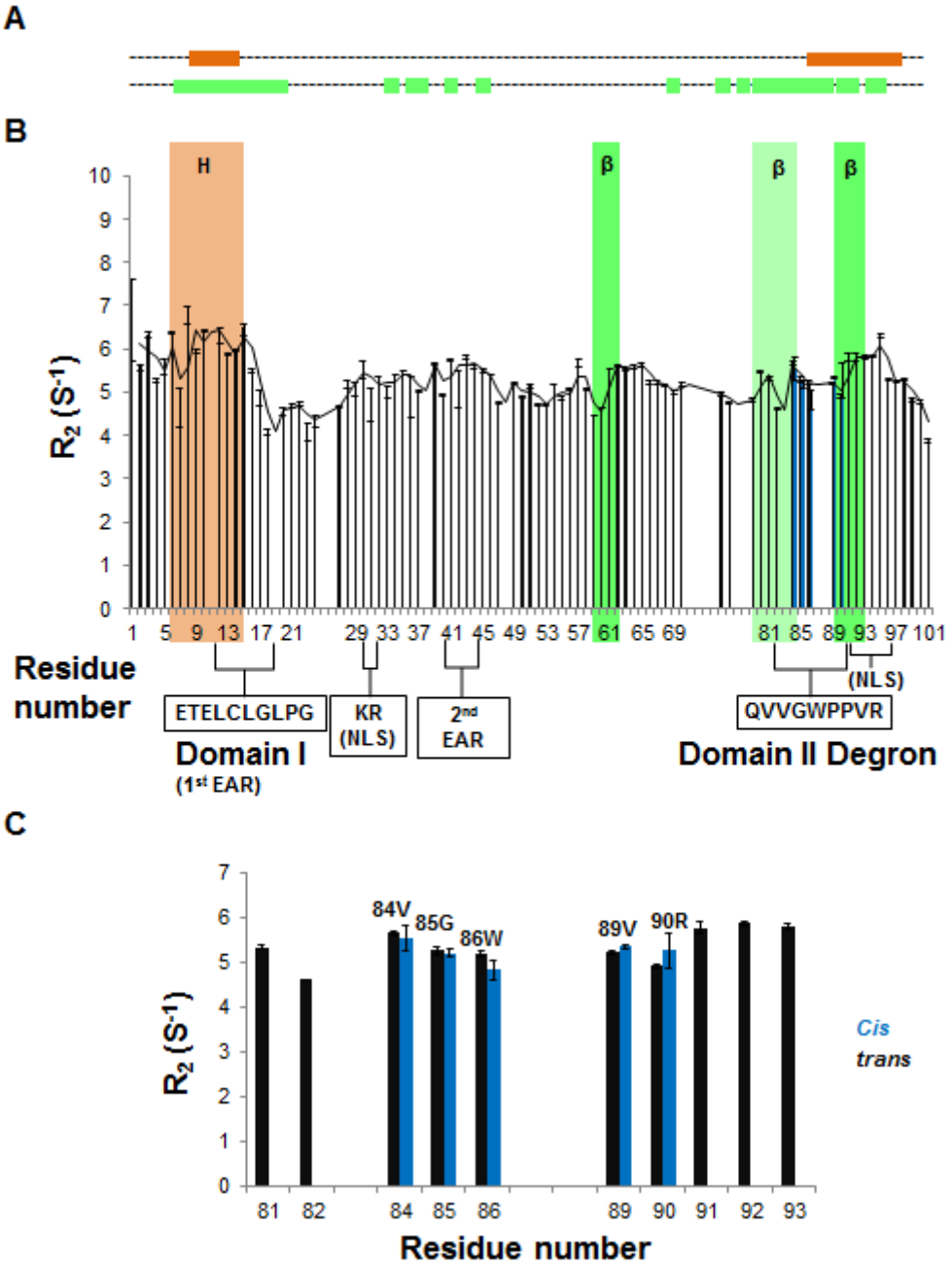

Figure 3.19 Comparison between R_2 relaxation rates and the consensus regions for secondary structure tendencies of AXR3 (DI and DII). (A) Secondary structure prediction for the AXR3 (DI and DII) amino acid sequence. Helical regions are shown in orange and β-secondary structure shown in green. (B) R_2 relaxation rate for residues along the carbon backbone of AXR3 (DI and DII). Relative increases in the R_2 rate are associated with regions of reduced flexibility. The R_2 data set is overlaid with consensus regions for secondary structure tendencies as indicated by the chemical shift indices. The data set is annotated with consensus sequences for functional domains I and II, including the nuclear localisation signal (NLS) KR motif which functions in partnership with a 2nd NLS at

Arg 90 to Val 96. Gaps in the R_2 data set are associated with Prolines and residues in signal dense regions preventing peak picking. (C) R_2 relaxation rate for residues in domain II. Showing the R_2 rates for the *cis* and *trans* conformations of degron residues Val 84 to Arg 90.

3.3 Discussion

3.3.1 The N-terminal AXR3 (DI and DII) protein is dominated by regions of intrinsic disorder

Our results are consistent with the hypothesis that the majority of the N-terminal half of the Aux/IAA protein AXR3 (DI and DII) is intrinsically disordered. This was indicated by the low signal dispersion observed in the ^{1}H-^{15}N HSQC spectrum. The extent of this disorder was most substantial in a large region of the carbon backbone between DI and DII, indicated by the $\Delta\delta$ indices for the $^{13}C_{\alpha,}$ and $^{13}C'$ signals.

The disordered region is enriched in prolines and is a feature consistent with other intrinsically disordered proteins (Theillet *et al*., 2013). This region appears to from a disordered loop interspersed by smaller more structured regions of possible β-strands associated with increases in the R_2 rate. One of these structural elements from V 59 to D 63 is supported in the $\Delta\delta$ indices. The function of these possible β-strands within the disordered loop separating the functional domains is currently unknown. However, a conserved KR motif which acts as part of a nuclear localisation signal, identified in early sequence analysis of Aux/IAA proteins is observed adjacent to one of these potential β-strands (Abel *et al*., 1994).

3.3.2 Identification of a possible recognition element adjacent to the EAR motif of domain I

Our results suggest a region of DI adjacent to the primary EAR motif of LXLXL has a tendency to form helices. The EAR motif forms a key interface for the recruitment of TPL, resulting in the transcriptional repression of auxin regulated genes (Tiwari *et al*., 2004; Szemenyei *et al*., 2008; Causier *et al*., 2012; Wang and Estelle, 2014). Crystallography suggests that the EAR motif

is sufficient to form an interaction with TPL and raises the question of the biological significance of helices adjacent to the motif in the AXR3 protein (Ke *et al*., 2015). It is a possibility that the observed tendency to form helices supports the interaction with the TPL domain acting as another recognition element, alongside the EAR motif.

Possible support for this hypothesis is from the observation of a second EAR motif within the disordered loop of AXR3 at residues positions 40 to 44, within a region of less stable structural elements. This second LXLXL motif is considered to be less efficient at forming the interaction with TPL and suggests that the EAR motif in DI is enhanced by a more prominent recognition element (Lee *et al*., 2016).

3.3.3 Identification of a possible recognition element C-terminal to the degron core of AXR3

C-terminal to the di-proline motif (Pro 87 and Pro 88) at the centre of the degron core is a region with a tendency to form β-secondary structure. This may represent an additional recognition element to support the interaction of the degron core with TIR1. This hypothesis assumes that the regions of intrinsic disorder in AXR3 are likely to remain in the unfolded state when forming the auxin receptor complex as typically seen in other IDPs (Hazy and Tompa, 2009; Gruet *et al*., 2016). In these circumstances elements of secondary structure can form binding interfaces which are either pre-formed or triggered to fold upon binding (Fuxreiter *et al*., 2004; Mészáros *et al*., 2007).

Our observation of a possible β-strand from Val 89 to Arg 93 in the AXR3 protein is not observed in the crystal structure of the peptide of AXR2 (Tan *et al*., 2007). Presumably this lack of secondary structure in AXR2 is due to a residue change at position 93, occupied by asparagine in AXR2 and arginine in AXR3. This hypothesis is based on the possibility that the peptide may not provide a sufficient sequence context to observe the secondary structure tendency of this region. Alternatively this may be due to the observation that arginine has a slightly higher propensity for β-secondary structure formation (Smith *et al*., 1994).

3.3.4 Identification of *cis-trans* isomer states within the degron

Analysis of hCAnCO and hCACO spectra indicated that only Pro 87 out of the ten prolines in AXR3 was associated with an additional prominent signal, distinct from the background signals. This indicates that the *cis* isomer of Pro 87 has a considerably higher population then the other prolines which conform to the expected low level of population (around 10%) of the *cis* isomer in an intrinsically disordered context. This indicated that a *cis-trans* isomerisation equilibrium of the prolyl bond was occurring within the highly conserved core of the degron which forms the main interface with TIR1 (Tan *et al*., 2007).

The *cis* conformation of Pro 87 was associated with an up-field chemical shift for the $^{13}C_{\alpha}$ and $^{13}C_{\delta}$ signals consistent with previous reports (Richarz and Wüthrich, 1978). Unusually the *cis* conformation of the adjacent residue Trp 86 showed a down-field chemical shift. However there are no reports on the expected chemical shift of residues adjacent to a *cis-trans* di-proline motif and this motif is assume responsible for the observed down-field chemical shift. The $^{13}C_{\alpha}$ up-field chemical shift of 0.3 ppm was used to link *cis* and *trans* isomer states of Pro 87 with the pairs of NMR singles observed for the degron region Val 84 to Arg 90.

Overall our NMR analysis of the N-terminal half of AXR3 (DI and DII) has revealed a protein dominated by extensive regions of disorder which separate the functional domains I and II. Here, the domains have been shown to overlap regions with a tendency to form secondary structure, with helices at the N-terminus and potential β-strand tendencies towards the C-terminus. These two main regions of nascent secondary structure are likely to represent distinct recognition elements supporting protein-protein interactions mediated by the highly conserved sequence motifs of DI and DII. The functional implications of a tendency to form a β-strand adjacent to the degron, and the role of potential *cis-trans* isomerisation within the degron will be explored further to develop our understanding of the formation of the auxin receptor complex.

Chapter 4

Evidence for novel co-receptor functions in auxin perception

4.1 Introduction

4.1.1 Aux/IAA as a co-receptor for auxin

The molecular structure of the auxin receptor complex by Tan *et al*., 2007 inspired a simple model of auxin perception. In this model IAA bound first to TIR1 and acted as molecular glue at the base of the auxin binding pocket (Tan *et al*., 2007; Guilfoyle, 2007). It is by this process that IAA enhances the affinity of the receptor for the binding of the Aux/IAA transcriptional repressor proteins (Kepinski and Leyser, 2005; Dharmasiri *et al*., 2005).

More recently it has been proposed that Aux/IAA and TIR1 act together as co-receptors for auxin binding. This hypothesis was based on the observation that different Aux/IAA proteins and degron peptides were associated with a wide range of rate constants for the dynamics of the auxin receptor complex (Villalobos *et al*., 2012). Such a perspective places Aux/IAA as having a more prominent role in complex formation. Even with this new emphasis on Aux/IAA function, it is assumed that the co-receptors are not equal in their ability to bind IAA, as crystallography studies suggest auxin binding to TIR1 is the more prominent interaction (Tan *et al*., 2007). How the Aux/IAA may act as a co-receptor for auxin is currently poorly understood, and it is studied here.

4.1.2 The potential for aromatic-aromatic interactions in auxin perception

When studying the stabilising effect of IAA during the formation of the auxin receptor complex, it is important to consider the possible role of an aromatic interaction between IAA and Trp 86 of the Aux/IAA degron region, which may act as an important recognition element during auxin perception. The

crystal structure (2P1Q) of the auxin receptor complex (Tan *et al*., 2007) shows Trp 86 within the degron core in close proximity to the IAA ring structure when bound to the receptor TIR1. A key question is whether these aromatic ring structures interact during complex formation, providing a potential mechanism for Aux/IAA co-receptor function.

Aromatic–aromatic ring interactions can occur when an electron rich and electron poor regions of the planar aromatic rings come into contact. However, beyond this simplistic picture several other factors can come into play and include: the maximisation of van der Waals forces, electrostatics due to a charge distribution within the electron cloud for each molecule, and the minimisation of solvent exposure (Hunter *et al*., 2001). Although an aromatic–aromatic interaction is fundamentally weak it can have a very important role in biological functions, by providing shape and charge based specificity within a molecular interaction (Cozzi *et al*., 1995). This specificity arises due to the electrostatic contribution to the interaction, which is translated into the defined spatial the arrangement of the aromatic rings (Hunter and Sanders, 1990; Hunter *et al*., 2001; Waters *et al*., 2002; Martinez and Iverson, 2012).

There are three potential arrangements of aromatics rings that lead to electrostatic attraction (Figure 4.1A to F). The first scenario is the potential to form an edge-face geometry, where the aromatic rings are perpendicular to each other (Figurer 4.1C). The second is an offset stacked geometry, where the rings are only partly overlapped reflecting their charge distribution (Figurer 4.1D). Thirdly, face-face stacking where rings of opposite charge densities are positioned parallel to each other minimising solvent exposure and maximising van der Waals contacts (Figurer 4.1E to F). Face to Face arrangements are disfavoured between regions with the same charge density, resulting in the repulsion between the rings (Hunter and Sanders, 1990; Hunter *et al*., 2001, Waters *et al*., 2002; Martinez and Iverson, 2012).

Edge-face interaction is considered to be particularly prominent in proteins between aromatic side-chains of amino acids, including Phe, Tyr, and Trp. Such interactions act as a stabilising force, with an average free enthalpy of - 0.3 kcal mol^{-1} which can often be enough to make an interaction favourable

(Meyer *et al*., 2003). It is likely that a similar interaction could occur within the auxin binding pocket between IAA and Trp 86 based on the geometry between these two components in the crystal structure 2P1Q (Tan *et al*., 2007).

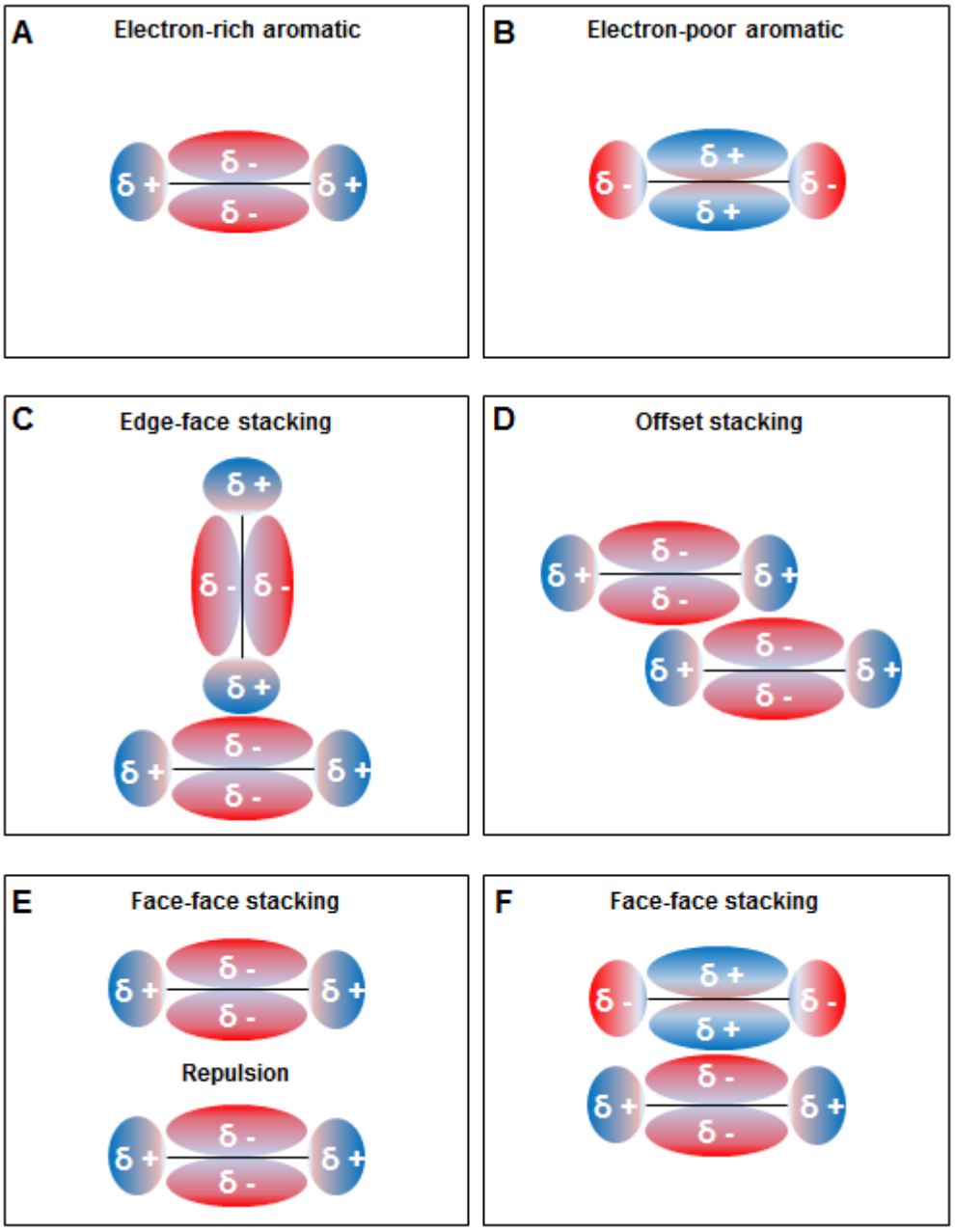

Figure 4.1 Schematic representations of the possible arrangements of aromatic–aromatic interactions. Electron clouds surrounding the planar structures are represented by elongated spheres with gradated colour. The colour coding is as follows: red indicates electron rich regions (δ -), and blue indicates electron poor regions (δ +). (A to B) Aromatics with enrichment of electrons centered above the ring are termed electron rich aromatics, while the opposite scenario is described by the electron poor aromatics. (C to D) The scenarios of an

edge-face interaction and offset stacking are shown here between two electron rich aromatics. (E to F) A face-face stacking will only be favoured between an electron-rich aromatic and an electron poor aromatic.

The IAA molecule has been shown to be an electron rich aromatic with an uneven distribution of the electron cloud, a key factor for establishing an aromatic interaction (Schmit *et al*., 2011). In this case the electron cloud is denser along the planar surface of the indole ring compared to the edges (Figure 4.2). This divergence in electrostatic polarity continues across this electron rich area with the N atom in the NH group of the indole ring establishing a centre of high electron density (Figure 4.2).

Differences in electrostatic potentials are also observed between IAA and when the indole ring is in isolation. This difference is due to the displacement of the electron cloud by the carboxyl side chain in IAA (Schmit *et al*., 2011). As the carboxyl chain re-orientates with respect to the IAA ring structure (Kaethner, 1977) the influence on the electron cloud of the indole ring is also considered to change (Schmit *et al*., 2011). The strongest displacement of electrons is believed to occur when the carboxyl chain is in an alignment perpendicular to the ring, enhancing the electrostatic polarity of the IAA ring structure.

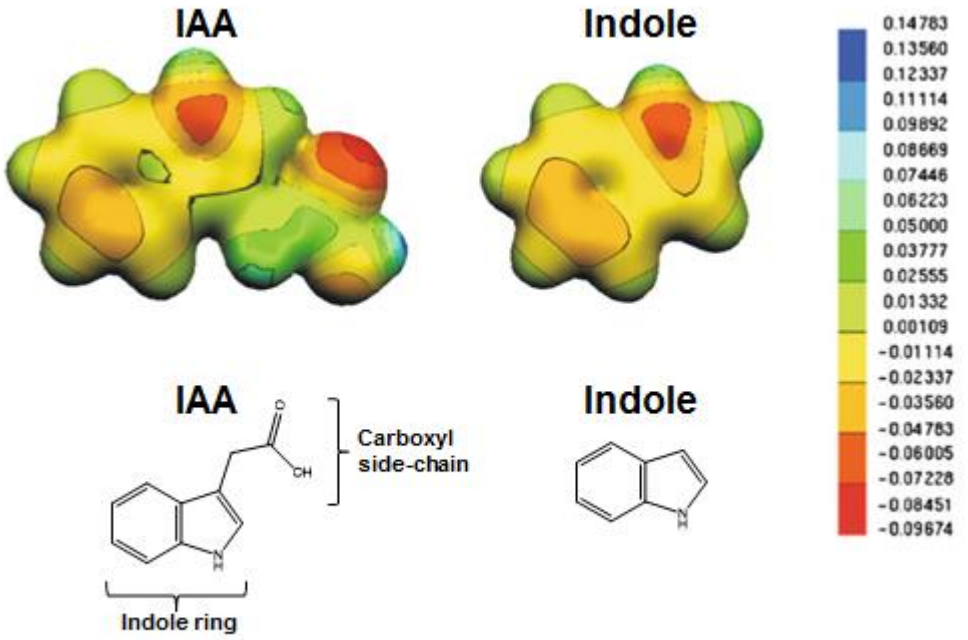

Figure 4.2 Molecular electrostatic potential of IAA and indole, adapted from Schmit *et al*., 2011. The molecular surface of IAA and indole are shown with contours colour coded for the electrostatic potential. The atomic units (a.u.) associated with each colour are presented, with blue tones representing electron deficient regions and red indicating electron rich regions. The chemical structures of IAA and indole are included for comparison with the molecular models. The indole ring in the IAA structure is considered to have a greater electrostatic polarity compared to the indole ring alone.

The ability of IAA to undergo a conformational change was first proposed by Kaethner in 1977, forming an early model for auxin binding (Kaethner, 1977). Within this model IAA goes from a recognition state to a modulation state, where the carboxyl chain becomes perpendicular to the indole ring (Figure 4.3). This conformational change was supported by the observation of IAA in the modulation conformation when bound to the auxin binding pocket of TIR1 (Tan *et al*., 2007).

Kaethner also proposed that the conformational change of IAA may only occur with a partner molecule, where simultaneous structural changes are promoted. This change in conformation of IAA is considered essential for any auxin to be functional. The exact mechanism for this functionality is unknown, but may relate to electrostatic polarisation and consequently the strength of any potential aromatic interactions formed by IAA.

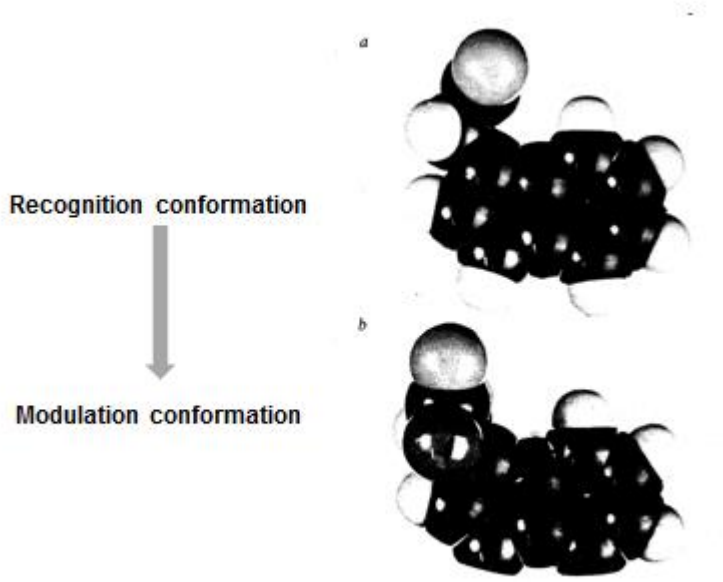

Figure 4.3 Molecular model of IAA in two conformational states, adapted from Kaethner, 1977. The molecular model shows IAA in a recognition conformation and a modulation conformation, where the carboxyl chain becomes perpendicular to the indole ring.

4.1.3 *Cis-trans* isomerisation and the importance of electrostatics

In addition to the role of electrostatics in auxin perception, *cis-trans* isomerisation is an area of increasing interest in auxin biology. The crystal structure of the auxin receptor complex by Tan *et al*., 2007 contains a *cis* prolyl amide bond in the degron core of the Aux/IAA peptide (Tan *et al*., 2007).

The *cis* and *trans* isomer states can be distinguished by the geometry of chemical groups around a structural unit. In this classification a *cis* isomer of

a peptide bond describes when the CO and NH groups are orientated on the same side of the amide bond, with the opposite scenario described by the *trans* isomer (Fischer, 2000). Conversion between cis and *trans* states is considered to be slow relative to a NMR chemical shift time scale which allows the detection of both isomer states, with the change in geometry resulting in chemical shift differences (Fischer, 2000).

Conversion between the two geometries requires rotation of the C-N peptide bond. Isomerases such as cyclophilin are usually required to reduce a high energy barrier for bond rotation, which is on average 80 kJ mol^{-1} at 60 ˚C (Fischer, 2000). It is due to this high energy barrier that exchange between the two states is slow (minutes). Proteins tend to adopt the *trans* conformation as it is the lowest energy state in the absence of other interactions from backbone conformation and neighbouring sidechains, as steric clashes are minimised (Hinderaker *et al*., 2003).

Even with the high energy barrier present access to *cis* conformation is not impossible and is favoured by specific sequence contexts. The *cis* conformation is most likely to occur when a peptide bond is established N-terminal to a proline. In this case, the energy required for bond rotation is considered equal for conversion between the isomer states with a lower energy barrier of 2.0 kJ mol^{-1} (Weiss *et al*., 1998, Fischer, 2000). This makes a prolyl bond a more favourable site for the *cis* conformation to exist.

Despite the equal energy barrier between *cis* and *trans* conformers, the proportion in the *cis* conformation adopted by prolyl bonds is low. This was shown in a previous study, where only 7-8 % of a test peptide with a prolyl bond reported displayed the *cis* isomer (Thomas *et al*., 2006). This value is observed to increase when an aromatic residue is adjacent to the proline, from 17 % with phenylalanine, 21 % with tyrosine, and 25 % with tryptophan (Wu and Raleigh, 1998). The increase in *cis* frequency with the type of aromatic residue correlates with how electron rich the orbitals of the aromatic ring are, which stabilises the *cis* conformation by an electrostatic stacking between the rings (Figure 4.4) (Thomas *et al*., 2006).

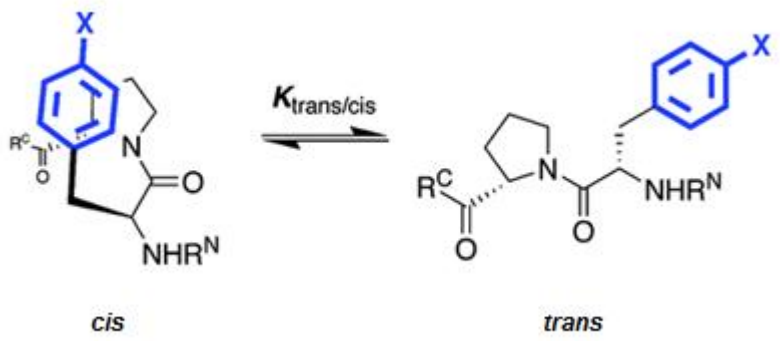

Figure 4.4 Arrangement of a proline and aromatic ring in the *cis* and *trans* states from Thomas *et al*., 2006. The rare *cis* state is more likely to form when the aromatic ring is electron rich as is the case for tryptophan. An enrichment of electrons will enhance an electrostatic interaction between the ring structures, stabilising the *cis* conformation. The aromatic ring is shown in blue within the diagram.

The electrostatic stacking of the aromatic ring and the proline ring may also influence the isomerisation rates. A recent report has shown the isomerisation rate from *cis* to *trans* decreases by 3 - 7 % in the presence of an aromatic residue, in contrast to a 1.6 - 3 % decrease from *trans* to *cis* (Wu and Raleigh, 1998). The slower isomerisation rate from *cis* to *trans* demonstrates the stabilising effect of the aromatic residue on the *cis* conformation. In addition the di-proline motif in the degron core is also likely to contribute to a higher *cis* frequency (Dasgupta *et al*., 2007).

The significance of a *cis* conformation within the degron in the receptor bound state is unknown and raises further questions on how the auxin receptor complex forms. A central question which will be studied here is the possibility of conformational selection, between the *cis* and *trans* states of the degron during the formation of the auxin receptor complex.

Here NMR spectroscopy was used to examine the role of conformation selection in auxin perception, focusing on whether the Aux/IAA protein AXR3 must be in the *cis* or *trans* states to form the auxin receptor complex. Furthermore, NMR spectroscopy and surface plasmon resonance (SPR)

assays have been used here to investigate a possible co-receptor function of Aux/IAA for the binding of IAA. Together, these studies provide evidence for a putative model for auxin receptor complex formation.

4.2 Results

4.2.1 Degron core displays almost equal occupancy in *cis* and *trans* isomer states

Trp 86 is part of the highly conserved degron core of an Aux/IAA and forms the motif WPP. The prolyl amide bond between Pro 87 and Trp 86 is in a *cis* isomer conformation within the crystal structure 2P1Q published by Tan *et al*., 2007. This arrangement is shown in our own analysis of the crystal structure using the computational modelling software Maestro Schrodinger suite (Figure 4.5A and B). My analysis of the crystal structure is described in more detail in chapter 5 (sections 5.3.1 to 5.3.3).

The observation of a *cis* conformation raised the possibility of *cis-trans* isomerisation within the Aux/IAA degron core. My assignment of the NMR data for the protein AXR3 (DI and DII) identified duplicate NMR signals associated with residues within the degron from Val 84 to Arg 90. Such duplicate signals are consistent with *cis* and *trans* isomers being present. These isomer populations were distinguished in the NMR spectrum, with the *cis* population showing an up-field chemical shift of around 0.3 ppm for $^{13}C_{\alpha}$ as reported in chapter 3 (section 3.3).

The occupancy within the isomer states was estimated from the height and volume of the duplicate NMR signals of Trp 86 HN cross peak, from the ^{1}H-^{15}N HSQC spectrum of AXR3 (DI and DII) (Figure 4.5C and D). This analysis revealed approximately equal abundance between the *cis* and *trans* isomer populations.

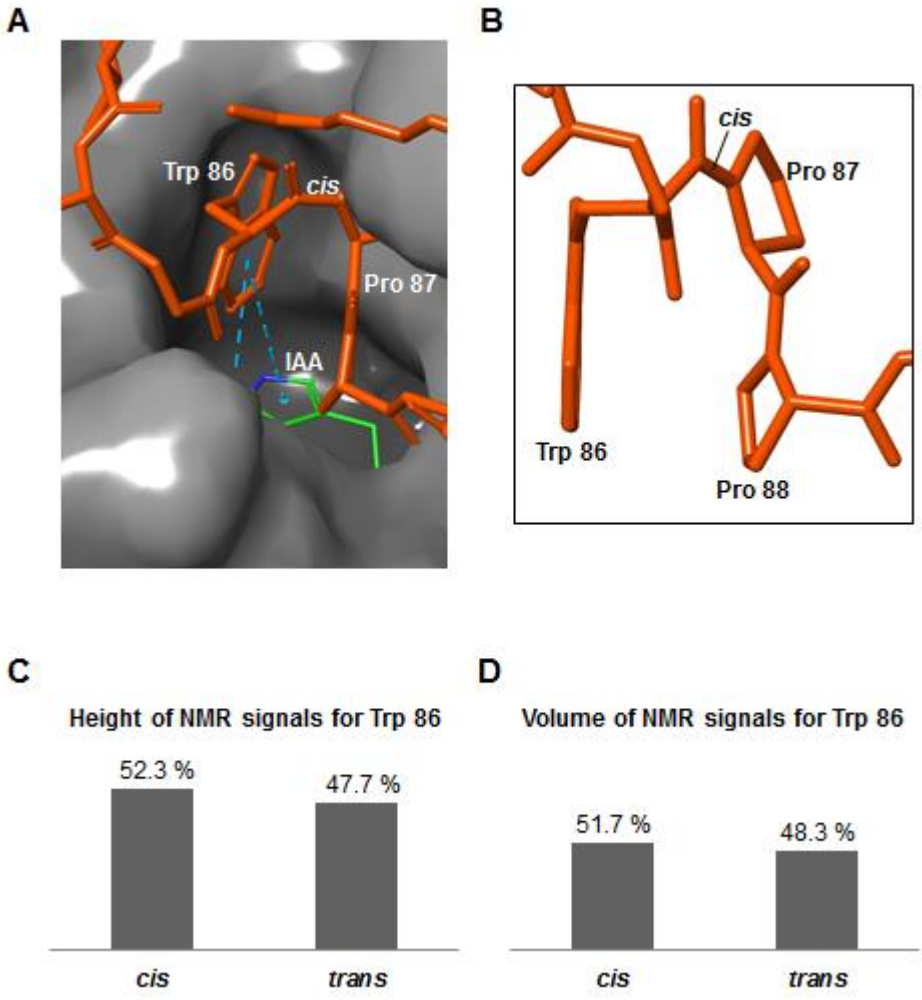

Figure 4.5 Approximately equal abundance in *cis* and *trans* isomer states of Pro 87 within the degron core. (A) Molecular model of the auxin receptor complex composed of TIR1 (shown in grey), IAA (annotated and shown in green), and a peptide of the AXR2 degron (shown in orange).The molecular model presented is my own analysis of the crystal structure 2P1Q published by Tan *et al*., 2007. A prolyl amide bond between Pro 87 and Trp 86 is observed in the *cis* isomer state. (B) Molecular model of the AXR2 degron core in the bound conformation, viewed without the molecular surface of TIR1. The peptide bond in the *cis* conformation is annotated. (C) and (D) The height and volume respectively of NMR signals from a ^{1}H-^{15}N HSQC spectrum of AXR3 (DI and DII) protein, estimating the abundance of the *cis* and *trans* isomer states as measured by Trp 86 H_{α}-N_{α}. The ^{1}H-^{15}N HSQC spectrum of AXR3 (DI and DII) was performed at 17˚C.

4.2.2 Conformational selection of the central degron core (WPP) for the interaction with TIR1

The crystal structure 2P1Q of the AXR2 degron was used to create a model of the AXR3 peptide. This involved using Maestro Schrodinger suite to replace Asn 91 with serine followed by energy minimisation of the strucutrue (Figure 4.6A). Analysis of this strucuture is shown for the AXR3 degron core in the *cis* conformation within the context of the auxin bindng pocket (Figure 4.6A). This observation of the *cis* isomer of the degron in the bound state raised the possiblity of conformational selection during the formation of the auxin receptor complex.

The NMR experiment ^{1}H-^{15}N HSQC was used to study the interactions between the auxin receptor TIR1 and the confromational states of the AXR3 degron residues associated with *cis-trans* isomerisation of Pro 87. AXR3 (DI and DII) protein isotopically labelled with ^{15}N was studied with unlabelled TIR1 in the presence and absence of unlabelled IAA. The NMR signals recorded were overlaid for comparison and colour coded (Figure 4.6B). Changes in $^{15}N/^{1}H$ chemical shift, and/or decreases in signal intensity between the overlaid NMR signals, were used as indicators of binding.

The ^{1}H-^{15}N HSQC spectrum of AXR3 (DI and DII) shows two resonances for Trp 86 HN cross peak due to the presence of both *cis* and *trans* isomers of Pro 87 in solution. The Trp 86 HN cross peak associated with the *cis* isomer population of Pro 87 shows both a chemical shift change and a decrease in signal intensity in the presence of TIR1 compared to free AXR3 (DI and DII)(Figure 4.6C). This interaction was enhanced by IAA, leading to these the NMR signals no longer being observed in the NMR spectrum due to broadening to below the noise floor. This is in contrast to the to the equivalent signals from Trp 86 HN cross peak which occur when a *trans* Pro 87 is present, which displayed a limited chemical shift change even in the presence of IAA (Figure 4.6C).

Gly 85 is also part of the highly conserved degron core and is situated at the edge of the auxin binding pocket as the N-terminal half of the degron extends into the cavity (Figure 4.6A). The overlaid NMR spectra of AXR3 (DI

and DII) shows chemical shifts and decreases in signal intensity for both the Gly 85 HN cross peaks one of which can be associated with with the *cis* conformer of Pro 87 and the second the *trans* conformer; in the presence of TIR1, an effect enhanced by IAA (again to the point where no visible signals remain in the spectrum).

The equal binding ability of Gly 85 HN cross peak when Pro 87 is in the *cis* or *trans* conformations is not observed for Arg 90 HN cross peak. This difference may relate to the position of Arg 90 compared to Gly 85, as the two residues are on the opposite sides of a hair-pin structure formed by Trp 86 and the di-proline motif of the degron core in the AXR3 (DI and DII) protein (Figure 4.6A). The residue Arg 90 which is C-terminal to the hair-pin structure shows that the *cis* Pro 87 population binds more strongly to the receptor TIR1 when compared to the *trans* Pro 87 population, as indicated by the decreases in signal intensity in the spectrum (Figure 4.6E).

Importantly the region of the protein local to Arg 90 with a *trans* Pro 87 can still bind to TIR1, unlike the limited interaction displayed by region close to Trp 86 with Pro 87 in the *trans* conformation. In combination the NMR data shows that residues across the degron can interact with TIR1 even in the absence of IAA. This interaction with TIR1 can occur outside of the central degron core (WPP) when Pro 87 is in the *cis* or *trans* state but is selected for by the *cis* conformer of Pro 87 in the region on residue Trp 86 which promotes a stronger interacton.

There are also indications of more weaker interactions between TIR1 and regions of AXR3 away from the degron. This is shown by TIR1 and auxin induced chemical shift changes of Leu 42 and Lys 76 where the effect appears localised to the immediate surrounding residues. Residue 42 is intriguing as it is part of the secondary EAR motif. The function of these more transient interactions within the auxin receptor complex is uncertain.

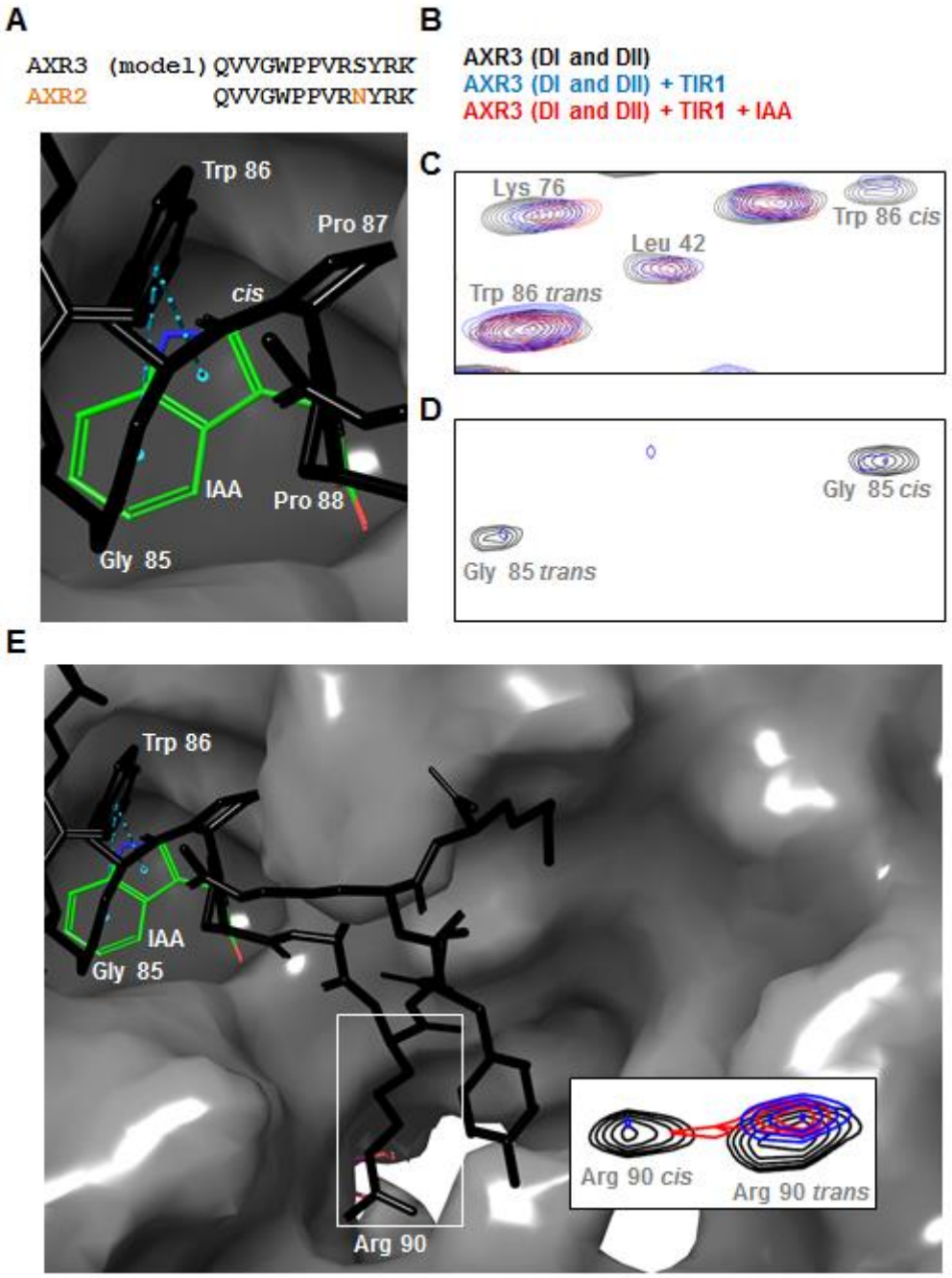

Figure 4.6 Conformational selection for the binding of the central degron core (WPP) to TIR1 and evidence for Aux/IAA binding to TIR1 in the absence of auxin. (A) Amino acid sequence of the AXR3 degron aligned with the AXR2 degron. Only residue 93 is different between the two peptides. Asn 91 in AXR2 was replaced with serine to model the AXR3 peptide. The peptide was modelled bound to the receptor TIR1 and IAA. The molecular model is shown below the degron sequence. The model presents a view above the auxin binding pocket with the degron core of AXR3 inserted into this pocket. The residue positions of Gly 85 and Trp 86 are annotated. (B) to (D) Gly 85 and Trp 86 were studied using a ^{1}H-^{15}N HSQC spectrum for AXR3 (DI and DII) as previously observed in Figure 3.17. (B)

Key for the colour coding of the NMR signals: AXR3 control (black), AXR3 and TIR1 (blue), AXR3 with TIR1 and IAA (red). (C) Two sets of NMR signals were observed for Trp 86 in *cis* and *trans* isomer states of Pro 87. These are annotated on the spectrum ^{1}H-^{15}N HSQC. Chemical shifts and a decrease in signal intensities were observed for the *cis* isomer in the presence of TIR1 with the effects enhanced with IAA. Small chemical shifts were observed for the *trans* isomer. Chemical shifts induced by TIR1 and IAA were observed for residues outside of the degron at residue positions Lys 76 and Leu 42. (D) The *cis* and *trans* isomer states for the Gly 85 NMR signals. (E) An extended view of the molecular surface of the auxin receptor complex focusing on the C-terminal end of the degron and residue Arg 90, which is observed orientated down into a second cavity on the TIR1 receptor. Arg 90 is highlighted by a white box. NMR signals of Arg 90 from AXR3 (DI and DII) protein are presented.

4.2.3 A small defined region C-terminal to AXR3 degron core interacts with TIR1

The molecular model of the AXR3 peptide forming the auxin receptor complex provides a limited view of the Aux/IAA interaction with the receptor TIR1 (Figure 4.7A to B). The C-terminal half of the degron is observed to extend out of the auxin binding pocket and into a second cavitity on the TIR1 surface, a feature discussed in more detail in chapter 5. Here, we investigate the extent of the interaction with TIR1 beyond the C-terminal half of the degron.

NMR was used to study the residues beyond Lys 94, following the NMR signals along the carbon backbone. The NMR data used for this analysis was from the ^{1}H-^{15}N HSQC experiment of AXR3 (DI and DII). As previously seen in section 4.3.2, spectra of the AXR3 (DI and DII) with TIR1 and in the presence and absence of IAA were overlaid. This allowed the comparison of the NMR signals for the identification of chemical shifts and decreases in signal intensity.

This analysis has included the degron residues Arg 90 and Ser 91, which both show signs of a strong interaction with TIR1, even with no IAA (Figure 4.7C). As previously seen in section 4.3.2, Arg 90 preferentially binds when Pro 87 is in the *cis* conformation. This is the last residue in this region of the

degron to display two distinct populations for *cis* and *trans* isomers, with only one NMR signal being observed for Ser 91.

Beyond the consenus sequence of the degron, Asn 95 shows a chemical shift and decreases in signal intensity in the presence of TIR1 (Figure 4.7C). Importantly, the signal intensity is observed to be equal for Asn 95 with TIR1 in the presence and absence of IAA and indicates that binding of this residue is auxin-independent. Further along the carbon backbone the extent of the chemical shifts and signal intensity differences diminishes from Val 96 and Met 97. Together, these results suggests a specific region C-terminal to the degron core interacts with TIR1.

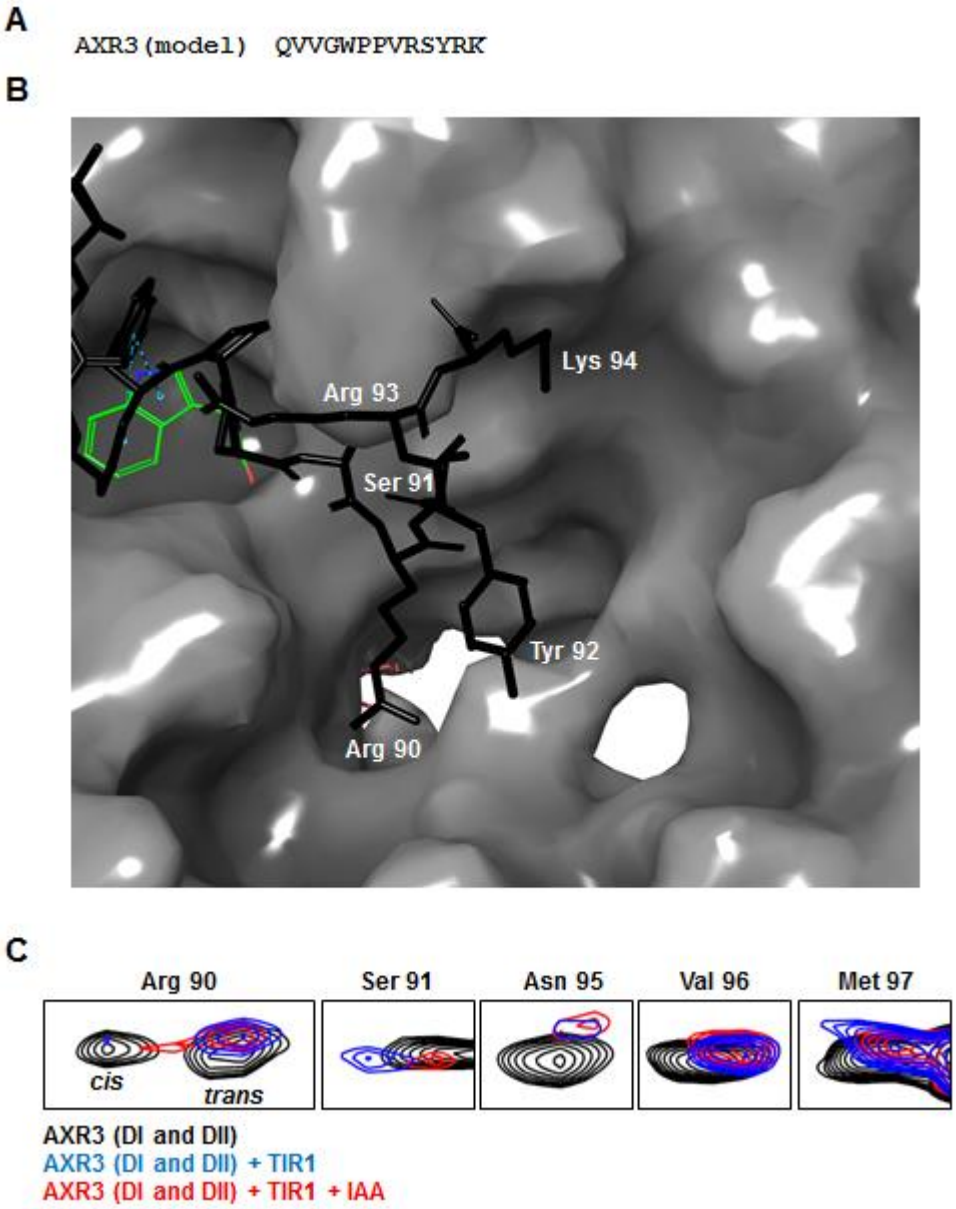

Figure 4.7 Specific region C-terminal to the degron core of AXR3 may interact with TIR1. (A) Amino acid sequence of the AXR3 degron used in the computational modelling of the auxin receptor complex. (B) Molecular model of the AXR3 degron peptide forming the auxin receptor complex. The presented view focuses on the C-terminal half of the degron positioned over the second cavity on TIR1. The modelled peptide was based on crystal structure 2P1Q and terminates at Lys 94. (C) NMR signals from ^{1}H-^{15}N HSQC spectrum of AXR3 (DI and DII). The NMR signals presented are of residues from Arg 90 and Ser 91 located within the modelled degron, and residues C-terminal to the degron up to Met 97. The key for the colour coding of the NMR signals is shown below this sequence of images.

In contrast residues N-terminal to the degron are observed to form limited interactions with TIR1 even in the presence of IAA (Figure 4.8). This was

shown by analysis of residues Ala 79 to Gln 82 from the ^{1}H-^{15}N HSQC spectrum of AXR3 (DI and DII). Overlaying spectra of the AXR3 (DI and DII) protein with TIR1 in the presence and absence of IAA showed limited chemical shifts and indicate weak interactions.

Modelling the auxin recptor complex formed by the AXR3 degron peptide using Maestro Schrodinger suite indicated that Gln 82, in the N-terminus of the peptide, is positioned outside of the auxin binding pocket (Figure 4.8). The weak interaction of the residues N-terminal to the degron (Ala 79 to Gln 82) coincide with an absence of further surface cavities in this particular location of the TIR1surface, which is in clear contrast to the C-terminal end of the degron.

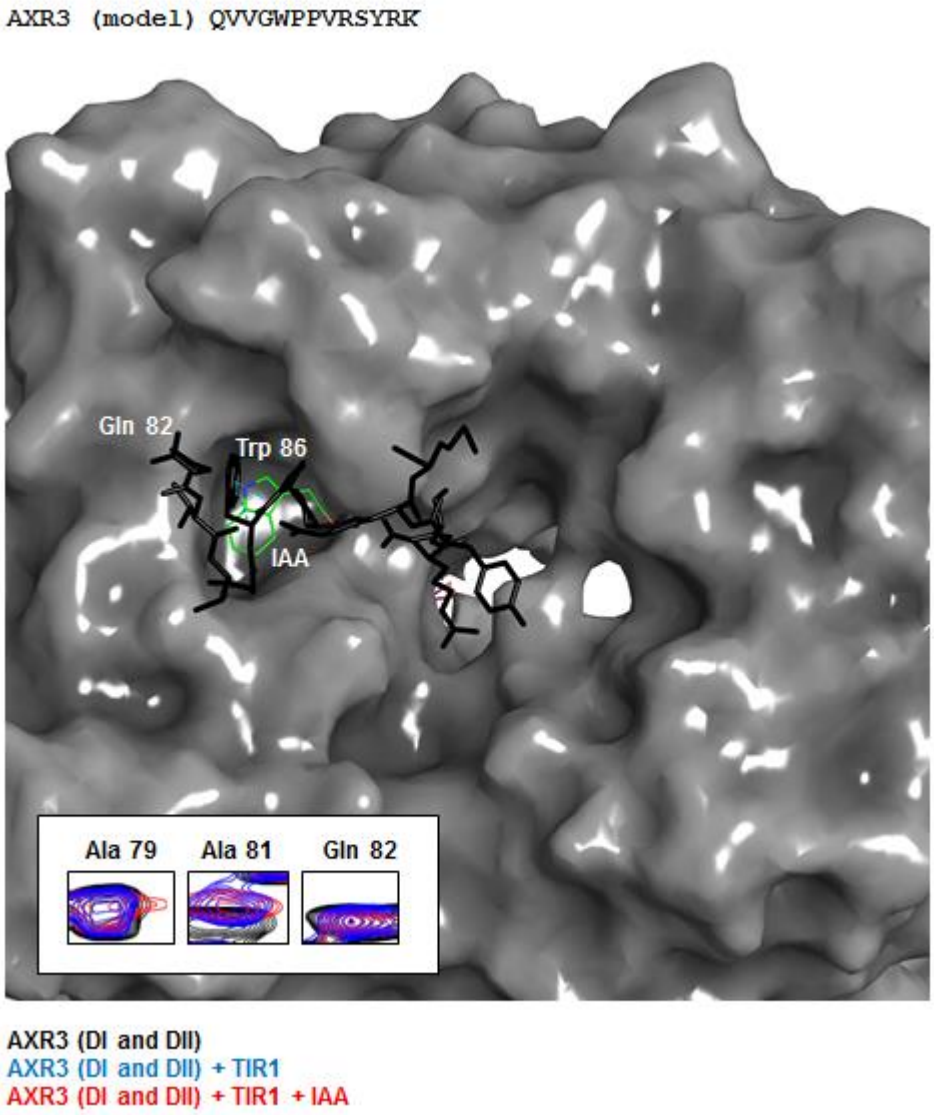

Figure 4.8 Limited binding to TIR1 observed for residues N-terminal to the degron. Molecular surface of the auxin receptor complex formed with the AXR3 degron peptide. The sequence of the AXR3 peptide modelled is shown above the image. The N-terminus of the peptide is at Gln 82 and is observed above the auxin binding pocket. Overlaid onto this model are images from the NMR analysis of the AXR3 (DI and DII) for residues immediately N-terminal to the degron. Ala 79 to Trp 86 were studied in the ^{1}H-^{15}N HSQC spectrum by overlaying spectra for the AXR3 (DI and DII) with TIR1 in the presence and absence of IAA. Key for the colour coding of the NMR signals: AXR3 control (black), AXR3 and TIR1 (blue), AXR3 with TIR1 and IAA (red). Limited chemical shifts were observed for these residues.

4.2.4 Evidence for co-receptor function of AXR3

Here we investigate a possible co-receptor function of the Aux/IAA protein AXR3. It is known from crystalography that the auxin molecule IAA binds to the same binding pocket of TIR1 as the degron peptide of an Aux/IAA protein. An interesting question is whether Aux/IAAs and auxin can interact independently of TIR1/AFBs.

We unexpectedly discovered evidence for this TIR1 independent interaction within an SPR assay. A high concentration of IAA (400 µM) was passed over a surface immobilised with AXR3 degron peptides (Figure 4.9A). The resulting response was recorded showing a binding curve (Figure 4.9B). This response curve showed a slow dissociation phase, which did not return back to base-line by the end of the experiment.

A further insight into the possible location of the interaction between IAA and the AXR3 degron is derived from my molecular model of the AXR3 degron. The model shows the possibility of an electrostatic interaction between the ring structures of IAA and Trp 86 when in close proximity within the auxin binding pocket (Figure 4.9C and D). This arrangement is studied further in chapter 5, focusing on the AXR2 degron peptide as part of our own analysis of the 2P1Q crystal structure.

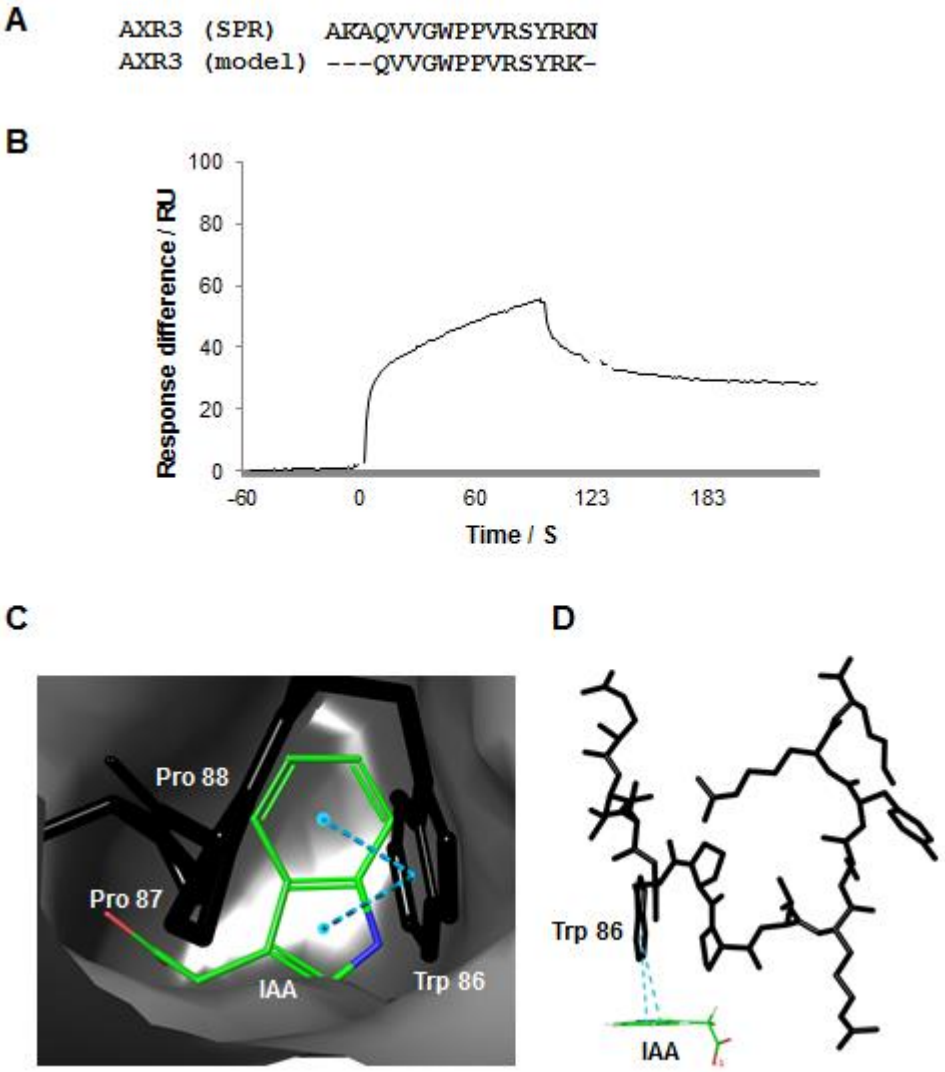

Figure 4.9 Evidence for IAA interacting with the degron of AXR3. (A) Sequence alignment between the AXR3 degron peptides used in SPR and in the molecular model. (B) SPR assay showing IAA interacting with the AXR3 degron in the absence of TIR1. (C) Molecular model of the auxin receptor complex with the AXR3 degron peptide, viewed from above the auxin binding pocket. The model of this complex indicated the potential for an electrostatic interaction (blue dashed-line) between the lower ring of Trp 86 and the two rings of IAA. (D) The electrostatic interaction between IAA and Trp 86 of the AXR3 degron peptide viewed with the molecular surface of TIR1 hidden.

The IAA interaction with the degron was further studied by using mutated peptides of the AXR3 degron series. This series of peptides contains residue replacements of the degron core, based on *axr3* mutants. The changes

include the replacement of Pro 88 with leucine in axr3-1, and Val 89 with glycine in axr3-3 (Figure 4.10A). These residue replacements did not abolish the interaction with IAA, with only small differences in the maximum responses levels between the peptides (Figure 4.10B). This SPR assay shows that the residues effected in axr3-1 and axr3-3 may not be directly involved in the interaction with IAA.

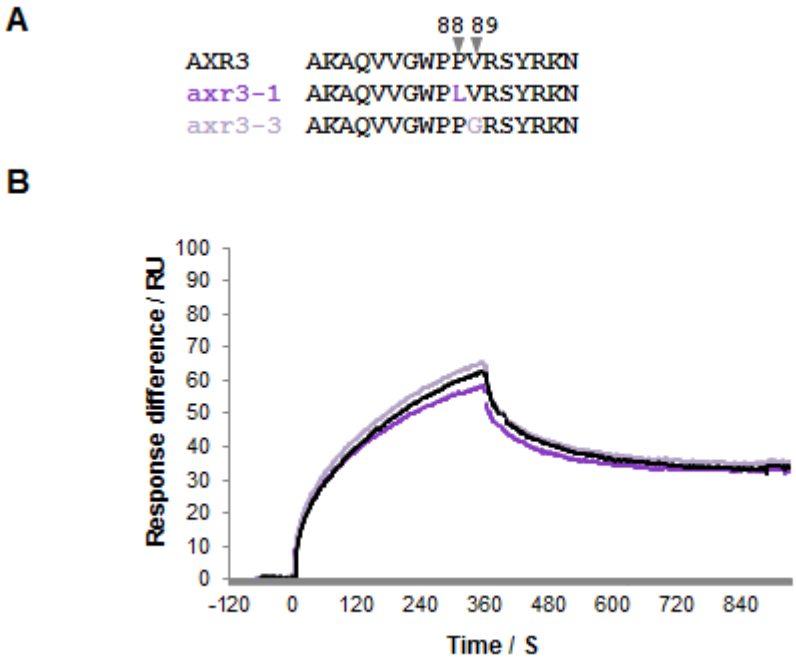

Figure 4.10 Residue changes in within the AXR3 degron series does not abolish the interaction with IAA. (A) Amino acid sequence alignment of the AXR3 series degron peptides used in the SPR assay. Changes to the amino acid sequence are coloured. The peptide axr3-1 sequence replaces Pro 88 with leucine, and axr3-3 replaces Val 89 with glycine. (B) SPR assay with the AXR3 series of degron peptides to screen for binding with IAA in the absence of TIR1. The response curves are colour coded according to the degron peptide of the AXR3 series: AXR3 (black-line), axr3-1 (dark-purple-line), axr3-3 (light-purple-line).

SPR was used to further explore the interaction between IAA and the AXR3 degron (Figure 4.11A) by expanding the assay to screen a larger range of compounds. These compounds included tryptophan, a metabolic precursor of IAA with no known auxin activity. The SPR response curve for this

compound showed a low response level which steadly decreased during the injection, indicating an unstable interaction with the degron (Figure 4.11B).

The synthetic auxins 2,4-D and 1-NAA showed similar low responses as tryptophan (Figure 4.11B). Such low responses reduce the confidence of describing these compounds as having a binding curve. Within this low response, small differences were observed between 2,4-D and 1-NAA, with 2,4-D forming a possible binding plateau almost immediately at the start of the injection. This is in contrast to 1-NAA which showed a gradual increase in its response during the injection of the compound. Both these compounds show an increase in the response level towards the end of the assay.

In contrast to the other synthetic auxins tested, picloram was observed to have a higher maximum response compared to IAA, followed by a rapid dissociation in contrast to the slow dissociation of IAA (Figure 4.11 B). These results show that not all synthetic auxins are as effective as IAA for interacting with degron, demonstrating structural specificity for a stable interaction.

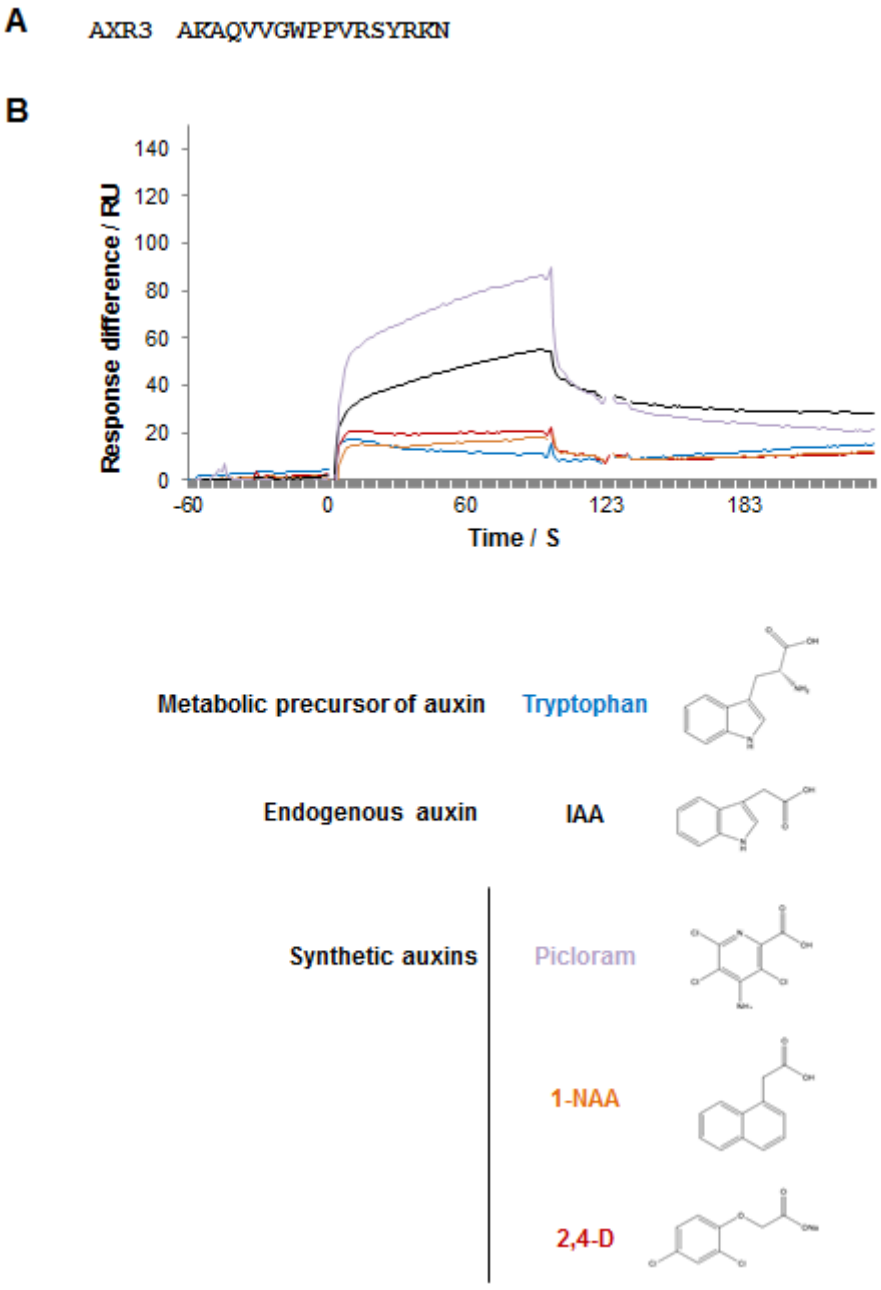

Figure 4.11 SPR assay for degron binding to synthetic auxins in the absence of TIR1. (A) Amino acid sequence of the AXR3 peptide used in the SPR assay. (B) SPR assay of the AXR3 degron peptide with a range of synthetic auxins in the absence of TIR1 protein. IAA is the positive control, compared with tryptophan which is a metabolic precursor of auxin with no known function in auxin signalling. Response curves are overlaid and colour coded according to the chemical compound. The colour coding associated with the chemical compounds tested in the SPR assay are the following: tryptophan (blue -line), IAA (indole-3-acetic acid) (black -line), picloram (4-amino-3,5,6-trichloropicolinic acid) (purple -line), 1-NAA

(1-naphthaleneacetic acid) (orange -line), and 2,4-D (2,4-dichlorophenoxyacetic acid) (red -line). All SPR response curves were corrected for non-specific binding.

The unexpected discovery of a potential low affinity interaction between IAA and the AXR3 protein was tested further with the ^{1}H WaterLOGSY NMR experiment. The WaterLOGSY experiment is based on the principle that the population of a small molecule binding to a larger molecule can be detected by a change in the signal intensity of the smaller molecule, after selectively inverting the water signal, due to enhanced magnetisation transfer via water bound to the larger molecule (Meyer and Meyer *et al*., 2001). In this study the signal intensities of the IAA molecule were recorded in a WaterLOGSY experiment in the presence and absence of the AXR3 protein (Figure 4.12A). The protein used was the full-length version of the AXR3 (DI to DIV) to achieve the required size difference for WaterLOGSY to be effective. A range of IAA concentrations were tested, from a AXR3:IAA ratio of 1:40 to a ratio of 1:200 with a protein concentration of 15 µM. Our analysis showed that a difference in signal intensity for IAA was recorded and this was dependent on the ratio of protein to ligand (figure 4.12A).

The data from WaterLOGSY shows evidence for a low affinity interaction. This data was used to estimate a theoretical dissociation binding constant (K_D) of approximately 430 µM. This was an average of K_D values calculated for each of the selected four proton signals associated with the ring structure of IAA within the NMR spectrum, at an IAA concentration of 1200 µM. The K_D values were calculated based on the equation 1. (Dalvit *et al*., 2001), where I is the recorded signal intensity difference of IAA in the presence and absence of the protein; L is free ligand concentration (IAA); and I_{max} is the maximum signal intensity recorded.

Equation 1: $K_D = [(I_{max} - I) / I]L$

Isothermal titration calorimetry (ITC) was used to further test this interaction. In this ITC experiment the N-terminal half of the AXR3 (DI and DII) protein was used. Injection of IAA (4 mM) into a solution of AXR3 (DI and DII) protein resulted in an exothermic signal for the interaction which decreases in intensity as the ratio of protein to ligand is increased (Figure 4.12B). Which is not seen in the control experiment when IAA (4 mM) is injected into

buffer (Figure 4.12C). This ITC result supports the SPR and WaterLOGSY observations.

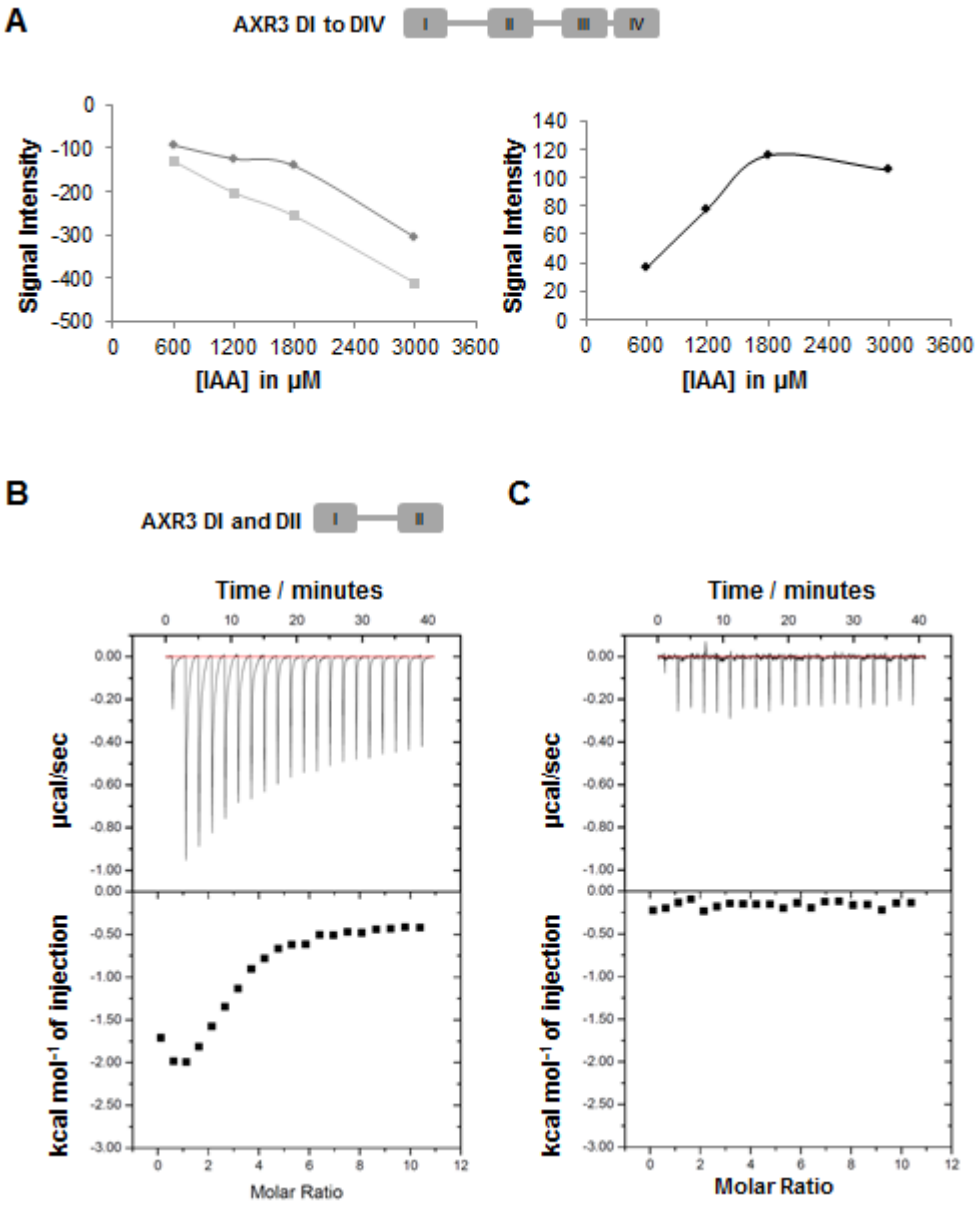

Figure 4.12 AXR3 forms a low affinity interaction with IAA. (A) ^{1}H WaterLOGSY NMR analysis of IAA and AXR3 (DI to DIV) full-length protein. Signal intensities were recorded for IAA over a range of IAA concentrations. The data set consist of: the control of IAA in absence of AXR3 (DI to IV) protein (grey-line), IAA in the presence of 15 µM AXR3 (dark grey-line), and the difference between these recorded signal intensities of IAA (black-line). The observed change in signal intensity indicates binding between IAA and the AXR3 (DI to DIV) protein. (B) ITC measurements of the injection of IAA into AXR3 (DI and DII) protein. Top panel shows the recorded injection peaks. Lower panel shows the area underneath each of the injection peaks. (C) The control data set of IAA injection into sample buffer.

4.2.5 Conformational selection for IAA binding to the degron

In this section, the effect of *cis-trans* isomerisation on the interaction between IAA and the degron has been investigated. The ^{1}H-^{15}N HSQC NMR experiments has been used to search for IAA binding in the two isomer populations for residues of the degron, from Val 84 to Arg 90. As this is a low affinity interaction only small $^{15}N/^{1}H$ chemical shifts were identifed by comparing the signals from ^{1}H-^{15}N HSQC spectra of AXR3 (D and DII) in the presence and absence of IAA (Figure 4.13). These small chemical shifts were observed for a specific subset of the degron residues. The *trans* isomer population for residues N-terminal to the di-proline motif from Val 84 to Trp 86 showed evidence for an interaction with IAA, indicated by a small chemical shift. Our results suggest there may be conformational selection for the binding to IAA to the N-terminal degron.

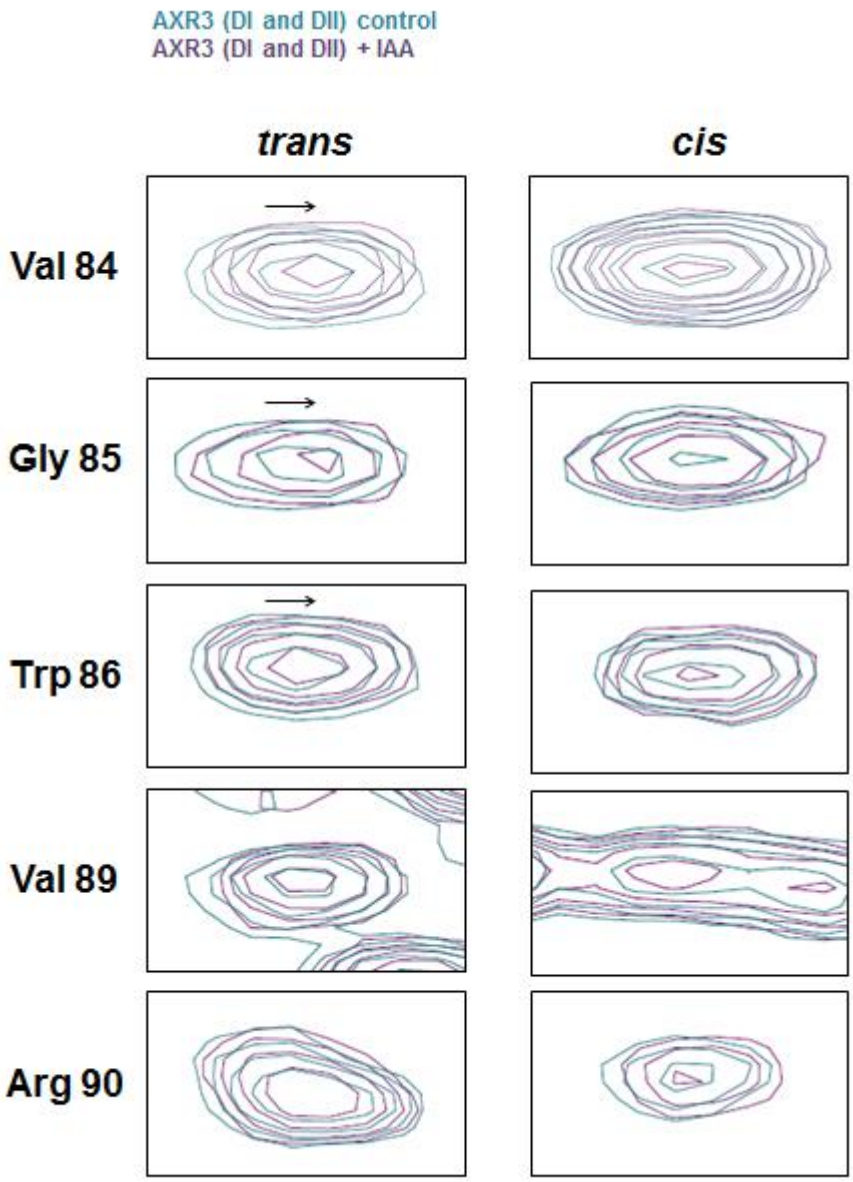

Figure 4.13 IAA forms a low affinity interaction with the N-terminal degron when Pro 87 is in the *trans* conformation. Overlaid NMR signals from HSQC spectra of AXR3 (DI and DII) protein in the presence and absence of IAA. The NMR signals are colour coded: the control with no IAA (blue-tone), plus IAA (purple). The residues presented here are from the AXR3 degron, Pro 87 and Pro 88 are not included. Each of these residues has distinct signals from the *trans* and *cis* isomer populations of the protein at residue Pro 87. The NMR signals for each residue have been presented in two columns for the *cis* and *trans* isomer states of Pro 87. A small chemical shift is observed with the addition of IAA (ratio of AXR3:IAA, 1:40). This shift is annotated with black arrows. The chemical shift was observed only for the residues within the N-terminal half of the degron and when Pro 87 is in the *trans* state.

4.3 Discussion

4.3.1 Conformational selection of the degron core (WPP) in AXR3, during auxin receptor complex formation

Our results are consistent with the hypothesis that conformational selection controls the binding of the central degron core of AXR3 to the receptor TIR1. Only a specific region of the AXR3 protein displays this conformational selection, where Trp 86 forms a hairpin structure with the di-proline motif of the central degron core, an arrangement observed by my analysis of the crystal structure 2P1Q. It is in the Pro 87 *cis* conformation that Trp 86 has been observed to bind strongly to the receptor with the *trans* state being considerably weaker.

Conformational selection of degron core (WPP) is consistent with previous observations from crystallography of the auxin receptor complex, which shows the prolyl amide bond between Pro 87 and Trp 86 in the *cis* conformation when bound to the receptor TIR1 (Tan *et al*., 2007). It is known from studies of peptides that a tryptophan adjacent to a prolyl bond promotes the occupancy of the *cis* state to 25 % (Wu and Raleigh, 1998). This is in contrast to our results for the prolyl bond in the N-terminal half of the Aux/IAA protein AXR3 (DI and DII) where the *cis* conformation is observed around 50 % of the time.

It is expected that the tryptophan adjacent to the prolyl bond in the degron will have a stabilising effect on the *cis* conformation due to electrostatic stacking between the rings (Thomas *et al*., 2006), which would normally be associated with an occupancy of around 25 % for a peptide (Wu and Raleigh, 1998). Furthermore, the di-proline motif is also likely to contribute to the *cis* frequency (Dasgupta *et al*., 2007). Since a higher population of the *cis* conformer is observed in our study, it suggests additional stabilising factors are involved from the wider protein structure of the N-terminal half of AXR3 (DI and DII).

The effects of the *cis-trans* isomerisation are not restricted to the prolyl amide bond between Pro 87 and Trp 86, as residues Val 84 to Arg 90 are

associated with pairs of NMR signals which can be assigned to states with the *cis* and *trans* isomers of Pro 87. This observation is consistent with previous studies on *cis-trans* isomerisation, where changes in geometry are propagated outwards from the site of bond rotation (Fischer, 2000).

Cis-trans isomer selectivity of the central degron core (WPP) for the binding to the receptor TIR1 and also appears to influence the strength of interaction for residues further along the carbon backbone, as seen for Arg 90 when Pro 87 is in the *cis* state. Our results indicate that Trp 86 is a key determinate of Aux/IAA binding to TIR1, where specificity is introduced into the interaction by *cis-trans* isomerisation of Pro 87. When Pro 87 is in the *cis* conformation a strong interaction with TIR1 is enabled, presumably by insertion of the WPP motif into the auxin binding pocket (Tan *et al*., 2007).

4.3.2 Evidence for an encounter complex phase during auxin receptor complex formation

Residues on either side of the central degron core hair-pin structure of AXR3 (WPP) appear to be able to bind to TIR1 when Pro 87 is in the *trans* state. As indicated by chemical shifts and intensity changes for the Gly 85, N-terminal to Trp 86 and Arg 90 in the C-terminal position. This is in contrast with Trp 86 which appears not to form a strong interaction with TIR1 when Pro 87 is in the *trans* conformation. These results may represent a transient or weaker interaction not captured by the crystallography of the auxin receptor complex (Tan *et al*., 2007).

Furthermore, an interaction between the degron of AXR3 (DI and DII) and TIR1 is observed in the absence of IAA. This IAA-independent binding was observed for all the degron residues studied with the exception of Trp 86 when Pro 87 is in the *trans* state. Residues Arg 90 to Met 97 are of particular interest as they can interact with TIR1 outside of the auxin binding pocket. Our analysis of the crystal structure 2P1Q shows this region of the degron within a second cavity adjacent to auxin binding pocket on the TIR1 surface.

In contrast, residues N-terminal to the degron, Ala 79 to Gln 82 (observed with only one NMR signal each), are observed to form weak interactions with TIR1. The computational modelling of the AXR3 degron peptide shows the

N-terminus is located immediately above the auxin binding pocket. It is therefore likely that residues N-terminal to the degron are positioned above the edge of the TIR1 receptor where there are apparently no further cavities to promote binding.

Although an interaction with TIR1 is possible without IAA, the small molecule is observed to increase the strength of the interaction. This latter observation is consistent with previous studies where IAA increases the affinity of the receptor for Aux/IAA binding, acting as molecular glue (Tan *et al*., 2007). Together, these results support a hypothesis where the degron of an Aux/IAA can form a transient encounter complex with TIR1, developing and enhancing our understanding of auxin receptor complex formation.

4.3.3 The co-receptor functions of AXR3

Our results have shown that IAA forms a low affinity interaction with the AXR3 protein; with an estimated K_D of approximately 430 µM. NMR spectroscopy has indicated the location of the interface is within the degron of AXR3, N-terminal to the di-proline motif which includes residues Val 84 to Trp 86. These findings support the hypothesis that an Aux/IAA acts as a co-receptor in auxin perception (Villalobos *et al*., 2012)

Even though this interaction was observed in the absence of TIR1, the low affinity binding of IAA to the AXR3 degron is most likely to occur with its co-receptor partner. This is consistent with the previously proposed co-receptor hypothesis (Villalobos *et al*., 2012). It is possible that TIR1 acts to bring together IAA and the Aux/IAA protein during an encounter complex phase, increasing the probability of this interaction occurring. For example, the auxin-independent binding of the Aux/IAA to TIR1 might stabilise the structural motif responsible for the apparent direct binding of IAA to the Aux/IAA. This idea of a functionally distinct encounter complex is especially intriguing in light of the finding that residues of the N-terminal degron (Val 84 to Trp 86) must be in the more open conformation when Pro 87 is in the *trans* state to enable the interaction with IAA. This is in contrast to the observed *cis* prolyl amide bond of the degron when bound inside the auxin binding pocket (Tan *et al*., 2007). The findings raise the possibility of an

encounter phase involving the *trans* conformation of Pro 87 in AXR3, where there is an opportunity for IAA to interact with the degron, either alone or in conjunction with TIR1, to aid complex formation. In this scenario, the assembly of the auxin receptor complex would then progress from the encounter complex phase with the isomerisation of the Pro 87 into the *cis* conformation for insertion into the auxin binding pocket. Such a scenario would not preclude the existence of other modes of complex formation, including the simple, sequential and independent binding of auxin and then the Aux/IAA to TIR1. In this case it is, however, worth noting that the affinity of IAA binding to TIR1 in the absence of Aux/IAA is very low (~40 µM (K_D), Quareshy and Ramans Harborough, unpublished).

The conformational changes within the degron core may also coincide with the reorientation of the IAA molecule and relates to one of the first models for auxin binding. The model proposed by Kaethner in 1977 consisted of the IAA structure changing its shape from a recognition conformation to a modulation state, where the carboxyl side chain becomes perpendicular to the plane of the indole ring (Kaethner, 1977). Within this IAA binding model conformational rearrangement of IAA was facilitated by a partner molecule. We propose that this partner for conformational change could be the Aux/IAA protein and may form part of the hypothesised co-receptor functions of AXR3.

Kaethner proposed that an auxin could only be functional if the molecule could undergo the reorientation of carboxyl side chain between the two main conformational states (Kaethner, 1977). We hypothesise that this functionality may be partly due to the ability IAA to interact with the degron. It is a possibility that the low affinity interaction reported here is due to an aromatic interaction between the ring structures of IAA and Trp 86, representing an important recognition interface for auxin perception (Cozzi *et al*., 1995).

The crystal structure 2P1Q shows these two aromatics arranged perpendicular within the auxin binding pocket (Tan *et al*., 2007). Therefore, it is likely that any aromatic interaction between these rings will correspond to an edge-face stacking model (Hunter and Sanders, 1990; Hunter *et al*.,

2001, Waters *et al*., 2002, Martinez *et al*., 2012). Such an interaction between Trp 86 and IAA may be enhanced when the carboxyl side chain of IAA is in the modulation state. This is because the electrostatic potential of the indole ring is considered to be increased by the carboxyl-side chain, displacing the electron cloud of the IAA ring structure (Schmit *et al*., 2011).

The observation that the synthetic auxins 2,4-D and 1-NAA may form limited interactions with the degron, while picloram can form a rapid association, may relate to changes in electrostatic potential across these molecules and their ability form an aromatic interaction with Trp 86. In the case of picloram the three Cl side groups are expected to displace the electron cloud to the margins of the ring structure and consequently alter the geometry of the aromatic stacking with Trp 86 (Hunter *et al*., 2001). A similar electrostatic distribution is expected for 2,4-D, but the longer side chain may create steric clashes as the molecule interacts with the degron limiting any potential interaction. In the case of 1-NAA the lack of an NH group is expected to decrease the polarisation across the ring structure and therefore the strength of the aromatic interaction. We suggest that these compounds should be modelled and analysed in ^{1}H-^{15}N HSQC NMR experiments to test these hypotheses.

Furthermore, a limited interaction between the degron and tryptophan is most likely to be associated with the longer carbon backbone of the carboxyl side chain compared to IAA. This may reduce the effectiveness of the carboxyl side chain to displace the electron cloud across the ring structure. Together these findings indicate how specificity is introduced into the molecular interaction with degron through electrostatics.

This study has presented evidence for an early phase in formation of the auxin receptor complex not observed in previous crystallography. NMR spectroscopy has shown that the interaction between the degron core and TIR1 involves conformational selection of the central degron core (WPP) in the AXR3 protein. We also propose that a transient encounter complex is formed by the degron when Pro 87 is in both the *cis* and *trans* states. By combining the results NMR spectroscopy with the SPR assays it seems possible that AXR3 may have a limited function as a co-receptor for IAA

binding. This possible co-receptor function is likely to occur in partnership with TIR1 to provide two halves of a binding interface for IAA. We believe this is most likely to occur in the encounter complex phase, as the interaction with IAA was promoted with the N-terminal degron when Pro 87 was in the *trans* state. It is during the interaction with the degron that specificity may be introduced by an aromatic interaction between Trp 86 and IAA, providing an additional recognition element to auxin perception.

Chapter 5

Binding of an Aux/IAA to TIR1 is not simply controlled through the essential degron core

5.1 Introduction

The Aux/IAA protein family displays a range of degradation dynamics in the plant cell. This difference is shown by IAA28 and AXR3 transcriptional repressor proteins. The full-length protein of IAA28 has a half-life of approximately 80 minutes in vivo and is in contrast to AXR3 which has a much shorter half-life of approximately 10 minutes (Dreher *et al*., 2006). This difference in half-life is likely to reflect the sequence variation in the degron, influencing the ability of these proteins to form an auxin receptor complex with TIR1/AFBs.

Here we are interested in understanding how specific sequence variation can fine tune the events of auxin perception. In this section we will review the effects of mutations within the degron core, revealing differences in the contribution that different residues make to receptor complex formation. Furthermore, we will consider the increasing number of reports which suggest regions outside of this core region can influence the degradation dynamics of Aux/IAA proteins.

The function of the degron core sequence of VGWPP has been well established as forming the main binding interface with the receptor TIR1 (Ramos *et al*., 2001; Tan *et al*., 2007). When this binding event is disrupted by the single amino acid replacement of any degron core residue it results in increased stability of that Aux/IAA protein within the plant cell (Ramos *et al*., 2001; Guseman *et al*., 2015). This accumulation of Aux/IAAs has severe implications on auxin signalling and therefore plant morphology (Worley *et al*., 2000), with the severity of the phenotype closely linked to the residue within the degron core which is mutated. This variation is observed in the *axr3* mutant series where *axr3-1* shows a more pronounced reduction in root length and agravitropic phenotype compared to *axr3-3* (Leyser *et al*., 1996;

Rouse *et al*., 1998). The residues affected in these two mutants are in close proximity which makes their difference in severity the more intriguing.

The *axr3-1* mutation replaces Pro 88 with leucine; while *axr3-3* replaces Val 89 with glycine. Two other mutations *shy2-2 and axr2-1 are* similar to *axr3-1* in that they affect the di-proline motif at the centre of the degron core. In this case, *shy2-2 and axr2-1* share the same modification where Pro 87 is replaced by serine (Tian and Reed, 1999; Nagpal *et al*., 2000). These mutations within the di-proline motif exhibit agravitropic root phenotypes and indicate that auxin signaling has been disrupted, presumably by altering the interaction with the auxin receptors in the plant.

Although a degron core modification may negatively affect receptor complex formation, it is possible that the interaction is not completely abolished. This was indicated by a previous study on peptides of the degron shy2-2. The peptide was shown to have a reduced interaction with TIR1, but still retained the ability to respond to IAA's promotion of complex formation (Tian *et al*., 2003).

Such changes to the degron core indicate that interactions between other regions of the degron and the TIR1 receptor may have a functional role, with sequence variation in these regions a possible factor to Aux/IAA degradation dynamics. The C-terminal half of the degron is of particular interest, as alanine replacement of residues Arg 93 and Lys 94 in the degron consensus sequence, increases Aux/IAA stability in the plant cell (Ramos *et al*., 2001).

Regions outside of the degron may also have an influence on Aux/IAA protein binding to the receptor. This has been demonstrated in truncation studies of Aux/IAAs where full-length and N-terminal (DI and DII) proteins have a more rapid degradation compared to proteins of just the DII region (Havens *et al*., 2012).

The un-conserved region of an Aux/IAA protein which links the degron (DII) and functional domain III may represent one of these additional binding interfaces with TIR1. It has been suggested that variation in the length of this region and not specific amino acid motifs influences Aux/IAA degradation dynamics (Moss *et al*., 2015). These findings are consistent with the previously reported truncation studies, suggesting that the regions C-

terminal to the degron core are an important influence on degradation dynamics of Aux/IAA proteins.

Here this study has used a combination of computational modelling and biophysical assays to investigate why modifications to the degron core have different severities in mutant phenotypes and how this may inform our interpretation on auxin receptor complex formation. In addition, we investigate the degron flanking motifs of IAA28 and AXR3 and their effects on the stability of the auxin receptor complex.

5.2 Results

5.2.1 The AXR2 degron peptide extends over two cavities on the TIR1 surface with only the degron core inserting into the auxin binding pocket

The computational modelling software Maestro Schrodinger suite was used to perform our own analysis of the Tan *et al.*, 2007 crystal structure (2P1Q) in order to explore the auxin receptor complex. The structure is composed of two different ligands bound to the same binding pocket on the TIR1 receptor. These ligands are: the auxin IAA, and a thirteen amino acid peptide, representing the degron sequence of the Aux/IAA protein AXR2.

The TIR1 upper surface is observed to form a concave shape with the centre of the depression dominated by two adjacent cavities (Figure 5.1A). The depression is at the centre of two concentric rings of secondary structure, an outer ring of α-helices and an inner ring of β-strands (Figure 5.1B). It is in this depression where the AXR2 peptide is observed to bind, with the centre of the peptide inserting into a binding pocket with IAA. This particular cavity on the receptor is the auxin binding pocket (Figure 5.1C). The peptide also extends into a second cavity separated from the auxin binding pocket by a ridge in the TIR1 surface.

The portion of the peptide inside the auxin binding pocket is composed of the highly conserved centre of the degron core: Trp 86, Pro 87 and Pro 88. The arrangement of these residues forms a distinctive structural motif, which

can be described as a hair-pin structure (Figure 5.1D). The two conserved prolines bend the carbon backbone projecting the tryptophan residue outwards where it interacts with the bound IAA molecule at the bottom of the binding pocket. The interaction consists of two Pi-Pi bonds between the 6-membered ring of Trp 86 and the two rings of the IAA molecule. The observation of only the six-membered ring of Trp 86 forming the interaction corresponds with a perpendicular arrangement with the IAA ring structure. This interaction with IAA inside the auxin binding pocket may not be alone in enhancing interactions between Aux/IAAs and TIR1. Another important molecule, the TIR1 co-factor inositol hexakisphosphate (IP_6) can be seen at the base of the second cavity (Figure 5.1E).

The AXR2 peptide extends into this second cavity by bending through a narrow gap which separates the two TIR1 pockets (Figure 5.1F). This gap is partly enclosed by the TIR1 residue Phe 351, which protrudes outwards and above the pocket-separating ridge of the TIR1 surface. The degron peptide is shown to bend through this gap to extend across the two major cavities of the TIR1 receptor surface.

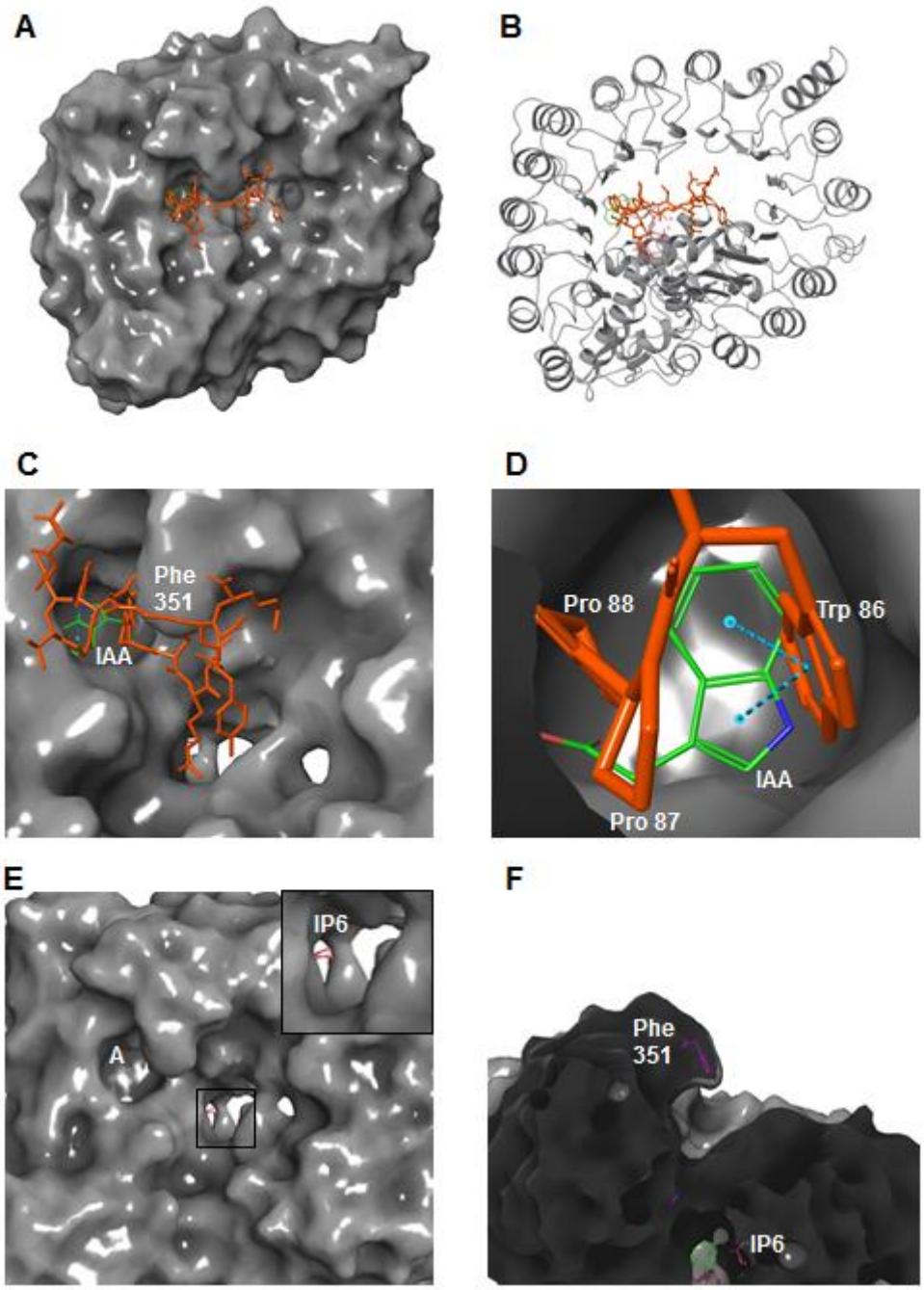

Figure 5.1 An observation of a major cavity adjacent to the auxin binding pocket in the TIR1 receptor. (A to B) The molecular model of the auxin receptor complex viewed from above. TIR1 receptor is shown in grey; AXR2 peptide is shown in orange; and IAA is displayed in green. (A) Shows the molecular surface of TIR1 and the location of the AXR2 peptide once bound. (B) Shows the secondary structure of TIR1 as a ribbon diagram. (C) A view above the TIR1 molecular surface where a large cavity is adjacent to the IAA binding pocket, separated by a ridge in the TIR1 surface. Phe 351 protrudes above this ridge structure. The AXR2 peptide is observed within the IAA pocket and extending into the second cavity. (D) A view directly above the IAA binding pocket. The residues Pro 87 and 88, and Trp 86 form

a distinct structure inside the IAA binding pocket where the ring structure of Trp 86 is perpendicular to the IAA ring. Two Pi-Pi bonds occur between these ring structures and are shown as dashed blue lines. (E) The molecular surface of TIR1 showing the two cavities without the peptide and IAA. The IAA pocket is labelled with a white capital A. IP_6 is visible at the base of the second cavity from its binding position underneath the TIR1 receptor. (F) A cross section through the molecular surface of TIR1 showing a profile of the space which separates the IAA pocket with the second cavity. The residue Phe 351 and co-factor IP_6 are annotated in the section.

5.2.2 Analysis of the degron core

The centre of the degron core extends into the auxin binding pocket from Val 89 with residues Pro 88, Pro 87, and Trp 86 directly within the pocket. Analysis of the auxin receptor complex has shown that the peptide bond between Trp 86 and Pro 87 is in a *cis* conformation (Figure 5.2A). The *cis* bond appears to bend the backbone allowing the Trp 86 ring structure to fit inside the binding pocket by positioning it parallel to the wall of the pocket. This tryptophan is adjacent to Gly 85 which leads the N-terminal end of the peptide outside of the auxin binding pocket.

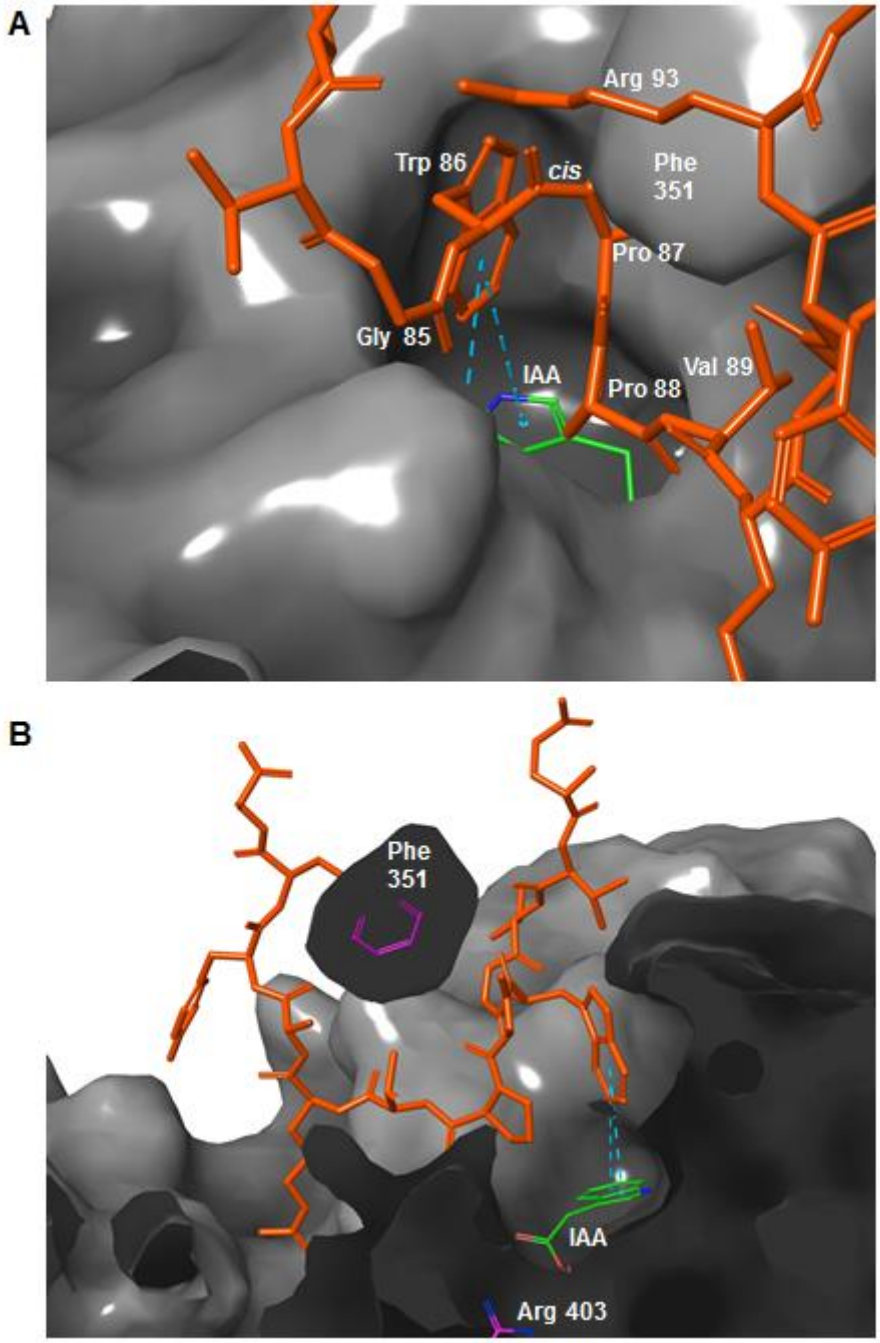

Figure 5.2 Computational model of the AXR2 peptide bound to the auxin binding pocket. (A) The molecular surface of TIR1 showing the approach to the IAA binding pocket and the structural arrangement of the AXR2 peptide carbon backbone (shown in orange). The carbon backbone of AXR2 enters the IAA binding pocket after Val 8, which is positioned above a ridge of the TIR1 surface separating the IAA pocket with the second cavity. Val 89 is directly underneath TIR1 residue Phe 351 which restricts access to the IAA pocket. Arg 93 of the peptide extends over the Phe 351 (TIR1). Pro 87 and Pro 88 bend the peptide backbone and together with Trp 86 form a distinct structure which occupies the upper half of the IAA binding pocket. The perpendicular orientation of Trp 86 relative to the IAA ring

(green) is clearly observed. (B) A cross section of the molecular surface of TIR1 showing a profile of the IAA binding pocket with the bound AXR2 peptide. The TIR1 residues Arg 403 and Phe 351 are annotated as they represent the lower and upper limits of the pocket respectively.

5.2.3 Residues of the C-terminal end of the degron peptide favour an orientation down into the second cavity

The second cavity is of particular interest both for its proximity to the auxin binding pocket and for the observation of IP_6 through gaps in the pocket's floor. The C-terminal end of the peptide is observed entering into this second cavity within the crystal structure. Our modelling has indicated that the preferred orientation of these C-terminal residues is to point downwards into the second cavity towards the negative charge of the IP_6 (Figure 5.3).

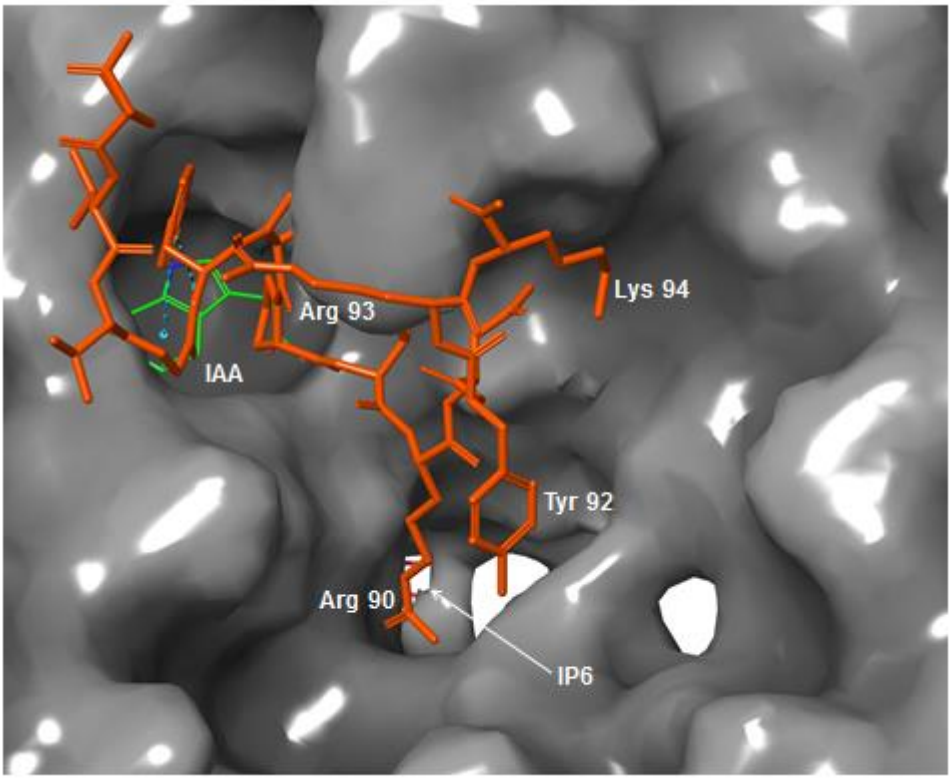

Figure 5.3 The AXR2 peptide extends down into the second cavity of theTIR1 receptor towards the location of IP_6. The IAA molecule and AXR2 peptide are shown bound to the molecular surface of the TIR1 receptor. Part of the AXR2 peptide is bound within the IAA binding pocket interacting with IAA molecule with two Pi-Pi bonds (blue dashed lines). The other half of the peptide extends down into

a large cavity which is observed adjacent to IAA binding pocket. This second cavity shows openings to the underside of TIR1 and to the location of IP_6. The molecular model shows the AXR2 peptide extending down into the second cavity with residues Arg 90, Tyr 92, and Lys 94 orientating towards the IP_6 molecule.

The possibility of IP_6 influencing the C-terminal end of the degron was further investigated through the spatial arrangement of these molecules. The best view of this arrangement came from removing the molecular surface of the receptor. This revealed the close proximity of the degron to both IAA and IP_6 (Figure 5.4A). The postion of IP_6 is intriging, as the molecule is not directly underneath the auxin binding pocket, but is instead centred underneath the degron.

The removal of the molecular surface of TIR1 from the model also reveals the full shape of the degron peptide. It is in this view that the unusual shape adopted by the centre of the degron core can be best appreciated. The model shows the carbon backbone bending at the location of the conserved di-proline motif to form the hair-pin motif with Trp 86 (Figure 5.4A and B). It is in this conformation that Trp86 interacts with IAA in the auxin binding pocket, a view now clear in this analysis.

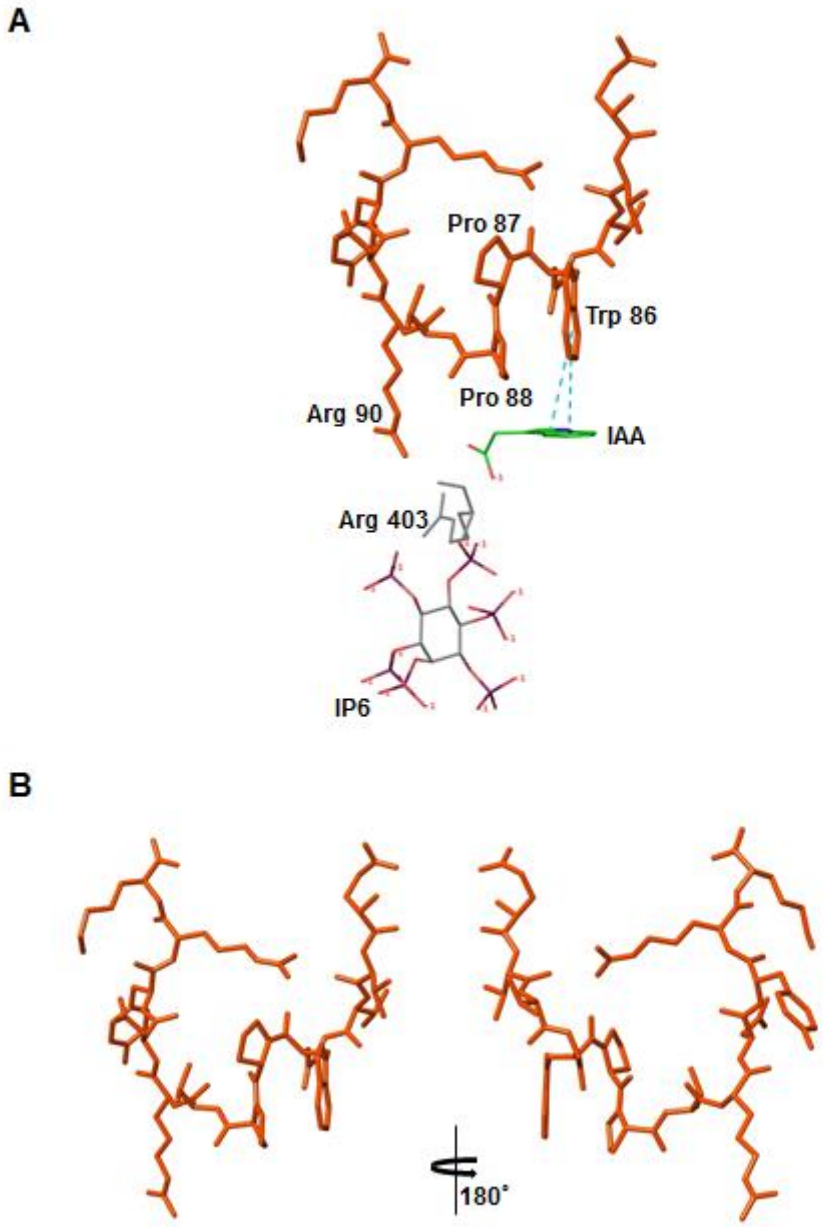

Figure 5.4 A view of the bound AXR2 peptide with the TIR1 surface not displayed. (A) The AXR2 peptide (orange) is shown in its bound form to the receptor with IAA (green); the co-factor IP_6; and the residue Arg 403 which forms part of the floor of the IAA binding pocket. The TIR1 receptor has not been displayed to allow a clear view of the structural conformation of the central degron core formed from Trp 86, Pro 87 and Pro 88. The model shows that Trp 86 interacts with IAA by forming two Pi-Pi bonds represented by the dashed blue lines. (B) Two profiles of the AXR2 peptide rotated 180˚.

5.2.4 Modifications in the AXR3 degron series affect residues at key postions in the interface with receptor TIR1

SPR assays were used to study the AXR3 degron series, which contain residue modifications within the conserved degron core. The two variants of the AXR3 degron sequence investigated here are: axr3-1 where Pro 88 is replaced with a leucine; and axr3-3 where Val 89 is replaced with a glycine (Figure 5.5A). Peptides of this degron series show very different responses in SPR assays (Figure 5.5B). The degron axr3-1 is observed to have the most severe effect in the SPR sensorgram with a maximum response very close to the base-line. Unlike axr3-1, the peptide axr3-3 more readily forms the auxin receptor complex but shows a faster dissociation phase, where k_{off} = 5.7 x 10^{-6} s^{-1} (The following X^2 value was obtained as a percentage of maximum response: = 20.17 %) compared to AXR3 = 3.7 x 10^{-3} s^{-1} (X^2 = 0.11 %). This results in the axr3-1 degron forming a binding plateau far more quickly than the unaltered AXR3 degron.

The Maestro Schrodinger suite was used to model these modifications to the AXR3 degron, with the degron peptides bound to the TIR1 receptor. When these models are overlayed. small differences in the predicted alignment between the carbon backbones are observed (Figure 5.5C).

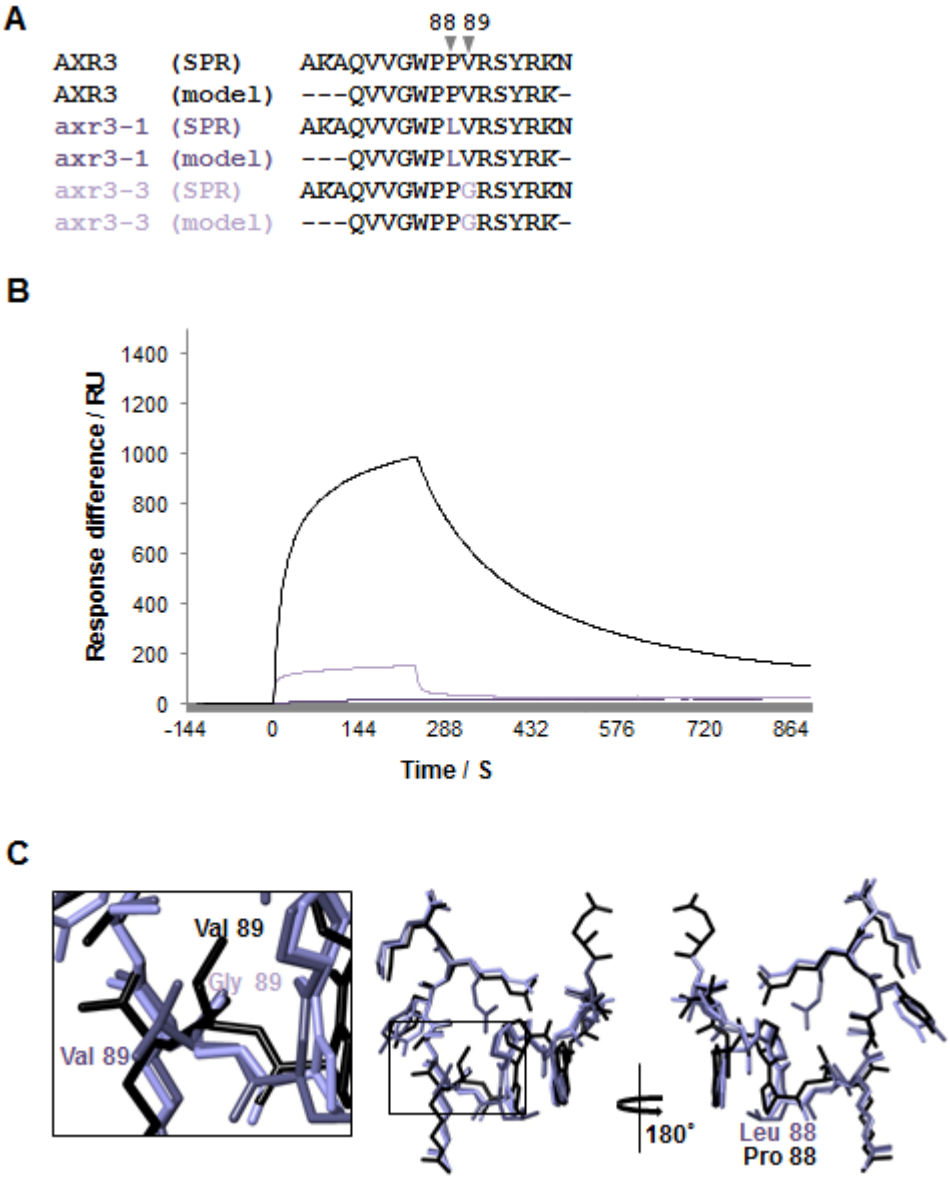

Figure 5.5 Observation on the biophysical effects of replacing residues in the degron core which from the AXR3 series. (A) Sequence alignment between the peptides of AXR3 series used in SPR analysis and those used in computational modelling. The axr3-1 peptide contains a valine to glycine modification relative to the AXR3 degron; axr3-3 contains a proline to leucine modification. These variations from the AXR3 degron sequence are coloured according to the peptide. (B) Sensorgrams from SPR analysis of the AXR3; axr3-1; and axr3-3 peptides represented by the black; dark purple and light purple lines respectively. The data are plotted as response units against time. The axr3-1 shows the lowest maximum response with a response curve close to the base-line. The axr3-1 peptide shows a lower maximum response compared to the AXR3 degron. The axr3-3 response curve forms a plateau soon after the injection of TIR1 and IAA. At the end of this

injection the dissociation of the axr3-3 peptide from the rest of the auxin receptor complex is observed to be rapid when compared to AXR3. The following k_{on} rates (M^{-1} s^{-1}) were calculated: AXR3 = 7.7 x 10^3, axr3-3 = 8.9 x 10^3. From the dissociation phase, the following k_{off} (s^{-1}) rates were calculated: AXR3 = 3.7 x 10^{-3}, axr3-3 = 5.7 x 10^{-6}. The following X^2 values as a percentage of the maximum binding response were obtained: AXR3 = 0.11 %, axr3-3 = 20.17 %. (C) Model of the carbon backbones of axr3-1 (light purple); axr3-3 (dark purple); and ARX3 peptides overlayed for comparison in their bound conformation. Two views of the peptide are shown at a 180˚ rotation. Differences in the backbone alignment are observed particularly at the sites of residue change, valine to glycine and leucine to proline. The positions of these residues are annotated on the peptide models.

The axr3-1 modification of Pro 88 to Leu 88 is located directly within the hydrophobic hairpin of the degron core (Figure 5.6A and B). Computer models of the axr3-1 and AXR3 peptides show this residue change alters the shape of the degron core, forcing Trp 86 to reorientate away from Leu 88 (Figure 5.6C). Despite this strucutral change, the axr3-1 modification does not alter the overall bend in the carbon backbone at the degron core as Pro 87 still remains. The model also indicated that conformational changes due to Leu 88 were not restricted to the degron core and extend along the carbon backbone, altering the orientation of Val 89 (Figure 5.6C).

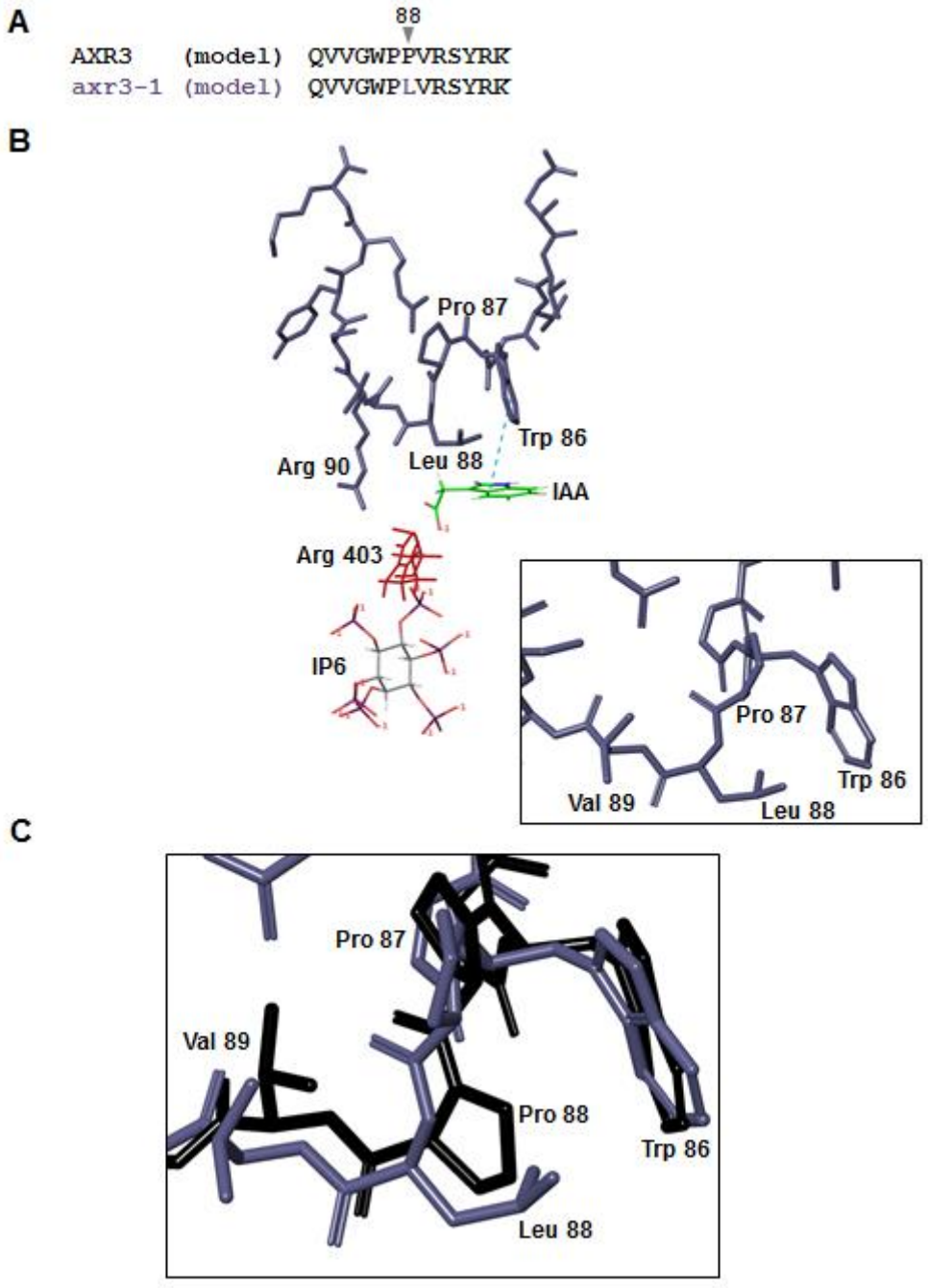

Figure 5.6 Molecular model of the axr3-1 degron. (A) Sequence alignment between the AXR3 and axr3-1 degron peptides used in computational modelling. (B) Model of the carbon backbone of axr3-1 viewed in the conformation when bound to TIR1. The molecules IAA and IP_6 are displayed along with the residue Arg 403 which represents the position of the auxin binding pocket floor. An enlarged image of the degron core is also presented, clearly showing the axr3-1 change of Leu 88. (C) A comparison between the computer models of the degron core for axr3-1 shown in dark purple and AXR3 shown in black. The residue change from

proline to leucine at position 88 is observed to alter the alignment of the carbon backbone in the degron core.

The axr3-1 peptide was modelled within the confines of the auxin binding pocket as the model was dependent on the orginal AXR2 peptide in the crystal structure 2P1Q. Consequently, the structural changes that are reported for axr3-1 had an impact on the auxin binding pocket within the model resulting in the reorientation of the TIR1 residues (Figure 5.7).

Such changes in TIR1 residue positions were observed by overlapping the models of AXR3 with axr3-1 (Figure 5.7A and B). A cross section through the molecular surface of TIR1 revealed that the residues affected were from positions all around the binding pocket and resulted in the auxin binding pocket being required to adopt a more open conformation to accommodate the axr3-1 peptide (Figure 5.7C). This is particularly noticeable in the upper regions of the pocket (Figure 5.7D).

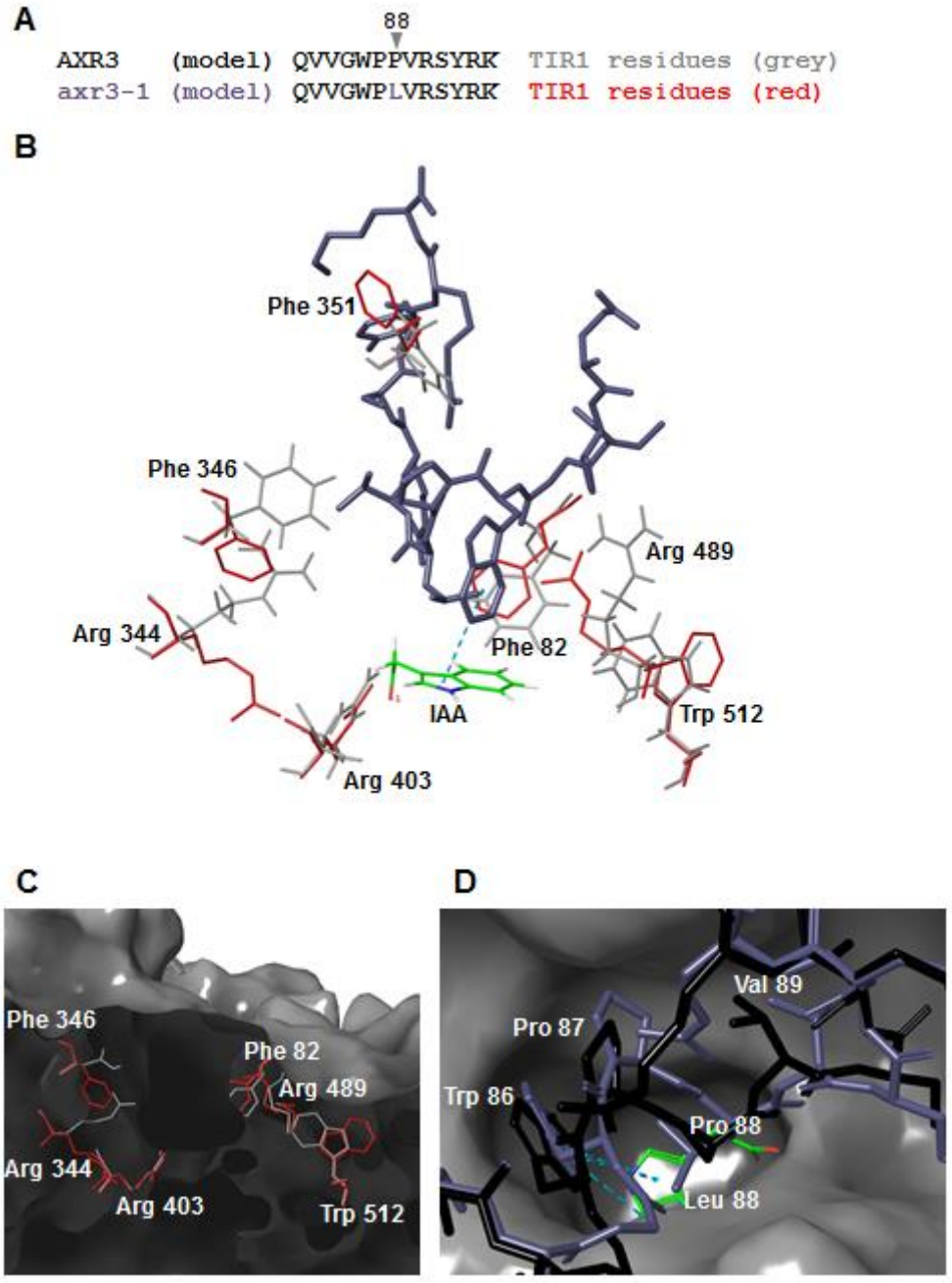

Figure 5.7 Computational modelling shows the residues of the binding pocket change position to fit axr3-1. (A) Sequence alignment of the residues of AXR3 peptide shown in black and axr3-1 with the residue Leu 88 highlighted in dark purple. These were the sequences used in computational modelling. The positions of TIR1 residues which change position are colour coded according to the computer model of the bound degron peptide. Grey indicates the TIR1 residues position when the AXR3 peptide is bound. Red indicates the new position of the TIR1 residues when axr3-1 is bound to the receptor (B) Computer model of axr3-1 carbon backbone showing the TIR1 residues of the binding pocket which change position

between the AXR3 and axr3-1 models. (C) Cross section through the molecular surface of the TIR1 receptor. The outline of the auxin binding pocket is observed surrounded by the residues of TIR1 which change position. (D) A view above the molecular surface of TIR1 above the auxin binding pocket from the axr3-1 bound computer model. The degron peptides of AXR3 (black) and axr3-1 (dark purple) are both displayed in their bound positions. The changes in the carbon backbone alignment between the two degron cores are clearly observed. The computer modelling fits the axr3-1 peptide inside a more open conformation of the auxin binding pocket.

The axr3-3 modification of replacing Val 89 with Gly is of particular interest (Figure 5.8A) as the change is affecting the region of the degron which forms the interface with the pocket separating ridge on the TIR1 surface (Figure 5.8B). Conformational changes due to the axr3-3 modification were studied by overlaying the modelled peptide of AXR3 onto axr3-3 model (Figure 5.8C). From this comparison only limited changes in the backbone alignment were observed with the Gly 89 modification causing a shift in the postion of the backbone into the auxin binding pocket (Figure 5.8D).

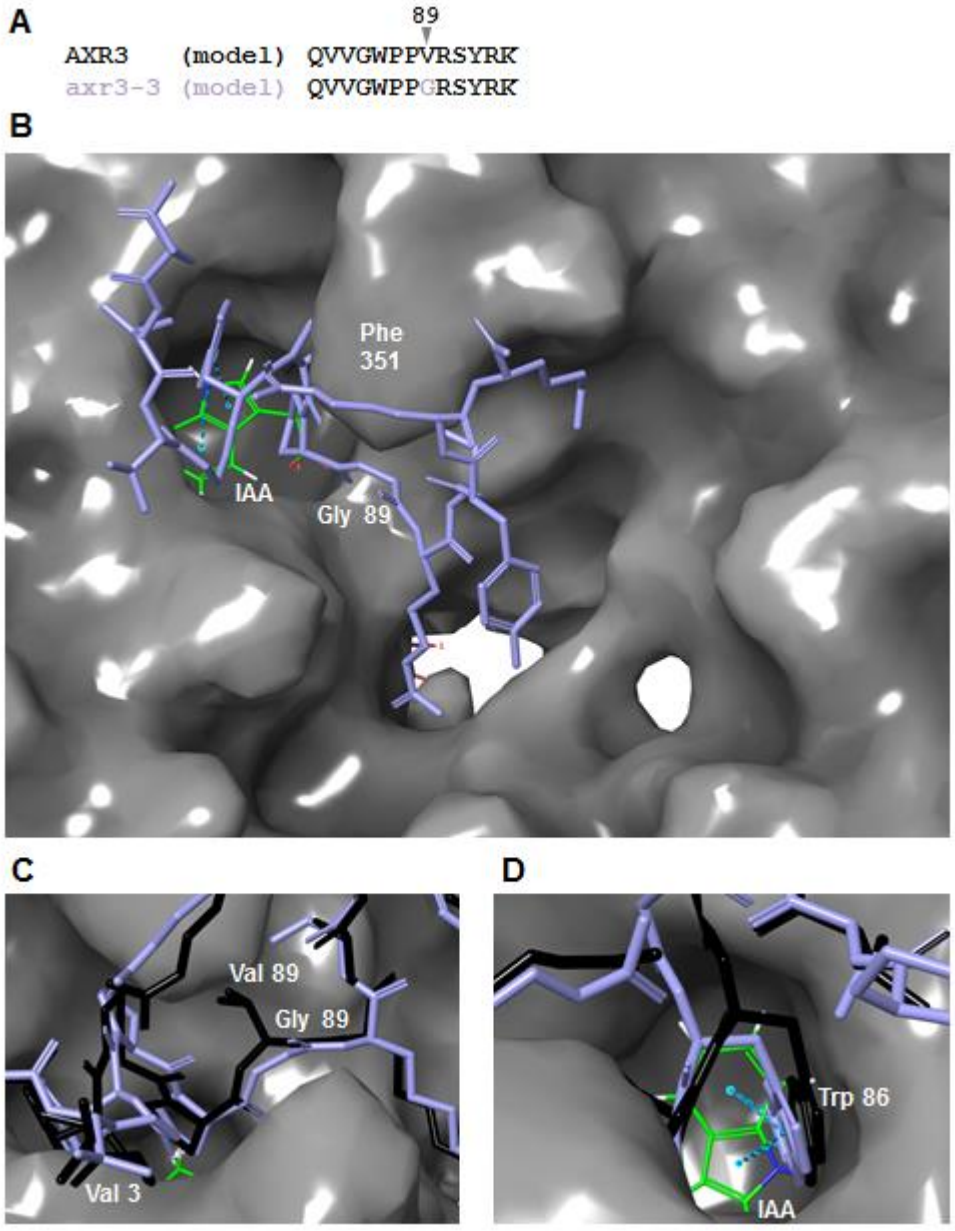

Figure 5.8 The residue at position 89 is where the degron peptide extends over a ridge separating the auxin binding pocket from the second cavity. (A) Sequence alignment of the residues of AXR3 shown in black, and the residue variation in axr3-3 is shown in light purple. These were the peptides used in computational modelling. The axr3-3 peptide contains one residue change from valine to glycine at position 89. (B) Computational model of the molecular surface of TIR1 viewed from above the second cavity. The axr3-3 peptide is displayed in light purple forming the auxin receptor complex. The position of Gly 89 in axr3-3 is annotated along with the IAA molecule in its binding pocket. (C) An enlarged image of the carbon backbone of axr3-3 at Gly 89 is displayed. The AXR3 peptide (black) is overlaid onto the model for comparison. The residue change at position 89 between AXR3 and axr3-3 is observed to occur above the TIR1 ridge which

separates the auxin binding pocket from the second cavity. (D) A view above the auxin binding pocket from the axr3-3 model. This shows the alignment of the carbon backbone between axr3-3 and the overlaid AXR3 degron core.

These observed conformational changes for the axr3-3 peptide resulted in only small changes in orientation for the majority of residues lining the auxin binding pocket (Figure 5.9A to C). Only the TIR1 residue Arg 489 was observed to show a large change in position (Figure 5.9B). This residue is situated within the upper region of the auxin binding pocket at the interface with the N-terminal degron region, where the peptide descends into the auxin binding pocket (Figure 5.9C). Our analysis showed that the misalignment of the axr3-3 backbone affected the orientation of Val 84 positioned directly above the TIR1 residue of Arg 489. Consequently, Arg 489 was observed to shift orientation.

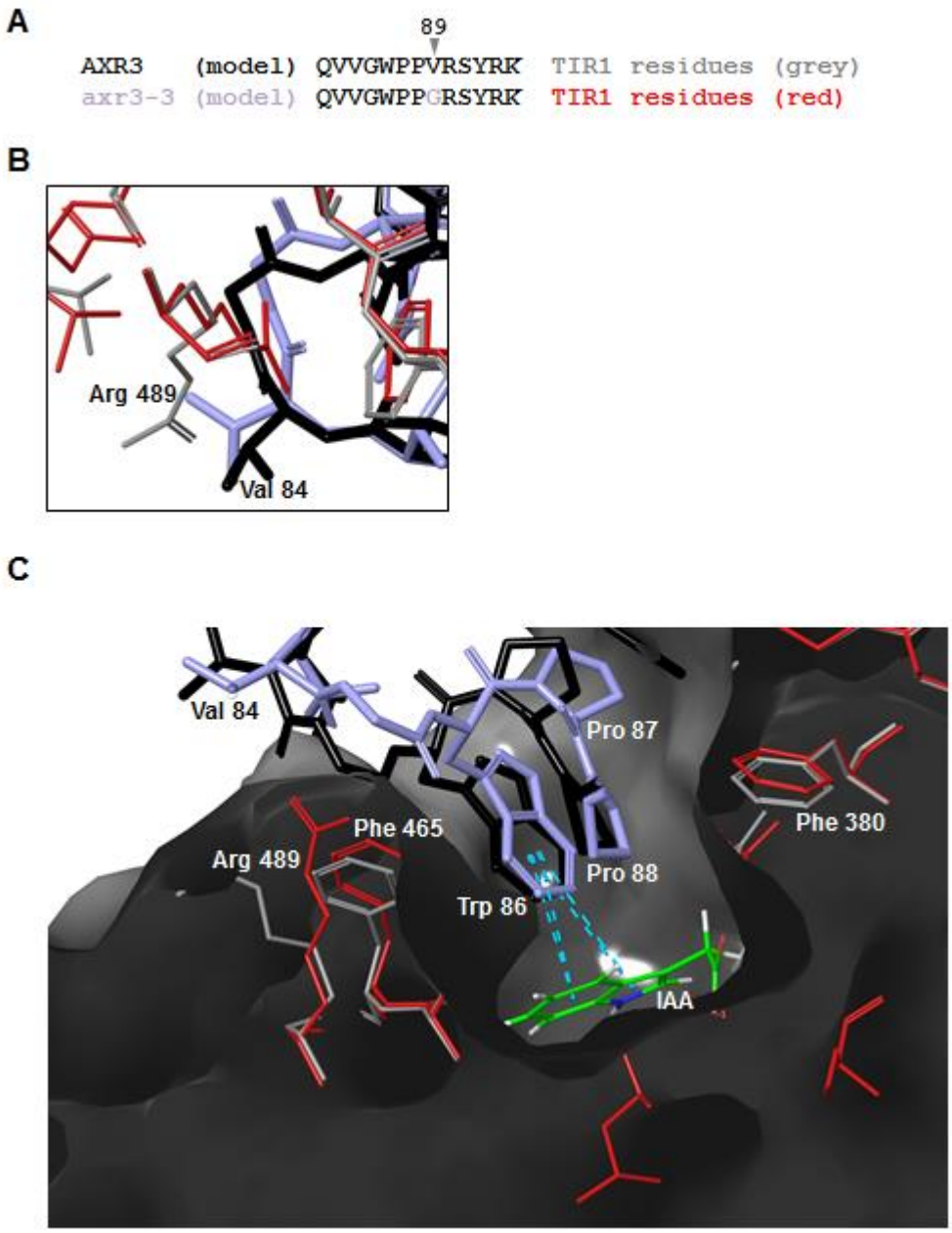

Figure 5.9 Changes in the auxin binding pocket associated with axr3-3 binding. (A) Sequence alignment for the degron peptides used in the computer modelling. The AXR3 sequence is shown in black and the residue change at position 89 in axr3-3 is highlighted in light-purple. Alongside the sequences are marked the colour coding used to display the TIR1 residues derived from the computer models associated with each peptide. (B) Computer model of axr3-3 peptide (light-purple) forming the auxin receptor complex. The TIR1 residues from this model are displayed red. Overlaid are the carbon backbone of AXR3 peptide (black) and the position of the TIR1 residues from the AXR3 model are shown in grey. The image focuses on Val 84 of the degron peptides which re-orientates between the two models. The TIR1 residue Arg 489 is observed to change position

from grey to red due to the repositioning of Val 89. (C) Computer model displaying a cross section through the molecular surface of TIR1. The image shows the repositioning of the TIR1 residue Arg 489 at the entrance to the auxin binding pocket. Smaller changes in the positions of residues around the binding pocket are also displayed. These include the TIR1 residues Phe 465 and Phe 380, which are also located towards the top of the auxin binding pocket.

5.2.5 The residue change of Val 83 to Ile alters the orientation of Trp 86 in the shy2-2 peptide

The peptide axr2-1 is a variant of the AXR2 degron with the conserved Pro 87 replaced with Ser. This residue change is also replicated in shy2-2, a variant similar to the AXR3 degron (Figure 5.10A). The degron shy2-2 peptide replicates an additional natural modification outside of the degron core where Val 83 is replaced with Ile. This modification occurs in a position of the degron directly above Trp 86 which is projected outwards to form the hydrophobic hairpin of the degron core (Figure 5.10B).

The computational model of axr2-1 shows that the modified Ser 87 does not affect the orientation of Trp 86 when the peptide is modelled within the confines of the auxin binding pocket (Figure 5.10C). This is in contrast to the model of shy2-2 where the Trp 86 shifts positon by 4.6 Å. This is a major change in the degron core conformation and corresponds with the residue change from Val 83 (AXR3) to Ile 83.

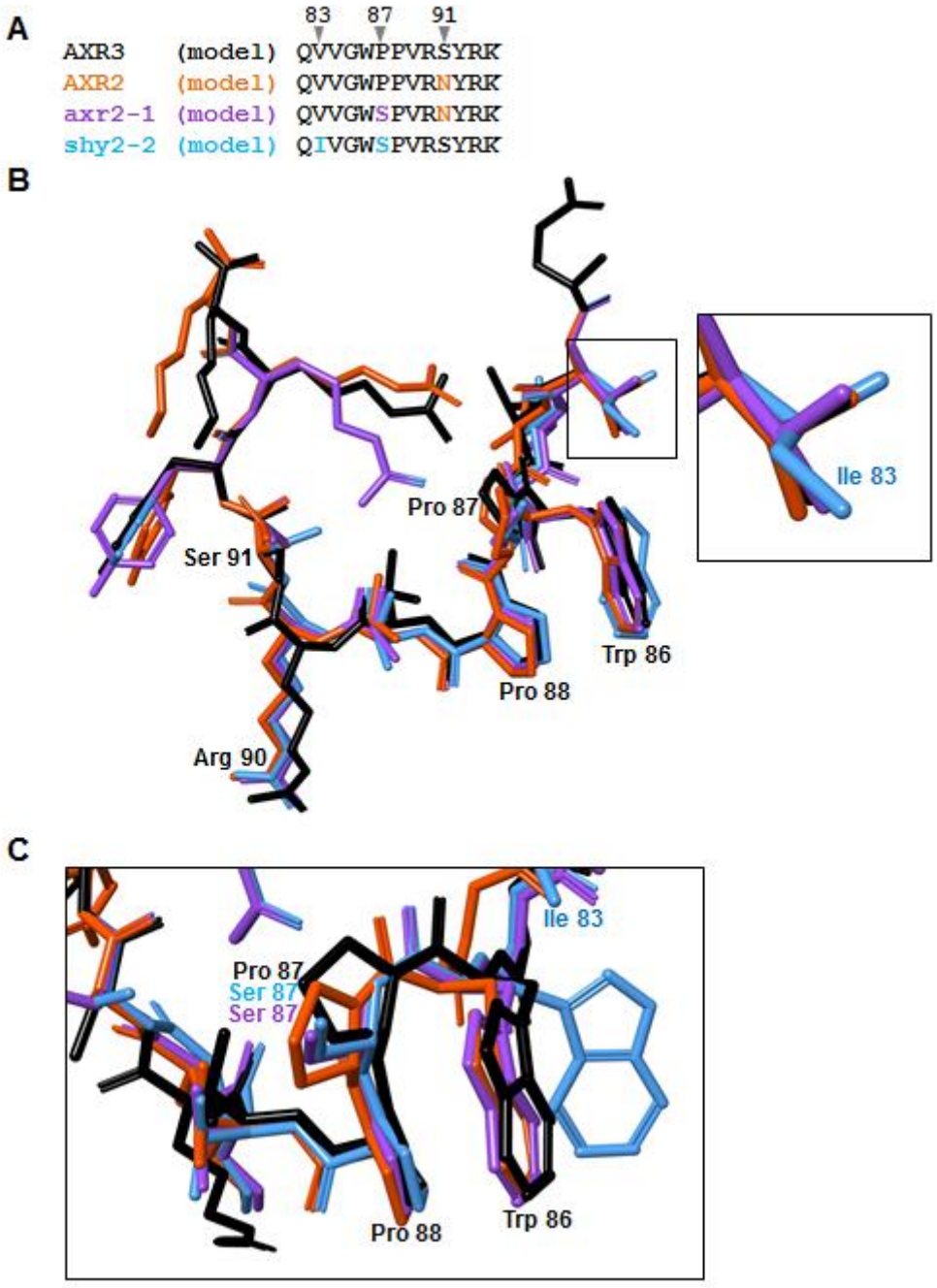

Figure 5.10 Residue Val 83 in the degron peptide is an important influence on the position of Trp 86. (A) Sequence alignment between the degron peptides used in the computer modelling. The sequence for AXR3 peptide is shown in black. Residue variation from the AXR3 sequence is highlighted for each peptide. (B) Computational model of the overlaid carbon backbones for the degron peptides: AXR3 (black); AXR2 (orange); axr2-1 (purple); shy2-2 (light blue). The peptides shown are in their bound conformation. An enlarged image focuses on the residue change in shy2-2 at position 83 from valine to isoleucine. Position 83 is in close proximity to Trp 86 in the degron core. (C) The peptides axr2-1 and shy2-2 both

contain the residue change of proline to serine at position 87. In addition shy2-2 contains the valine to isoleucine modification which can be seen above Trp 86. The shy2-2 model repositions Trp 86, with the residue moving by 4.6 Å from its position in the AXR3 peptide.

The new postion of Trp 86 is observed to alter the orientation of TIR1 residues forming the walls of the auxin binding pocket (Figure 5.11). The model shows that the more open conformation of the degron core is accommodated by shifting the orientation of the TIR1 residues particularly at the interface with Trp 86, with further adjustments extending around the pocket.

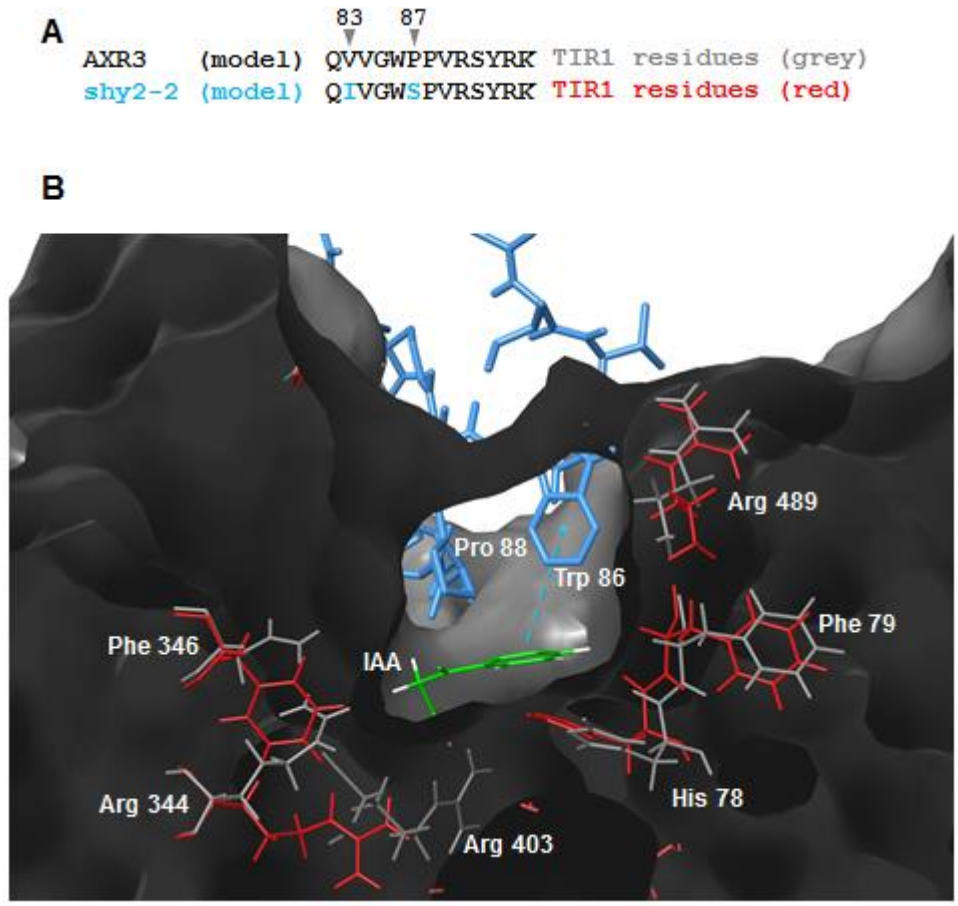

Figure 5.11 The auxin binding pocket changes shape to accommodate the new position of Trp 86 in shy2-2. (A) Sequence alignment between AXR3 and shy2-2 degron peptides modelled with Maestro Schrodinger suite. The change in TIR1 residue positions between the models are colour coded (Figure 17A). Only residues which show a change in position are displayed. TIR1 residue positions from the AXR3 bound model are shown in grey. These positions are overlaid onto the model for shy2-2 forming the auxin receptor complex. The new positions of

TIR1 residues as a result of fitting shy2-2 into the auxin binding pocket are shown in red. The changes are observed all around the auxin binding pocket. Arg 403 is displayed as a reference for the base of the binding pocket and is not observed to change position.

5.2.6 Regions of the degron outside of the auxin binding pocket affect the stability of the entire complex

Computational modelling and biophysical assays were used to investigate how residue variation in the regions flanking the Aux/IAA degron core (GWPPV) can influence association and dissociation of the auxin receptor complex. Such sequence variation is demonstrated by the auxin transcriptional repressor proteins AXR3 and IAA28, where the degron is different by only three residues (Figure 5.12A). Despite this small variation my SPR assays show that IAA28 degron peptide has a slower association phase and a faster dissociation phase compared to the AXR3 degron peptide (Figure 5.12B). Such different biophysical responses raised the question of conformational differences between the degrons.

To investigate this possibility, the Maestro Schrodinger suite software was used to simulate the structures of the AXR3 and IAA28 degron peptides. This was achieved by using the Maestro software to change the residues within the crystal structure of the AXR2 degron peptide. The resulting models were aligned to compare the carbon backbones of the AXR3 and IAA28 degrons in their receptor bound conformations. The resulting alignment showed limited conformational change between the two degrons (Figure 5.12C).

Our results highlighted that the sequence variation between AXR3 and IAA28 was occurring in the degron regions outside of the auxin binding pocket. The N-terminal sequence EVAP motif of IAA28 was only partly represented by the proline residue (Pro 82), which formed the terminus of this end of the degron within the crystal structure. This proline was positioned above the auxin binding pocket. At the opposite end of the peptide the C-terminal motif of SSRR was observed in the upper region of the second cavity (Figure 5.12D). Even though these changes were outside

of the auxin binding pocket, the residue modifications did cause the IAA28 degron core to adjust its position within the pocket (Figure 5.12E).

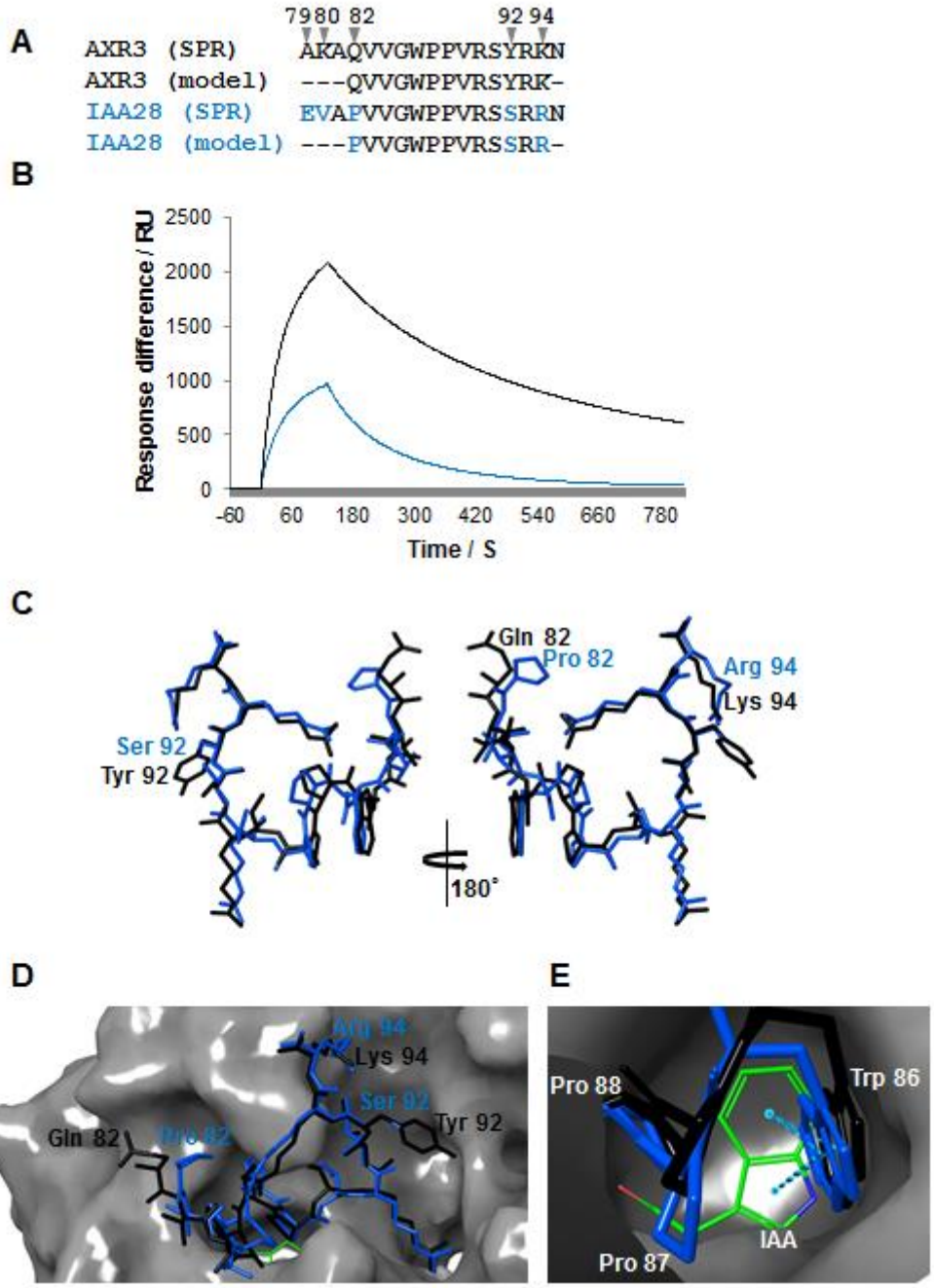

Figure 5.12 The degron peptides of IAA28 and AXR3 show different dynamics in auxin receptor complex formation and dissociation. (A) Sequence alignment between the peptides used in SPR analysis and the peptides used in computational modelling for both IAA28 and AXR3 degrons. Residues which are the same between IAA28 and AXR3 are shown in black and the differences in IAA28 are displayed in blue. (B) SPR analysis studying the IAA28 and AXR3 degrons. A sensorgram is shown as response units (RU) against time (seconds). The response curve for IAA28 is represented by the blue -line and the response curve of AXR3 is

represented by the black -line. A lower maximum response is observed for IAA28 compared to AXR3. The auxin receptor complex is observed to dissociate faster from the IAA28 peptide than the AXR3 peptide. (C) Model of the carbon backbones of IAA28 (blue) and AXR3 (black) peptides in the bound conformation. The models are displayed overlapped and show limited conformational divergence. The residues which vary between IAA28 and AXR3 are annotated and coloured corresponding to the peptide. (D) Model of the molecular surface of the receptor TIR1 displayed with the peptides IAA28 and AXR3 overlaped. The model shows that the residue variation between IAA28 and AXR3 are located outside of the IAA binding pocket. (E) A view above the model of the molecular surface of TIR1 showing the conformation of the degron core. A small change in the position of the degron core within the IAA binding pocket is observed between IAA28 and AXR3. The Pi-Pi interactions (blue dashed lines) between Trp 86 and the IAA ring are observed for both peptide models.

The biophysical differences between these degron peptides were further investigated, focusing on the effects of the IAA28 N-terminal and C-terminal sequence motifs within the AXR3 degron. Peptides were synthesised to replicate sets of IAA28 residue changes to the AXR3 degron sequence. This included the transition-P peptide, which refers to the replacement of glutamine 89 with a proline in the AXR3 degron sequence, as is the case in IAA28 (Figure 5.13A). The results showed that the new proline residue did not alter the association or dissociation of the auxin receptor complex with transition-P peptide, showing a similar sensorgram to AXR3 (Figure 5.13B). Computational modelling was used to visualise the transition-P peptide in its TIR1 bound state (Figure 5.13C). Comparison in the carbon backbone alignment of this transition peptide with AXR3 degron showed limited changes, with the degron modification occurring above the auxin binding pocket.

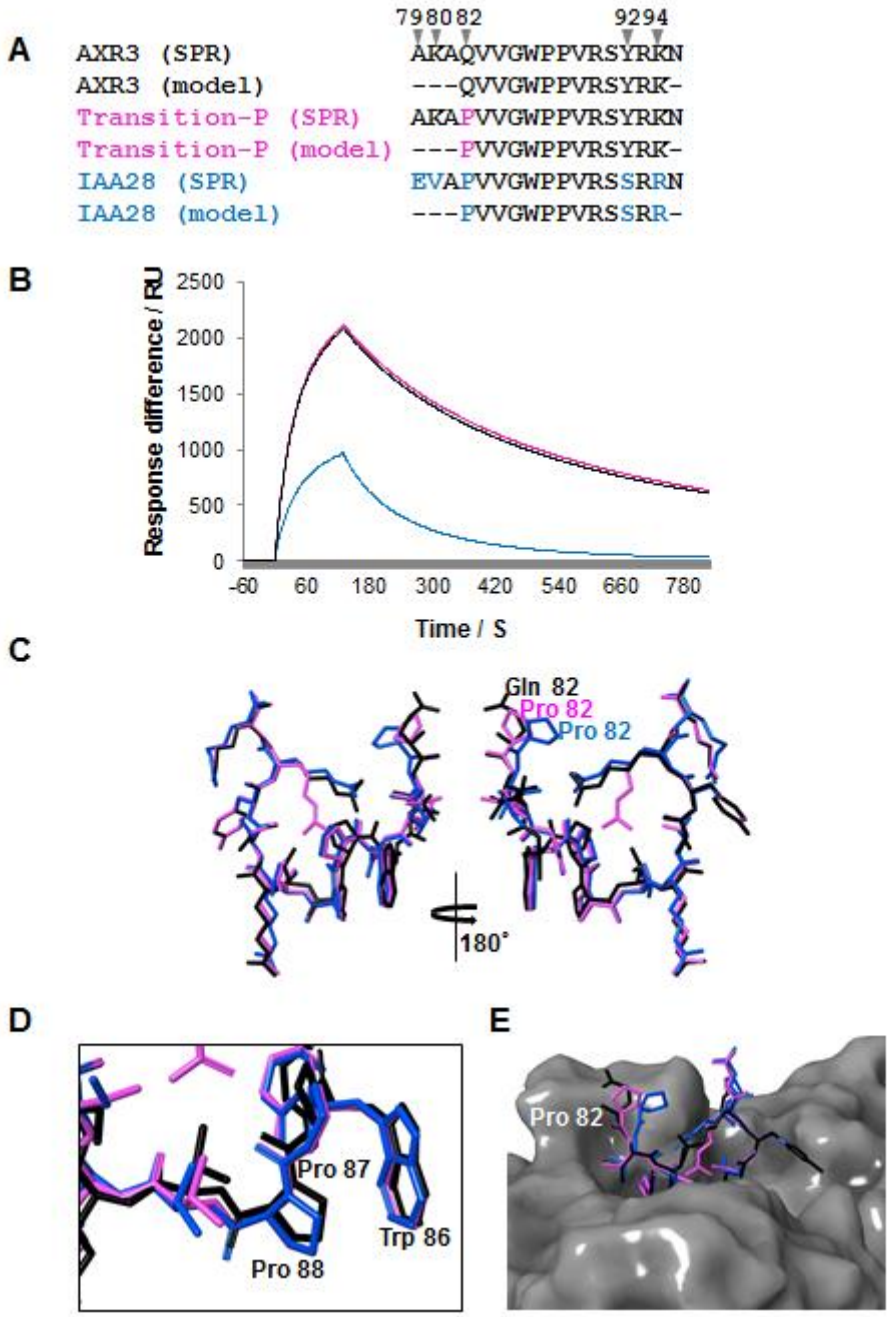

Figure 5.13 Transition-P peptide shows a similar SPR response to the AXR3 peptide. (A) Sequence alignment between the peptides used in SPR analysis and the peptides used in computational modelling. The sequences shown are for the transition-P peptide compared to the IAA28 and AXR3 degrons. Residues which are consistent with the AXR3 degron are displayed in black with variations coloured according to the peptide. The transition-P peptide has one residue change, glutamine to proline, from the AXR3 degron sequence. (B) Sensorgram from SPR analysis of the transition-P peptide represented by the pink -line compared to the IAA28 and AXR3 peptides, represented by the blue and black lines respectively. The data is plotted as response units against time (seconds) and shows that the

proline modification in transition-P results in a very similar response curve to that of AXR3. (C) Model of the carbon backbones of IAA28 (blue) and AXR3 (black) peptides overlayed with the transition-P peptide (pink) all observed in the bound conformation. The models show limited conformational divergence in the centre of the structures with changes in residue orientation towards the termini. The position of the gluatamine to proline modification is annotated with the labels coloured according to the peptides displayed. (D) Model of the degron core structural motif for the transition-P peptide compared toIAA28 and AXR3 models. Only small changes in the backbone orientation are observed within this region. (E) Model of the molecular surface of the TIR1 receptor with the tranisition-P peptide overlaid with models of IAA28 and AXR3. The proline modification in transition-P is annotated and is observed to occur above of the auxin binding pocket.

The IAA28 C-terminal motif SSRR was investigated by first studying the SS and RR motifs separately, introducing the residue changes within the AXR3 degron peptide. Transition-SS peptide replaces tyrosine 92 with serine; and transition-RR peptide replaces lysine 94 with an arginine. In all of these peptides the Pro 82 modification is also included in the transition of the degron to IAA28 (figure 5.14A).

SPR assays show transition-SS peptide with a slower association and dissociation with the auxin receptor complex compared to AXR3. The opposite effect is observed for the transition-RR peptide which shows a faster association and dissociation compared to AXR3 (Figure 5.14B). This is seen in the calculated k_{on} rates (M-1 s-1): transition-SS = 4.61 x 10^3, transition-RR = 6.56 x 10^3, AXR3 = 5.4 x10^3. The k_{off} (s^{-1}) rates consisted of the following: transition-SS = 5.85 x 10^{-3}, transition-RR = 2.21 x 10^{-3}, AXR3 = 3.57 x 10^{-3} (the following X^2 values were obtained: transition-SS = 2.72 %, transition-RR = 6.54 %, AXR3 = 3.46 %).

Computational modelling was used to simulate these degron variants (Figure 5.14C). Overlapping the models of these peptides shows limited structural changes to overall shape of the transition degrons in the receptor bound state (Figure 5.14D). This is consistent with the previously compared alignments of the IAA28 and AXR3 peptides. The models also show that these C-terminal modifications with their different biophysical properties are

affecting the region of the degron which is positioned over the second cavity of the TIR1 molecular surface (Figure 5.14E).

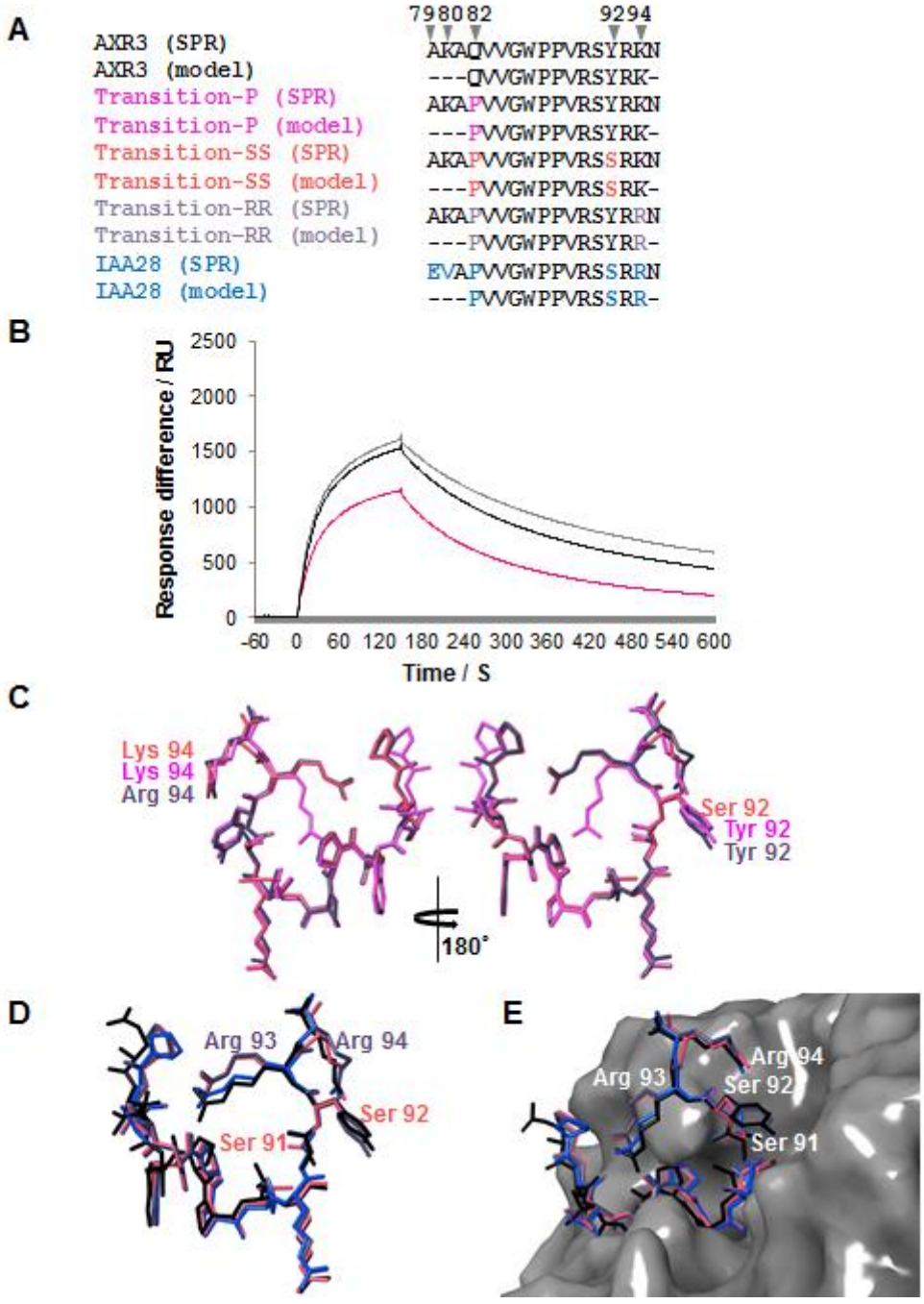

Figure 5.14 The transition-SS and transition-RR peptides show opposite effects in SPR assays. (A) Sequence alignment between the peptides used in SPR analysis and the peptides used in computational modelling. The transition-SS and transition-RR peptides are compared against the transition-P; IAA28; and AXR3 peptide sequences. Residues which are consistent with the AXR3 degron are displayed in black with variations coloured according to the peptide. The transition-SS and transition-RR peptides replicate the double serine and double arginine motifs observed in the C-terminal end of the IAA28 degron. (B) Sensorgram from

SPR analysis of the transition-SS; transition-RR; and AXR3 peptides represented by the light -red; grey and back lines respectively. The data is plotted as response units against time per second. The results show that the auxin receptor complex dissociates faster with the transition-SS peptide compared to AXR3. The double arginine motif in transition-RR peptide slows the dissociation of the auxin receptor complex compared to both transition-SS and AXR3 degrons. The following k_{on} rates (M^{-1} s^{-1}) were calculated: transition-SS = 4.61 x 10^3, transition-RR = 6.56 x 10^3, AXR3 = 5.4 x10^3. From the dissociation phase, the following k_{off} (s^{-1}) rates were calculated: transition-SS = 5.85 x 10^{-3}, transition-RR = 2.21 x 10^{-3}, AXR3 = 3.57 x 10^{-3}. The following X^2 values were: transition-SS = 2.72 %, transition-RR = 6.54 %, AXR3 = 3.46 %. (C) Model of the carbon backbones of transition-SS (light-red) and transition-RR (grey) peptides overlaid with the transition-P peptide (pink) all observed in the bound conformation. The models show limited conformational divergence particularly in the region of the degron core. The modifications of Lysine to Arginine in transition-RR peptide and the tyrosine to serine in transition-SS are annotated. (D) Model of the carbon backbones of the transition peptides SS and RR compared to the IAA28 (blue) and AXR3(black) peptide models. The double arginine and double serine motifs are labelled in the colours of their respective transition peptides. (E) Model of the molecular surface of TIR1 showing the positions of the bound transition-SS and transition-RR peptides compared to the IAA28 and AXR3 peptide models.The double serine and double arginine motifs are observed to occur outside the IAA binding pocket, above the adjacent second cavity.

The combination of the IAA28 C-terminal SS and RR motifs were analysed by SPR using the transition-SSRR peptide.This contained both the Ser 92 and Arg 94 modifications to the AXR3 degron sequence (Figure 5.15A).

SPR analysis showed a faster association of the transition-SSRR peptide to the auxin receptor complex compared to both the AXR3 and IAA28 peptides (Figure 5.15B). This is shown in the calculated k_{on} rates (M^{-1} s^{-1}), where transition-SSRR = 3.92 x 10^3, AXR3 = 3.83 x 10^3, IAA28 = 2.53 x10^3 (X^2: transition-SSRR = 4.33 %, AXR3 = 6.23 %, IAA28 = 5.36 %).

The fast association phase resulted in a high maximum response level in the SPR sensorgram for transition-SSRR peptide. This effect is also likely to be enhanced by a slower dissociation phase compared to AXR3 and IAA28 as seen in the calculated k_{off} (s^{-1}) rates: transition-SSRR = 5.35 x 10^{-3},

AXR3 = 3.61 x 10^{-3}, IAA28 = 3.27 x 10^{-3} (X^2: transition-SSRR = 4.33 %, AXR3 = 6.23 %, IAA28 = 5.36 %).

The changes observed in this SPR assay are not associated with large scale conformational changes in the chimeric peptide when viewed in the receptor-bound state (Figure 5.15C). Instead, the significance of C-terminal degron modification may be indicated by where this region of the degron interfaces with the TIR1 receptor (Figure 5.15D). As has been shown for the SS and RR motifs, the C-terminal end of the degron is positioned above and extending into the second cavity on the TIR1 surface.

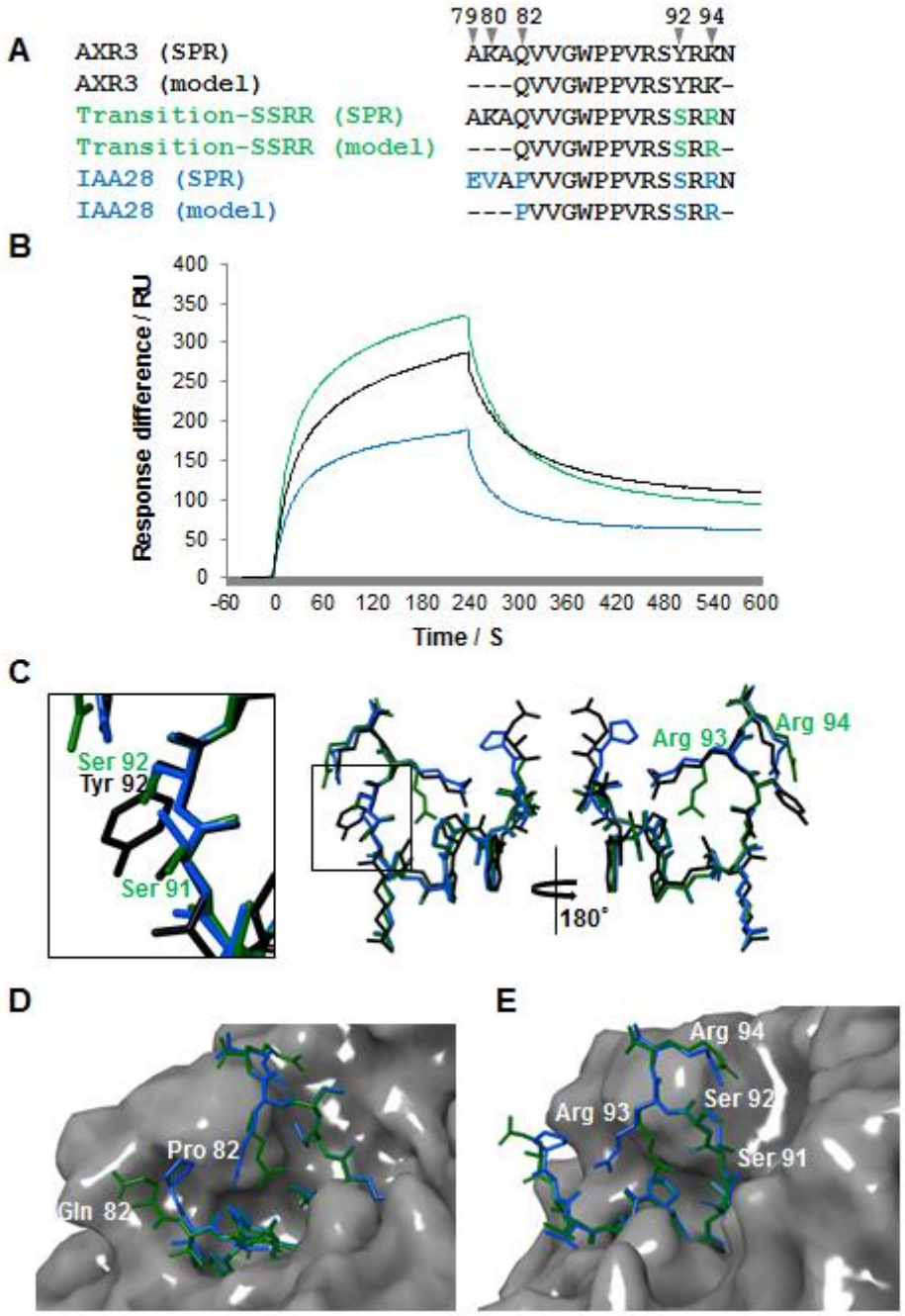

Figure 5.15 The C-terminal SSRR degron motif enhances association to the auxin receptor complex. (A) Sequence alignment between the peptides used in SPR analysis and the peptides used in computational modelling. The transition-SSRR peptide is compared against the IAA28 and AXR3 peptide sequences. Variations from the AXR3 sequence are coloured according to the peptide. The transition-SSRR peptide diverges from the AXR3 degron sequence with the double serine and double arginine motif as observed in the C-terminal end of the IAA28 sequence. (B) Sensorgram from SPR analysis of the transition-SSRR; IAA28; and AXR3 peptides represented by the green; grey and back lines respectively. The data is plotted as response units against time per second. The combination of the

SS and RR motifs results in a higher maximum response compared to AXR3 and IAA28. The following k_{on} rates (M^{-1} s^{-1}) were calculated: transition-SSRR = 3.92 x 10^3, AXR3 = 3.83 x 10^3, IAA28 = 2.53 x10^3. From the dissociation phase, the following k_{off} (s^{-1}) rates were calculated: transition-SSRR = 5.35 x 10^{-3}, AXR3 = 3.61 x 10^{-3}, IAA28 = 3.27 x 10^{-3}. The following X^2 values were obtained as a percentage of maximum response: transition-SSRR = 4.33 %, AXR3 = 6.23 %, IAA28 = 5.36 %. (C) Model of the carbon backbone of transition-SSRR peptide (green) overlaid with the models for IAA28 (blue) and AXR3 (black) observed in the bound conformation. These models are shown rotated 180˚ with the position of the double serine and double arginine motifs annotated. (D) molecular surface of the TIR1 receptor showing the position of the bound transition-SSRR peptide overlaid with the IAA28 model. The residue variation at the N-terminal of the displayed peptides occurs above the IAA binding pocket. (E) The SSRR motif is observed to be positioned outside of the IAA binding pocket above the adjacent second cavity.

5.2.6.1 N-terminal sequence motif of the IAA28 degron destabilizes the auxin receptor complex

The N-terminal IAA28 degron motif EVAP was investigated using the transition-EVAP peptide. In this peptide the AXR3 degron sequence was modified by changing Ala 79 to glutamic acid; Lys 80 to valine; and Gln 82 to proline (Figure 5.16A). SPR analysis of the transition-EVAP showed a substantial reduction in the maximum response level compared to the AXR3 degron. This observation was a result of a slower association phase and dissociation phase compared to the AXR3 and IAA28 peptides (Figure 5.16B). These results show that the IAA28 N-terminal modification to the AXR3 degron forms an unstable auxin receptor complex.

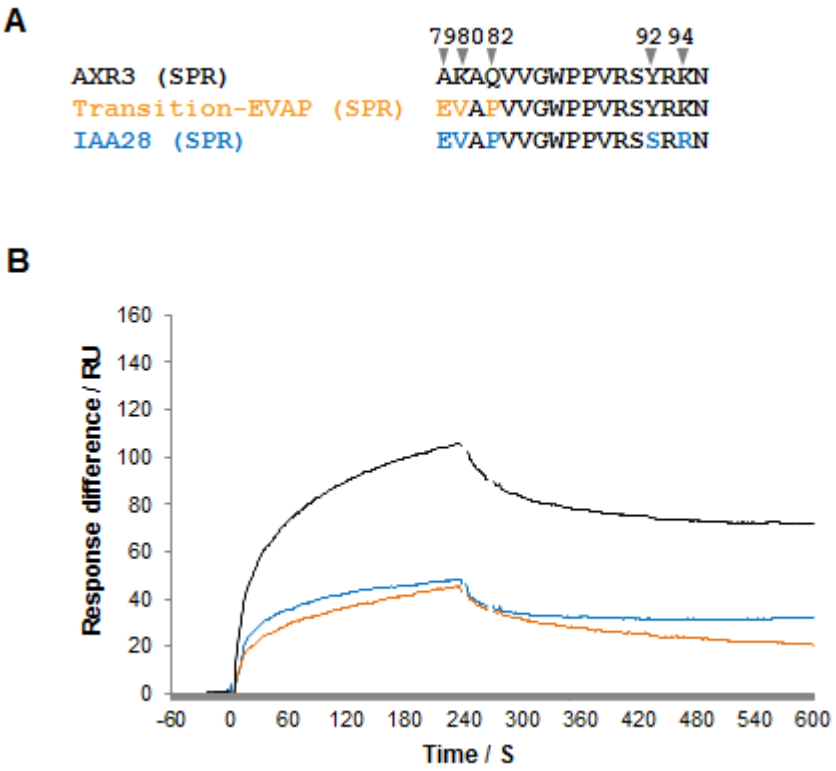

Figure 5.16 Chimeric degron peptide with the N-terminal EVAP motif of IAA28 destabilises the auxin receptor complex. (A) Sequence alignment between the peptides used in SPR analysis. Residues which are the same between IAA28 and AXR3 are shown in black and the differences in IAA28 are displayed in blue. The transition-EVAP peptide contains the N-terminal degron motif of IAA28 and the C-terminal sequence of AXR3. The EVAP sequence motif is highlighted in orange, signifying the motif's unique sequence context. (B) SPR analysis studying the transition-EVAP peptide in comparison with the IAA28 and AXR3 degrons. A sensorgram is shown as response units against time (seconds). The response curve for IAA28 is represented by the blue -line; the transition-EVAP is shown as the orange -line; and the response curve of AXR3 is represented by the black -line. A lower maximum response is observed for the transition-EVAP peptide compared to IAA28. The transition-EVAP peptide is observed to associate slower and dissociate faster compared to the IAA28 degron peptide. The AXR3 peptide is observed to associate faster to the auxin receptor complex compared to all the other degrons in this assay.

The N-terminal replacement of the AXR3 degron with that of IAA28 created a chimeric peptide, with large scale changes to the degron's interaction with the other components of the auxin receptor complex. To further characterize these changes, data from the SPR assay of transition-EVAP was used to

estimate the rate constants. This analysis showed that transition-EVAP peptide had a much lower K_D of approximately 559 µM than both AXR3 and IAA28, with estimated K_D values at 47 µM and 76 µM respectively (Table 5.1). The lower binding constant of the transition-EVAP peptide was due to a slow on rate and fast off rate compare to the IAA28 and AXR3.

Table 5.1 Rate constants for the chimeric peptide Transition-EVAP. Values were calculated from simulated binding curves for each SPR response. The values for X^2 are shown as a percentage of the maximum response value recorded for each individual SPR response. Values below 5 % are considered to represent a good fit between the simulated binding curve and the real data.

Degron	K_D **(nM)**	k_{on} **(M-1 s-1)**	k_{off} **(s-1)**	X^2
AXR3	47	5370	2.5×10^{-4}	3.6 %
Transition-EVAP	559	2850	1.6×10^{-3}	4.2 %
IAA28	76	5220	4.0×10^{-4}	4.9 %

Our investigation of the EVAP motif was further refined by focusing on the residues Glu 79 and Val 80 within the sequence. A chimeric peptide based on the AXR3 degron but containing the EV modification was analysed within an SPR assay (Figure 5.17A). Analysis of the binding responses showed that the EV motif decreases the maximum binding response relative to the AXR3 degron, with an 11-fold decrease of the k_{on} rate compared to AXR3 (Figure 5.17A). The transition-EV peptide was observed to have a similar binding profile as the IAA28 degron peptide, with an approximately equal k_{off} of 0.3×10^{-2} s^{-1} (X^2: transition-EV = 0.02 %, IAA28 = 0.02 %). Together this data indicates the importance of Glu 79 and Val 80 within the EVAP sequence to destabilise the auxin receptor complex.

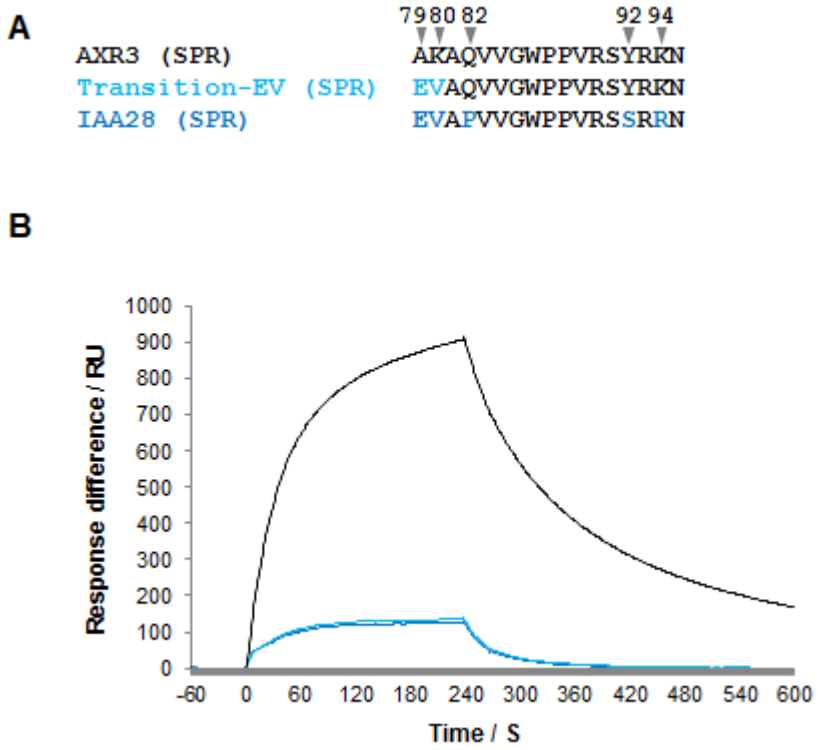

Figure 5.17 SPR study of the transition-EV peptide. (A) Sequence alignment between the peptides used in the SPR analysis. Residue changes in the transition-EV peptide are highlighted in light -blue. (B) SPR analysis studying the transition-EV peptide in comparison with the IAA28 and AXR3 degrons. The response curve for IAA28 is represented by the dark -blue-line; the transition-EVAP is shown as the light -blue-line; and the response curve of AXR3 is represented by the black -line. The following k_{on} rates (M^{-1} s^{-1}) were calculated: AXR3 = 3.9 x 10^3, transition-EV = 343, IAA28 = 10.9. From the dissociation phase, the following k_{off} (s^{-1}) rates were calculated: AXR3 = 5.8 x 10^{-3}, transition-EV = 0.3 x 10^{-2}, IAA28 = 0.3 x 10^{-2}. The following X^2 values were obtained: AXR3 = 8 %, transition-EV = 0.02 %, IAA28 = 0.02 %.

5.3 Discussion

It is well known that the Aux/IAA degron core (GWPPV) is critical for the formation of the auxin receptor complex (Kepinski and Leyser, 2004; Dharmasiri *et al*., 2005; Tan *et al*., 2007). This is demonstrated when any one of the core degron motif residues is modified as it results in disrupting the Aux/IAA degradation dynamics (Ramos *et al*., 2001). Our study has used computational and biophysical techniques to analyze modifications to the

core degron in order to gain an insight into the assembly of the auxin receptor complex.

An important insight into the function of the degron core has come from previous studies which show residue modifications within the degron core are not equal in their severity. This was clearly demonstrated by the *axr3* mutant series, particularly *axr3-1* and *axr3-3* (Leyser *et al*., 1996; Rouse *et al*., 1998). SPR analysis on degron peptides showed that unlike AXR3, the axr3-1 peptide was unable to form a stable complex with IAA and TIR1. Computational modelling of the axr3-1 peptide bound to the auxin receptor complex indicated that the Leu 88 modification was within a hydrophobic hair-pin structure, formed by the centre of the degron core (WPP). This modification had adjusted the conformation of the entire axr3-1 peptide, especially for the hair-pin motif. Modelling of this degron peptide showed that the central degron core could only fit inside the auxin binding pocket by forcing the pocket to adopt a more open conformation, particular in the upper region above the IAA molecule.

Such major conformational shifts in the auxin binding pocket are unlikely to occur naturally, especially when a previous study observed only limited flexibility of the auxin binding pocket (Tan *et al*., 2007). Therefore, we propose that axr3-1 is unable to insert into the auxin binding pocket, preventing a secure interaction with the rest of the complex.

In contrast, the axr3-3 peptide is better able to insert into the auxin binding pocket compared to axr3-1 as indicated by the presented computational models. SPR assays also indicate that axr3-3 peptide has a faster dissociation rate from the complex compared to AXR3. This may be due to the location of the axr3-3 modification at residue 89, situated where the C-terminal half of the degron peptide descends into the auxin binding pocket. This replacement of Val 89 with Gly may result in increased flexibility due to a shorter side chain, allowing axr3-3 peptide to more readily manoeuvre in and out of the auxin binding pocket.

The Aux/IAA SHY2 / IAA3 contains an interesting natural variant of the consensus sequence outside of the degron core where Val 83 is replaced by isoleucine. In addition to this natural variation, the mutation *shy2-2* is similar

to *axr3-1* in that the residue change of Pro 87 is at the centre of the degron core (Tian and Reed, 1999). The modelling of a shy2-2 degron peptide showed that the Pro 87 modification is within the hair-pin motif of the central core degron. This modification is also replicated in another Aux/IAA mutation *axr2-1* (Nagpal *et al*., 2000).

Despite this shared modification of the degron core the model of shy2-2 showed the greater change in conformation compared to the axr2-1 peptide, with a major shift in the orientation of Trp 86. This change is likely to be a result of the natural variant IIe 83; and fits in with a previous report that the double valine motif of the degron, which includes Val 83 can influence degradation dynamics of an Aux/IAA (Guseman *et al*., 2015).

The previously reported increase in shy2-2 binding with TIR1 due to IAA is intriguing especially when the modelled orientation of Trp 86 may prevent docking into the auxin binding pocket (Tian *et al*., 2003). This would suggest that regions flanking the degron core form an important interface with the receptor.

The importance of the flanking regions was demonstrated in my SPR analysis of the IAA28 and AXR3 degron peptides, which both show very different SPR responses. The low SPR response of IAA28 seems to reflect the long half-life of 80 minutes for full-length IAA28 in the plant cell (Dreher *et al*., 2006). This is further supported by the opposite trends for AXR3. Such differences in SPR responses of the degron peptides and half-life of full-length proteins reflect an ability to form an auxin receptor complex. Critical to this must be residue variation around the degron core as the SPR responses for the peptides were clearly distinct.

A central focus was to identify which combinations of residue motifs were important for the low SPR response of the IAA28 degron. The data suggest that N-terminal and C-terminal flanking motifs of IAA28 make distinct contributions to binding, particularly in the association phase of the auxin receptor complex. In this situation, the low SPR response for IAA28 may only be possible if the rapid association phase contributed by the C-terminal SSRR motif is overridden by the effects of the N-terminal EVAP motif.

The identification of specific effects of different motifs of IAA28 flanking regions adds to a previous observation, where replacing Arg 93 and Lys 94 in the consensus degron sequence with alanine increases protein accumulation within a plant cell (Ramos *et al*., 2001). Interestingly these are the same residue positions as the arginine residues in the SSRR motif. The IAA28 motifs can now refine this previous study which was not able to identify the effects of specific motifs, but did show that the flanking regions influenced protein stability as a sum of all parts (Ramos *et al*., 2001). Our study has now used the IAA28 flanking motif to demonstrate this in fascinating detail.

The findings presented here add to a growing consensus that the binding of an Aux/IAA is not simply controlled through the essential degron core (Ramos et al., 2001; Havens *et al*., 2012; Moss *et al*., 2015). Remarkably, the flanking motifs are able to influence the stability of the receptor complex outside of the auxin binding pocket and raise the question whether sequence variations at other interfaces with TIR1 determine Aux/IAA selectivity. As such changes may influence the occupancy of *cis* and *trans* states within the degron core.

In this investigation, it has been shown how the axr3-1 and shy2-2 influence the hydrophobic hair-pin structure at the centre of the degron core and consequently their ability to fit into the auxin binding pocket. However, the presented results on axr3-3 indicate that it is not simply enough to insert into this pocket. Residues outside the centre of the core degron, as seen in the IAA28 flanking motifs, have a key role in determining how well an Aux/IAA can bind. Here we propose that although the degron core is critical, the residues flanking the core can determine the stability of the auxin receptor complex with distinct effects between the N- and C-terminal of the degron.

Chapter 6

General discussion

The formation of the auxin receptor complex

Our understanding of auxin signal transduction within the plant cell nucleus has advanced significantly over the last 15 years, aided by the first genetic and biochemical studies and more recently structural analysis of the key elements within the mechanism (Weijers and Wagner, 2016). These studies include the crystal structure of the DNA binding domain of ARF1 and domains III and IV of ARF7, the auxin receptor TIR1, and studies of the Aux/IAA transcriptional repressor proteins (Boer *et al*., 2014; Korasick *et al*., 2014; Tan *et al*., 2007; Han *et al*., 2014; Ke *et al*., 2015).

Currently there is no complete structure of an Aux/IAA protein which is composed of four functional domains (DI to DIV). DI contains the motif required for co-repressor recruitment (Tiwari *et al*., 2004; Szemenyei *et al*., 2008; Causier *et al*., 2012; Wang and Estelle, 2014). DII is the location of the degron which forms the critical interface with TIR1 (Kepinski and Leyser, 2005; Dharmasiri *et al*., 2005; Tan *et al*., 2007). DIII and DIV mediate dimerisation between other Aux/IAA proteins and ARF transcription factors (Korasick *et al*., 2014; Han *et al*., 2014).

Crystallography has revealed fragments of the Aux/IAA transcriptional repressors, the most complete being the C-terminal half containing DIII and DIV (Han *et al*., 2014; Dinesh *et al*., 2015). Until now the N-terminal half of the protein has been less well characterised with the only structural data from peptides of the EAR motif from functional domain I (IAA10 and IAA1), and the AXR2 degron peptide of DII (Ke *et al*., 2015; Tan *et al*., 2007).

Our results now provide a context for these important binding sites within the N-terminal half of AXR3 (DI and DII). We have shown that this part of the Aux/IAA protein is intrinsically disordered with tendencies to form elements of secondary structure. Importantly the main regions of secondary structure

were associated with DI and DII, with helices forming part of DI and a tendency for a β-strand C-terminal to the degron core within DII. These results complement the crystal structure of the highly ordered C-terminal half of AXR3 (DIII and IV) (Han *et al*., 2014).

The structural characterization of AXR3 (DI and DII) by NMR provides an opportunity to study how this disordered protein interacted with TIR1 to form the auxin receptor complex. The results from our investigation support the degron forming the key binding interface with TIR1, with more transient interactions formed by localized points (Leu 42, and Lys 76) in the unconserved region of the protein between DI and DII. The extensive disorder within AXR3 (DI and DII) raised questions concerning its biological function.

6.1 The role of intrinsically disordered regions in the N-terminal half of AXR3 (DI and DII)

The unconserved sequences of Aux/IAA proteins have previously been assumed to function only as filler loops between the functional domains (Reed, 2001). Here, we suggest additional roles of such filler loops in Aux/IAA proteins based on recent developments in the literature.

IDRs typically disfavor protein-protein interactions, with many IDPs remaining disordered upon binding (Hazy and Tompa, 2009; Gruet *et al*., 2016). In such cases binding is focused within defined areas which contribute the majority of the binding free energy (Wright and Dyson, 2015). The disordered regions defined in our structural characterization of AXR3 (DI and DII) may have a similar function, focusing the binding interface with TIR1 to the degron region (Ramos, 2001; Tan *et al*., 2007).

6.1.1 Intrinsic disorder and the tripartite degron system

The disordered regions of AXR3 (DI and DII) may also participate in the ubiquitin-mediated degradation of the protein in the plant cell. This idea corresponds with a recent report on degron systems across a wide range of protein families (Guharoy *et al*., 2016). The report suggests protein

degradation is not mediated by only one instability element within a target protein and describes a tripartite system.

According to this system the primary degron of an Aux/IAA is most likely to correspond with the core degron motif (VGWPP), which identifies the protein as a substrate for ubiquitin-mediated degradation (Ramos, 2001). The secondary site for degradation is usually defined by at least one lysine residue in close proximity to the primary degron and functions as the site for ubiquitin modification (Guharoy *et al*., 2016). This corresponds with truncation studies of Aux/IAA proteins where molecular reporters containing just the DII region are still degraded in plants, although the degradation rates are reduced (Havens *et al*., 2012). The exact site for polyubiquitination of Aux/IAAs is currently unknown, with potential candidate lysine residues (80 and 84) on both sides of the degron core in AXR3. However, a recent study on the Aux/IAA protein IAA1 suggests lysine residues are unlikely to be the site of ubiquitin modification in this protein family. As substituting all lysine residues with arginine did not stop the rapid degradation of IAA1 and suggest alternative sites must be involved (Gilkerson *et al*., 2015).

The third part of the degradation model is a long disordered segment usually located within ten residues of the primary degron region, as observed in AXR3 (DI and DII). According to the tripartite model a disordered region may initiate the unfolding of the protein at the 26S proteasome (Guharoy *et al*., 2016). Together, it is likely that the defined disordered regions of the N-terminal half of the AXR3 protein, and in other Aux/IAAs, have a greater functional importance than previously thought.

6.2 The possible effects of the N-terminal flanking region on *cis-trans* isomerisation

Replacement of residues N-terminal to the degron, where the motif AKAQ (positions 82 to 79) in AXR3 is replaced by the IAA28 motif EVAP, was shown to reduce the formation of the auxin receptor complex in our SPR studies. This replacement of residues increased the K_D of the chimeric degron approximately ten-fold for TIR1 binding compared to the AXR3 degron (Chapter 5, section 5.2.6.1). This effect was intriguing especially

when NMR analysis showed that this N-terminal flanking region was limited in its ability to interact with TIR1 (Chapter 4, section 4.2.3).

One possible hypothesis is that the residue replacements in the N-terminal region flanking the degron may alter the *cis-trans* isomerisation of the prolyl amide bond between Pro 87 and Trp 86. We have previously discussed the importance of aromatic residues adjacent to a prolyl bond, but this alone cannot account for the *cis* abundance observed in AXR3 (DI and DII) (Wu and Raleigh, 1998; Thomas *et al*., 2006). The additional propensity for the *cis* conformation is likely to be due to the regional effects within the AXR3 (DI and DII) protein.

In this scenario we hypothesise that the EVAP motif may negatively affect the propensity for the *cis* conformation. Our NMR data indicates TIR1 displays conformational selection for the binding of the central degron core (WPP) to the auxin binding pocket. A lower abundance of the *cis* state would be expected to limit the ability of a degron to bind to the auxin pocket of TIR1, consistent with the observed binding response of the chimeric EVAP peptide. The potential influence on *cis-trans* isomerisation of the regions flanking the degron core may also relate to the previous observation of increased degron peptide accumulation in plants, as a result of alanine replacement of the N- and C-terminal flanking sequences (Figure 3, Ramos *et al*., 2001).

6.3 The AXR3 degron series

The AXR3 degron series of mutations within the degron core was investigated by SPR analysis for an interaction with IAA alone (chapter 4, section 4.3.4), and with the full auxin receptor complex (chapter 5, section 5.3.4). Our results suggest that IAA can form an interaction with the components of this degron series, indicated by similar binding responses for AXR3, axr3-1, and axr3-3. This was in contrast to the SPR studies with TIR1 forming the full auxin receptor complex where major differences in binding responses were observed within the degron series, corresponding to the severity of the mutant phenotypes observed in plants (Leyser *et al*., 1996; Rouse *et al*., 1998).

The computational analysis of axr3-3 shows that the degron core can insert into the auxin binding pocket, but the change from Val 89 to glycine may introduce flexibility into the degron allowing for a far more dynamic interaction with the auxin binding pocket in TIR1. This was supported by the observation of the axr3-3 degron dissociating faster from TIR1 with a k_{off} rate 10^3 faster than the AXR3 degron and suggests axr3-3 is unable to form a stable interaction with the auxin binding pocket.

The SPR assay showed that the axr3-1 degron had a binding response close to the base-line indicating only a very low affinity interaction. This was consistent with the computational modelling which suggested the axr3-1 degron could not fit into a rigid auxin binding pocket. This raises the possibility that the recorded SPR response for axr3-1 and axr3-3 was detecting a potential encounter complex phase, previously suggested in our NMR analysis of the complex with AXR3.

6.4 A comparison of degron secondary structures between auxin and jasmonate perception

Although the plant hormones auxin and jasmonate share a similar mechanism of perception through F-box proteins, it appears that the form of secondary structure used as potential recognition motifs is different in the two signaling systems. Crystallography has revealed that the degron peptide of the JAZ transcriptional repressor protein involved in jasmonate perception forms a conserved α-helix in the context of its receptor COI1 (Sheard *et al*., 2010). This appears to be a more well-defined structural element compared to the more transient β-strand in AXR3 and may relate to the subtle differences in function of the degrons for the two systems.

Unlike the auxin receptor complex where the degron core inserts into the upper region of the well-defined auxin binding pocket, the JA-Ile molecule occupies its entire pocket in COI1. Consequently the main contact between the N-terminal half of JAZ1 peptide and COI1 is a single leucine (Leu 201) which binds to a small pocket above the JA-Ile cavity (Sheard *et al*., 2010). To ensure a stable complex, the JAZ C-terminal degron forms a helix which fills an adjacent cavity in COI1 and blocks the JA-Ile from dissociating. This blocking function by the JAZ secondary structure element does not appear

to be required in auxin perception. Instead, we propose that the apparent bipartite degron structure of AXR3 may have evolved to stabilise the interaction with TIR1. In this binding process, the tendency for a β-strand formation in the C-terminal degron may guide the IDRs of the AXR3 protein into position on the TIR1 surface.

6.5 Schematic over-view of auxin receptor complex formation

Here, we present a possible model for the formation of the auxin receptor complex. The results in this study indicate the potential for an earlier transient phase of the complex, not observed in the previous crystallography studies (Tan *et al*., 2007). This phase may include the presented recognition function of a β-strand formed by the C-terminal half of the degron and *cis-trans* isomerisation within the degron core (A and B, Figure 6.1).

The auxin binding pocket appears to display conformational selection of the degron core (WPP), where the Pro 87 is required to be in the *cis* conformation for a secure interaction with the receptor, presumably by inserting into the auxin binding pocket as observed in the previous crystallography study (Tan *et al*., 2007). Our NMR results also indicate that this insertion of the Trp 86 can occur in the absence of IAA, an observation not previously reported. This binding event was observed to be enhanced with the addition of IAA consistent with early investigations (Kepinski and Leyser, 2005; Dharmasiri *et al*., 2005).

Previous crystallography has shown that different types of auxins (IAA, 1-NAA, 2,4-D) can bind to the pocket independent of the AXR2 degron peptide (Tan *et al*., 2007). At first this seems to contradict the early model of auxin binding where the IAA molecule was believed to undergo a transition of conformational states with the reorientation the carboxyl tail, from a recognition state to a modulation state promoted by a binding partner (Kaethner, 1977). We have proposed that this partner for conformational change is unlikely to be the TIR1/AFB protein, but may be the Aux/IAA co-receptor. The crystallography suggests that auxin molecules in the modulation conformation may bind to the pocket by chance. These

scenarios indicate a far more dynamic process than previously thought with IAA and the degron core inserting in and out of the auxin binding pocket, with a stable complex only forming when both Aux/IAA protein and auxin are present with TIR1.

We argue that within the spectrum of possible binding mechanisms of fuzzy complexes, the auxin receptor complex is most similar to a flanking model which displays conformational selection (Sharma *et al*., 2015). This mechanism describes the binding of structural elements in partnership with adjacent disordered regions, similar to the bipartite degron structure of AXR3. A contact between the C-terminal half of the degron and TIR1 is likely to be promoted by attractive forces between a positively charged degron region and the negative charges of $IP_{6,}$ a molecule observed through the base of the second cavity (Tan *et al*., 2007).

A possible transient encounter complex phase between TIR1 and AXR3, where the degron is in the *trans* state may influence the affinity of the proposed electrostatic interaction between IAA and the N-terminal degron. We assume that the conformation of the degron core when Pro 87 is in the *trans* state, orientates above the auxin binding pocket while the flanking regions form transient interactions with the receptor. A possible scenario is that this arrangement induces further conformational adjustments to the degron core and the establishment of a temporary hydrophobic pocket which would promote an electrostatic interaction with IAA. All these events including the β-strand of the C-terminal degron may aid the assembly of the intrinsically disordered AXR3 protein onto the TIR1 surface to form a stable auxin receptor complex.

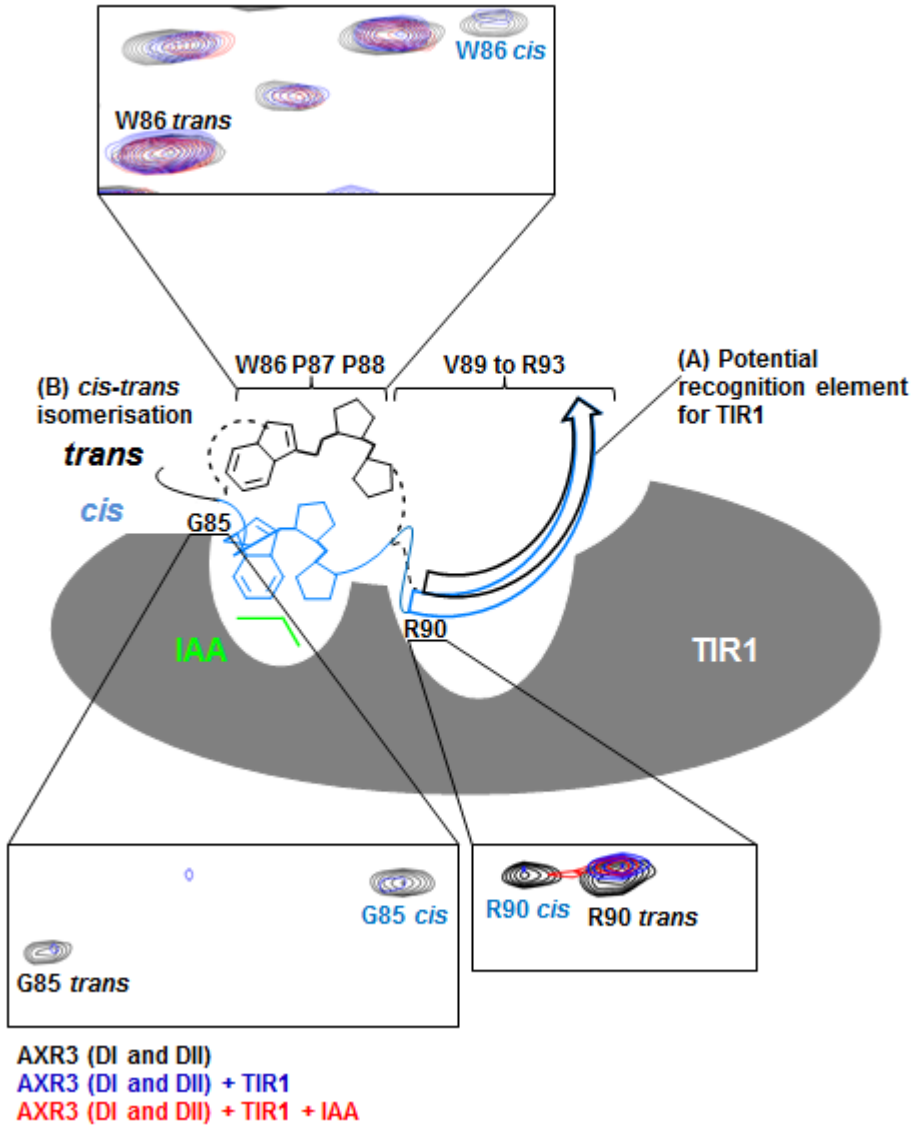

Figure 6.1 Schematic representation of a model for the formation of the auxin receptor complex. The TIR1 receptor is represented in dark grey with the two main surface cavities of the upper surface. IAA shown in green indicates the auxin binding pocket. The AXR3 degron is shown in black, including the central degron core motif WPP when Pro 87 is in the *trans* state. The conformation of the degron when Pro 87 is in the *cis* state is coloured light-blue. The alternative conformation of the carbon backbone is represented by the dashed-lines. The different binding abilities of the *cis* and *trans* isomers of residues Gly 85, Trp 86, and Arg 90 are indicated by the previously reported NMR HSQC data from chapter 4, section 4.3.2. A colour coded key for the spectra is shown at the base of the figure. The spectra are linked to the respective residues within the model. This data-set indicates the possibility of transient interactions between TIR1, and the regions flanking the

central degron core (WPP) in both *cis* and *trans* states. A more stable binding event occurs when the central degron core is in the *cis* state and IAA is present. The tendency for the formation of a possible β-strand by the C-terminal half of the degron is represented by an arrow. This element of secondary structure is likely to fit into the second cavity of TIR1, adjacent to the auxin binding pocket. It is possible that this site may also accommodate other molecules and represents a potential target site for future development of synthetic auxins.

6.6 Future prospects

Our investigation has raised further questions regarding the formation of the auxin receptor complex. There are five key questions we suggest should be investigated further. Firstly, the possibility that the encounter complex enhances the affinity of a likely electrostatic interaction between the degron and IAA should be tested. Secondly, we suggest further experiments to determine if Trp 86 is the primary site of this low affinity interaction with IAA. Thirdly, we believe axr3-3 protein should be tested for interacting with TIR1 during an encounter complex phase. Fourth, SPR analysis suggests the N-terminal flanking region to the degron core is an important influence on the binding stability of the auxin receptor complex. One possible hypothesis is that the N-terminal degron influences the *cis-trans* isomerisation within the degron core. Fifth, we believe the C-terminal half of the degron may form a recognition element for TIR1. Residue changes within this region seem to influence the k_{on} rate of the complex. A hypothesis is that such changes influence the propensity for secondary structure formation. This effect may also occur for residue changes in the N-terminal flanking region. In this section we have proposed experiments to test these questions.

6.6.1 Testing for an enhancement of an interaction between IAA and the degron (*trans*) in complex with TIR1

Future experiments are required to test the hypothesis that the affinity of the electrostatic interaction between IAA and the N-terminal degron is enhanced when the degron core is above the auxin binding pocket. This could be tested by blocking IAA from entering the auxin binding pocket by replacing

the residues which form the upper levels, possibly with branched amino acids (Leu, Ile, Val). The affinity could then be measured by a WaterLOGSY NMR experiment.

6.6.2 A possible interaction between Trp 86 and IAA

Our NMR analysis indicates that IAA changes the local chemical environment of the degron residues N-terminal to the di-proline motif in the *trans* conformation. We hypothesise that this is due to an interaction with Trp 86. This hypothesis may be tested by a phenylalanine replacement of Trp 86 within the AXR3 (DI and DII) protein. The residues of the degron would be studied for potential chemical shifts induced by the titration of IAA in a HSQC NMR experiment.

Furthermore, the potential aromatic stacking between Trp 86 and IAA may result in exciton coupling between the aromatic rings, where the excitation of electrons would spread across the two ring systems. Consequently the excited state is split into two and the electron transition back to the ground will result in the emission of energy in the form of a couplet. This can result in a characteristic excitation band detected by far-UV circular dichroism spectroscopy (CD) (Grishina and Woody, 1994). This has been demonstrated in a previous study on the photoreceptor UVR8, where tryptophan stacking resulted in a CD trough at 221 nm followed by a peak at 234 nm (Christie *et al*., 2012). CD spectroscopy at similar wavelengths can be used as a positive indicator of an aromatic interaction in our system. Additionally stopped-flow may be used for rapid mixing of the auxin receptor components to detect aromatic ring stacking during formation of a transient encounter complex (Gibson, 1969).

6.6.3 The possibility that axr3-3 can participate in the proposed encounter complex phase

We have hypothesised that axr3-3 may be able to form a transient encounter complex with the auxin receptor but unable to form a stable interaction with the auxin binding pocket. To test this hypothesis an HSQC experiment with

TIR1 and N-terminal axr3-3 (DI and DII) protein in the presence and absence of IAA is recommended. The degron residues would be studied for chemical shifts induced by the auxin receptor complex.

6.6.4 Studying the possible effects of EVAP motif on *cis-trans* isomerisation within the degron core

A key question raised by our research is whether the EVAP motif of the N-terminal flanking region of the IAA28 degron can influence the *cis-trans* isomerisation of the prolyl bond between Pro 87 and Trp 86. An HSQC NMR experiment can be used to detect the relative abundance between the *cis* and *trans* isomer states in a modified version of the AXR3 (DI and DII) protein, where the AKAQ motif at positions 82 to 79 is replaced by the EVAP motif. The results from this protein would then be compared to the relative abundance of the *cis* state observed in AXR3 (DI and DII).

6.6.5 A study of the N- and C-terminal regions flanking the degron core

Within this study the SSRR motif at positions 91 to 94 was observed to enhance the k_{on} rate of the auxin receptor complex. One hypothesis is that these residue changes may enhance the tendency for β-strand formation as a recognition element, enhancing TIR1 binding. This can be tested by a NMR assignment experiment of the carbon backbone of a modified AXR3 (DI and DII) protein containing the SSRR motif. Measuring the $^{13}C_{\alpha,}$ $^{13}C'$, and $^{13}C_{\beta}$ chemical shift indices will indicate the tendency for secondary structure within the C-terminal half of the degron. The chemical shift differences would then be compared to values of the AXR3 (DI and DII) protein.

A similar experiment can also be performed on residue changes in the N-terminal flanking region (positions 79 to 82). Although this region has a weaker trend for a potential β-strand in AXR3 the propensity may change with natural sequence variations observed in other Aux/IAAs. Together, these proposed studies may continue to improve our knowledge of how the

auxin receptor complex forms and reveal the earliest events of auxin perception.

6.6.6 Outlook: anti-auxins and the auxin receptor complex

An interesting area not explored in this research is the possible roles of anti-auxins on the auxin receptor complex. Early studies indicated the molecules CNB, NMSA, NMSP, and PCIB act as anti-auxins by antagonising IAA promoted growth (Audus and Das, 1955). PCIB is particularly interesting as it can enhance growth at concentrations below 10^{-6} molar (Burström, 1950). Currently the molecular mechanism of PCIB action is unknown.

It is a possibility that PCIB directly affects auxin signal transduction within the plant cell nucleus. This was suggested by the observation that PCIB disrupts normal regulation of Aux/IAA genes and lower Aux/IAA transcript levels (Oono *et al*., 2003). One hypothesis is that PCIB competes with IAA for binding to the auxin binding pocket which could disrupt receptor complex formation, potentially leading to elevated Aux/IAA protein stability. Consequently this may lead to down-regulation of Aux/IAA gene expression. This hypothesis is consistent with an in-silico docking study on the anti-auxins BH-IAA and auxinol. The study showed that these molecules can fit into the auxin binding pocket of TIR1 (Hayashi *et al*., 2012).

There may be an opportunity to test the effect of the anti-auxin PCIB on the binding of the Aux/IAA protein with an NMR HSQC experiment, examining the chemical shifts of degron residues induced by TIR1 with and without the anti-auxin. Furthermore, it is possible that PCIB displays selective binding to the other members of the auxin receptor family. Consequently any future studies should expand the range of auxin receptors studied.

6.7 Summary of conclusions

The results presented in this thesis have shed light on structural and biophysical determinants of TIR1/AFB-Aux/IAA-based auxin perception, revealing a more complex picture of the earliest events of complex formation. Central to this is the confirmation of extensive intrinsic disorder in

the amino-terminal half of the Aux/IAA AXR3. A surprising observation of this work was that one of the 10 Pro residues in this region of the protein, Pro 87, shows equal occupancy of the *cis* and *trans* conformations. This ratio of *cis* and *trans* confirmation of an amide bond is unprecedented, even for a Pro residue preceded by a Trp residue. This finding is even more remarkable given the paucity of recognisable structure within the amino-terminal region of AXR3. Further experiments based on the mutation of residues adjacent to the core Trp-Pro-Pro degron motif will determine the extent to which these flanking sequences, in which traces of secondary structure have been recorded, might result in a propensity to adopt the *cis* form of Pro 87.

Until now, a more static view of the fully-docked TIR1/AFB-auxin-Aux/IAA receptor complex, as resolved by crystallographic analysis, has by necessity, dominated. Here, because the auxin molecule is sandwiched between the TIR1/AFB and Aux/IAA co-receptors it has been suggested that the auxin binds first to TIR1, independently of the Aux/IAA, before becoming entombed by the subsequent docking of the Aux/IAA degron. Our finding that AXR3 and TIR1 can form a complex in the absence of auxin raises the possibility of the existence of a topologically-distinct encounter complex. This is further supported by the finding that auxin-independent binding to TIR1 is observed regardless of whether the core degron Trp 86-Pro 87 bond in AXR3 is in *cis or trans.* This is significant because the '*trans'* form of the degron cannot occupy the canonical auxin binding pocket in TIR1. In this context, the discovery of direct, low-affinity binding of IAA to the AXR3 alone is intriguing, especially as this binding appears to be specific to the '*trans'* form of the degron. Together, these experimental observations suggest that the formation of the auxin receptor complex may involve more than the simple, sequential and independent binding of the three components, with the possibility of auxin and the Aux/IAA binding higher in the canonical auxin binding pocket and completing some or all of the transition to the fully docked ternary complex together. Further experiments, such as those outlined here, will be required to test these exciting hypotheses on the formation of a fuzzy auxin receptor complex.

References

Abel, S., *et al*. (1995). "ThePS-IAA4/5-like Family of Early Auxin-inducible mRNAs in Arabidopsis thaliana." *Journal of Molecular Biology* **251**(4): 533-549.

Abel, S., *et al*. (1994). "Early auxin-induced genes encode short-lived nuclear proteins." *Proceedings of the National Academy of Sciences* **91**(1): 326-330.

Audus, L. and N. Das (1955). "The interactions of auxins and anti-auxins in the stimulation of root growth." *Journal of Experimental Botany* **6**(3): 328-347.

Bhalerao, R. P. and M. J. Bennett (2003). "The case for morphogens in plants." *Nature cell biology* **5**(11): 939-943.

Boer, D. R., *et al*. (2014). "Structural basis for DNA binding specificity by the auxin-dependent ARF transcription factors." *Cell* **156**(3): 577-589.

Burström, H. (1950). "Studies on growth and metabolism of roots. IV. Positive and negative auxin effects on cell elongation." *Physiologia Plantarum* **3**(3): 277-292.

Causier, B., *et al*. (2012). "TOPLESS co-repressor interactions and their evolutionary conservation in plants." *Plant Signaling & Behavior* **7**(3): 325-328.

Chandler, J. W. (2016). "Auxin response factors." *Plant, cell & environment*.

Christie, J. M., et al. (2012). "Plant UVR8 photoreceptor senses UV-B by tryptophan-mediated disruption of cross-dimer salt bridges." *Science* **335**(6075): 1492-1496.

Cozzi, F., *et al*. (1995). "Polar Interactions between Stacked π Systems in Fluorinated 1, 8-Diarylnaphthalenes: Importance of Quadrupole Moments in Molecular Recognition." *Angewandte Chemie International Edition in English* **34**(9): 1019-1020.

Dalvit, C., *et al*. (2001). "WaterLOGSY as a method for primary NMR screening: practical aspects and range of applicability." *Journal of Biomolecular NMR* **21**(4): 349-359.

Dasgupta, B., *et al*. (2007). "Enhanced stability of cis Pro-Pro peptide bond in Pro-Pro-Phe sequence motif." *FEBS Letters* **581**(23): 4529-4532.

Dharmasiri, N., *et al*. (2005). "The F-box protein TIR1 is an auxin receptor." *Nature* **435**(7041): 441-445.

Dharmasiri, N., *et al*. (2005 a). "Plant development is regulated by a family of auxin receptor F box proteins." *Developmental Cell* **9**(1): 109-119.

Dinesh, D. C., *et al*. (2015). "Solution structure of the PsIAA4 oligomerization domain reveals interaction modes for transcription factors in early auxin response." *Proceedings of the National Academy of Sciences* **112**(19): 6230-6235.

Dogan, J., *et al*. (2014). "The binding mechanisms of intrinsically disordered proteins." *Physical Chemistry Chemical Physics* **16**(14): 6323-6331.

Dreher, K. A., *et al*. (2006). "The Arabidopsis Aux/IAA protein family has diversified in degradation and auxin responsiveness." *The Plant Cell* **18**(3): 699-714.

Drozdetskiy, A., *et al*. (2015). "JPred4: a protein secondary structure prediction server." *Nucleic Acids Research*: gkv332.

Fischer, G. (2000). "Chemical aspects of peptide bond isomerisation." *Chemical Society Reviews* **29**(2): 119-127.

Fonseca, S., et al. (2009). "(+)-7-iso-Jasmonoyl-L-isoleucine is the endogenous bioactive jasmonate." *Nature Chemical Biology* **5**(5): 344-350.

Friml, J. (2003). "Auxin transport—shaping the plant." *Current Opinion in Plant Biology* **6**(1): 7-12.

Fuxreiter, M., *et al*. (2004). "Preformed structural elements feature in partner recognition by intrinsically unstructured proteins." *Journal of Molecular Biology* **338**(5): 1015-1026.

Gibson, Q. H. (1969). "[6] Rapid mixing: Stopped flow." *Methods in Enzymology* **16**: 187-228.

Gilkerson, J., *et al*. (2015). "Lysine residues are not required for proteasome-mediated proteolysis of the auxin/indole acidic acid protein IAA1." *Plant Physiology* **168**(2): 708-720.

Grishina, I. B. and R. W. Woody (1994). "Contributions of tryptophan side chains to the circular dichroism of globular proteins: exciton couplets and coupled oscillators." *Faraday Discussions* **99**: 245-262.

Grossmann, K. (2010). "Auxin herbicides: current status of mechanism and mode of action." *Pest Management Science* **66**(2): 113-120.

Gruet, A., *et al*. (2016). "Fuzzy regions in an intrinsically disordered protein impair protein–protein interactions." *FEBS Journal*.

Guharoy, M., *et al*. (2016). "Tripartite degrons confer diversity and specificity on regulated protein degradation in the ubiquitin-proteasome system." *Nature Communications* **7**.

Guilfoyle, T. (2007). "Plant biology: sticking with auxin." *Nature* **446**(7136): 621-622.

Guilfoyle, T. J. and G. Hagen (2007). "Auxin response factors." *Current Opinion in Plant Biology* **10**(5): 453-460.

Guseman, J. M., *et al*. (2015). "Auxin-induced degradation dynamics set the pace for lateral root development." *Development* **142**(5): 905-909.

Han, M., *et al*. (2014). "Structural basis for the auxin-induced transcriptional regulation by Aux/IAA17." *Proceedings of the National Academy of Sciences* **111**(52): 18613-18618.

Havens, K. A., *et al*. (2012). "A synthetic approach reveals extensive tunability of auxin signaling." *Plant Physiology* **160**(1): 135-142.

Hayashi, K.-i. (2012). "The interaction and integration of auxin signaling components." *Plant and Cell Physiology* **53**(6): 965-975.

Hayashi, K.-i., *et al*. (2012). "Rational design of an auxin antagonist of the SCFTIR1 auxin receptor complex." *ACS Chemical Biology* **7**(3): 590-598.

Hayashi, K.-i., *et al*. (2008). "Small-molecule agonists and antagonists of F-box protein–substrate interactions in auxin perception and signaling." *Proceedings of the National Academy of Sciences* **105**(14): 5632-5637.

Hazy, E. and P. Tompa (2009). "Limitations of induced folding in molecular recognition by intrinsically disordered proteins." *Chemphyschem* **10**(9-10): 1415-1419.

Hinderaker, M. P. and R. T. Raines (2003). "An electronic effect on protein structure." *Protein Science* **12**(6): 1188-1194.

Hunter, C. A., *et al*. (2001). "Aromatic interactions." *Journal of the Chemical Society, Perkin Transactions* **2**(5): 651-669.

Hunter, C. A. and J. K. Sanders (1990). "The nature of. pi.-. pi. interactions." *Journal of the American Chemical Society* **112**(14): 5525-5534.

Jenik, P. D. and M. K. Barton (2005). "Surge and destroy: the role of auxin in plant embryogenesis." *Development* **132**(16): 3577-3585.

Kaethner, T. (1977). "Conformational change theory for auxin structure-activity relationships." *Nature* **267**(5606): 19-23.

Kagale, S. and K. Rozwadowski (2011). "EAR motif-mediated transcriptional repression in plants: an underlying mechanism for epigenetic regulation of gene expression." *Epigenetics* **6**(2): 141-146.

Ke, J., *et al*. (2015). "Structural basis for recognition of diverse transcriptional repressors by the TOPLESS family of corepressors." *Science Advances* **1**(6): e1500107.

Kepinski, S. and O. Leyser (2005). "The Arabidopsis F-box protein TIR1 is an auxin receptor." *Nature* **435**(7041): 446-451.

Kiefhaber, T., *et al*. (2012). "Dynamics and mechanisms of coupled protein folding and binding reactions." *Current Opinion in Structural Biology* **22**(1): 21-29.

Kielkopf, C. L., *et al*. (2001). "A novel peptide recognition mode revealed by the X-ray structure of a core U2AF 35/U2AF 65 heterodimer." *Cell* **106**(5): 595-605.

Korasick, D. A., *et al*. (2014). "Molecular basis for AUXIN RESPONSE FACTOR protein interaction and the control of auxin response repression." *Proceedings of the National Academy of Sciences* **111**(14): 5427-5432.

Lee, M.-S., *et al*. (2016). "Biological and molecular functions of two EAR motifs of Arabidopsis IAA7." *Journal of Plant Biology* **59**(1): 24-32.

Leyser, H., *et al*. (1996). "Mutations in the AXR3 gene of Arabidopsis result in altered auxin response including ectopic expression from the SAUR-AC1 promoter." *The Plant Journal* **10**(3): 403-413.

Leyser, O. (2005). "Auxin distribution and plant pattern formation: how many angels can dance on the point of PIN?" *Cell* **121**(6): 819-822.

Leyser, O. (2006). "Dynamic integration of auxin transport and signalling." *Current Biology* **16**(11): R424-R433.

Martinez, C. R. and B. L. Iverson (2012). "Rethinking the term “pi-stacking”." *Chemical Science* **3**(7): 2191-2201.

Mészáros, B., *et al*. (2007). "Molecular principles of the interactions of disordered proteins." *Journal of Molecular Biology* **372**(2): 549-561.

Meyer, E. A., *et al*. (2003). "Interactions with aromatic rings in chemical and biological recognition." *Angewandte Chemie International Edition* **42**(11): 1210-1250.

Mockaitis, K. and M. Estelle (2008). "Auxin receptors and plant development: a new signaling paradigm." *Annual Review of Cell and Developmental Biology* **24**: 55-80.

Moss, B. L., *et al*. (2015). "Rate motifs tune auxin/indole-3-acetic acid degradation dynamics." *Plant Physiology* **169**(1): 803-813.

Nagpal, P., *et al*. (2000). "AXR2 encodes a member of the Aux/IAA protein family." *Plant Physiology* **123**(2): 563-574.

Oono, Y., *et al*. (2003). "p-Chlorophenoxyisobutyric acid impairs auxin response in Arabidopsis root." *Plant Physiology* **133**(3): 1135-1147.

Parcy, F., *et al*. (2016). "A Glimpse beyond Structures in Auxin-Dependent Transcription." *Trends in Plant Science.*

Parry, G. and M. Estelle (2006). "Auxin receptors: a new role for F-box proteins." *Current Opinion in Cell Biology* **18**(2): 152-156.

Ramos, J. A., *et al*. (2001). "Rapid degradation of auxin/indoleacetic acid proteins requires conserved amino acids of domain II and is proteasome dependent." *The Plant Cell* **13**(10): 2349-2360.

Reed, J. W. (2001). "Roles and activities of Aux/IAA proteins in Arabidopsis." *Trends in Plant Science* **6**(9): 420-425.

Richarz, R. and K. Wüthrich (1978). "Carbon-13 NMR chemical shifts of the common amino acid residues measured in aqueous solutions of the linear tetrapeptides H-Gly-Gly-X-L-Ala-OH." *Biopolymers* **17**(9): 2133-2141.

Rouse, D., *et al*. (1998). "Changes in auxin response from mutations in an AUX/IAA gene." *Science* **279**(5355): 1371-1373.

Sassi, M. and T. Vernoux (2013). "Auxin and self-organization at the shoot apical meristem." *Journal of Experimental Botany*: ert101.

Schmit, M. C. P., *et al*. (2011). "Electronic structure and conformational properties of 1H-indole-3-acetic acid." *Journal of Molecular Modelling* **17**(6): 1227-1239.

Sharma, R., *et al*. (2015). "Fuzzy complexes: Specific binding without complete folding." *FEBS Letters* **589**(19PartA): 2533-2542.

Sheard, L. B., *et al*. (2010). "Jasmonate perception by inositol-phosphate-potentiated COI1-JAZ co-receptor." *Nature* **468**(7322): 400-405.

Shen, Y. and A. Bax (2010). "Prediction of Xaa-Pro peptide bond conformation from sequence and chemical shifts." *Journal of Biomolecular NMR* **46**(3): 199-204.

Smith, C. K., *et al*. (1994). "A Thermodynamic Scale for the. beta.-Sheet Forming Tendencies of the Amino Acids." *Biochemistry* **33**(18): 5510-5517.

Strader, L. C. and Y. Zhao (2016). "Auxin perception and downstream events." *Current opinion in plant biology* **33**: 8-14.

Szemenyei, H., *et al*. (2008). "TOPLESS mediates auxin-dependent transcriptional repression during Arabidopsis embryogenesis." *Science* **319**(5868): 1384-1386.

Tan, X., *et al*. (2007). "Mechanism of auxin perception by the TIR1 ubiquitin ligase." *Nature* **446**(7136): 640-645.

Teale, W. D., *et al*. (2006). "Auxin in action: signalling, transport and the control of plant growth and development." *Nature Reviews Molecular Cell Biology* **7**(11): 847-859.

Theillet, F.-X., *et al*. (2013). "The alphabet of intrinsic disorder: I. Act like a Pro: On the abundance and roles of proline residues in intrinsically disordered proteins." *Intrinsically Disordered Proteins* **1**(1): e24360.

Theologis, A. (1986). "Rapid gene regulation by auxin." *Annual Review of Plant Physiology* **37**(1): 407-438.

Thines, B., *et al*. (2007). "JAZ repressor proteins are targets of the SCFCOI1 complex during jasmonate signalling." *Nature* **448**(7154): 661-665.

Thomas, K. M., *et al*. (2006). "Electronic control of amide cis-trans isomerism via the aromatic-prolyl interaction." *Journal of the American Chemical Society* **128**(7): 2216-2217.

Tian, Q., *et al*. (2003). "Regulation of Arabidopsis SHY2/IAA3 protein turnover." *The Plant Journal* **36**(5): 643-651.

Tian, Q. and J. Reed (1999). "Control of auxin-regulated root development by the Arabidopsis thaliana SHY2/IAA3 gene." *Development* **126**(4): 711-721.

Tiwari, S. B., *et al*. (2004). "Aux/IAA proteins contain a potent transcriptional repression domain." *The Plant Cell* **16**(2): 533-543.

Tompa, P. and M. Fuxreiter (2008). "Fuzzy complexes: polymorphism and structural disorder in protein–protein interactions." *Trends in Biochemical Sciences* **33**(1): 2-8.

Tompa, P., *et al*. (2015). "Intrinsically disordered proteins: emerging interaction specialists." *Current Opinion in Structural Biology* **35**: 49-59.

Ulmasov, T., *et al*. (1997). "ARF1, a transcription factor that binds to auxin response elements." *Science* **276**(5320): 1865-1868.

Ulmasov, T., *et al*. (1999). "Dimerization and DNA binding of auxin response factors." *The Plant Journal* **19**(3): 309-319.

Ulmasov, T., *et al*. (1995). "Composite structure of auxin response elements." *The Plant Cell* **7**(10): 1611-1623.

Uversky, V. N., *et al*. (2005). "Showing your ID: intrinsic disorder as an ID for recognition, regulation and cell signaling." *Journal of Molecular Recognition* **18**(5): 343-384.

Vanneste, S. and J. Friml (2009). "Auxin: a trigger for change in plant development." *Cell* **136**(6): 1005-1016.

Vernoux, T., *et al*. (2011). "The auxin signalling network translates dynamic input into robust patterning at the shoot apex." *Molecular Systems Biology* **7**(1): 508.

Villalobos, L. I. A. C., et al. (2012). "A combinatorial TIR1/AFB–Aux/IAA co-receptor system for differential sensing of auxin." *Nature Chemical Biology* **8**(5): 477-485.

Walker, L. and M. Estelle (1998). "Molecular mechanisms of auxin action." *Current Opinion in Plant Biology* **1**(5): 434-439.

Wang, R. and M. Estelle (2014). "Diversity and specificity: auxin perception and signaling through the TIR1/AFB pathway." *Current Opinion in Plant Biology* **21**: 51-58.

Wang, R. and M. Estelle (2014). "Diversity and specificity: auxin perception and signaling through the TIR1/AFB pathway." *Current Opinion in Plant Biology* **21**: 51-58.

Waters, M. L. (2002). "Aromatic interactions in model systems." *Current Opinion in Chemical Biology* **6**(6): 736-741.

Weijers, D. and D. Wagner (2016). "Transcriptional responses to the auxin hormone." *Annual Review of Plant Biology* **67**: 539-574.

Weiss, M. S., *et al*. (1998). "Peptide bonds revisited." *Nature Structural & Molecular Biology* **5**(8): 676-676.

Wishart, D. S. and B. D. Sykes (1994). "The 13C chemical-shift index: a simple method for the identification of protein secondary structure using 13C chemical-shift data." *Journal of Biomolecular NMR* **4**(2): 171-180.

Worley, C. K., *et al*. (2000). "Degradation of Aux/IAA proteins is essential for normal auxin signalling." *The Plant Journal* **21**(6): 553-562.

Wright, P. E. and H. J. Dyson (1999). "Intrinsically unstructured proteins: re-assessing the protein structure-function paradigm." *Journal of Molecular Biology* **293**(2): 321-331.

Wright, P. E. and H. J. Dyson (2015). "Intrinsically disordered proteins in cellular signalling and regulation." *Nature Reviews Molecular Cell Biology* **16**(1): 18-29.

Wu, W. J. and D. P. Raleigh (1998). "Local control of peptide conformation: stabilization of cis proline peptide bonds by aromatic proline interactions." *Biopolymers* **45**(5): 381-394.